

1 **Thyroid hormone regulates distinct paths to maturation in pigment
2 cell lineages**

3
4 Lauren M. Saunders,^{1,2} Abhishek K. Mishra,² Andrew J. Aman,² Victor M. Lewis,^{1,2} Matthew
5 B. Toomey,^{3†} Jonathan S. Packer,¹ Xiaojie Qiu,¹ José L. McFaline-Figueroa,¹ Joseph C.
6 Corbo,⁴ Cole Trapnell,^{1*} David M. Parichy,^{2*}

7
8
9 ¹Department of Genome Sciences, University of Washington, Seattle, WA 98195, USA.

10 ²Department of Biology and Department of Cell Biology, University of Virginia, Charlottesville, VA
11 22904, USA.

12 ³Department of Pathology and Immunology, Washington University School of Medicine, St. Louis,
13 MO 63110, USA.

14
15 * Correspondence to: dparichy@virginia.edu, coletrap@uw.edu

16 † Present address: Department of Biological Science, University of Tulsa, Tulsa, OK 74104

17 **Abstract**

18 Thyroid hormone (TH) regulates diverse developmental events and can drive disparate cellular
19 outcomes. In zebrafish, TH has opposite effects on neural crest derived pigment cells of the adult
20 stripe pattern, limiting melanophore population expansion, yet increasing yellow/orange xanthophore
21 numbers. To learn how TH elicits seemingly opposite responses in cells having a common
22 embryological origin, we analyzed individual transcriptomes from thousands of neural crest derived
23 cells, reconstructed developmental trajectories, identified pigment cell-lineage specific responses to
24 TH, and assessed roles for TH receptors. We show that TH promotes maturation of both cell types
25 but in distinct ways. In melanophores, TH drives terminal differentiation, limiting final cell numbers. In
26 xanthophores, TH promotes accumulation of orange carotenoids, making the cells visible. TH
27 receptors act primarily to repress these programs when TH is limiting. Our findings show how a
28 single endocrine factor integrates very different cellular activities during the generation of adult form.

29 **Introduction**

30 Mechanisms that synchronize developmental signals and integrate them across cell types and organ
31 systems remain poorly defined but are fundamentally important to both development and evolution of
32 adult form (Atchley and Hall, 1991; Ebisuya and Briscoe, 2018). A powerful system for elucidating
33 how organisms coordinate fate specification and differentiation with morphogenesis is the array of
34 cell types that arise from embryonic neural crest (NC), a key innovation of vertebrates (Gans and
35 Northcutt, 1983). NC cells disperse throughout the body, contributing peripheral neurons and glia,
36 osteoblasts and chondrocytes, pigment cells and other derivatives. Differences in the patterning of
37 these cells underlie much of vertebrate diversification.

38 Thyroid hormone (TH) coordinates post-embryonic development of NC and other derivatives
39 through mechanisms that are incompletely characterized (Brent, 2012; Brown and Cai, 2007; Sachs
40 and Buchholz, 2017; Shi, 1999). During the abrupt metamorphosis of amphibians, TH drives
41 outcomes as disparate as tail resorption and limb outgrowth. In the more protracted post-embryonic
42 development of zebrafish—which has similarities to fetal and neonatal development of mammals
43 (Parichy et al., 2009)—TH coordinates modifications to several traits including pigmentation.
44 Remarkably, TH has seemingly opposite effects on two classes of NC-derived pigment cells,

50 curtailing the population of black melanophores yet promoting development of yellow/orange
51 xanthophores; fish lacking TH have about twice the normal number of melanophores and lack visible
52 xanthophores (**Figure 1A**) (McMenamin et al., 2014).

53 We asked how a single endocrine factor can have such different effects on cells sharing a
54 common embryonic origin. Using transcriptomic analyses of individual cell states, we
55 comprehensively defined the context for TH activities by identifying populations and subpopulations
56 of adult NC derivatives. We then assessed the consequences of TH status for lineage maturation
57 across pigment cell classes. Our analyses showed that TH drives maturation of cells committed to
58 melanophore and xanthophore fates through different mechanisms, promoting terminal
59 differentiation and proliferative arrest in melanophores, and carotenoid-dependent repigmentation in
60 xanthophores. These mechanisms reflect different developmental histories of melanophores and
61 xanthophores, and yield different cell-type abundances when TH is absent. Our findings provide
62 insights into post-embryonic NC lineages, contribute resources for studying adult pigment cells and
63 other NC-derived cell types, and illustrate how a circulating endocrine factor influences local cell
64 behaviors to coordinate adult trait development.

65 Results

66 Post-embryonic NC-derived subpopulations revealed by single cell RNA-sequencing

67 To explain the pigment cell imbalance of hypothyroid fish, we envisaged two models for TH activity
68 during normal development (**Figure 1B**). In the first model, TH influences states of specification,
69 directing multipotent cells away from one fate and towards the other, or preventing the
70 transdifferentiation of cells already committed to a particular fate. In the second model, TH influences
71 cells that are already committed, and remain committed, to their fates. In this scenario discordant
72 effects across lineages might be observed if TH promotes a cellular process in one lineage that
73 amplifies its population, while simultaneously inhibiting the same process in the other lineage to
74 restrain its population.

75 To evaluate the applicability of these models to TH-dependent regulation of pigment cell
76 populations, we sought to capture the range of intermediate states through which these cells transit
77 during normal and hypothyroid development. Accordingly, we sequenced transcriptomes of
78 thousands of individual NC-derived cells isolated from trunks of euthyroid and hypothyroid fish
79 (**Figure 2—figure supplements 1 and 2**). Dimensionality reduction (Becht et al., 2018; Cao et al.,
80 2019) followed by unsupervised clustering identified melanophores, xanthophores and a third class
81 of NC-derived pigment cells, iridescent iridophores (**Figure 2A and B; Supplementary File 1**). A
82 cluster likely corresponding to multipotent pigment cell progenitors (Budi et al., 2011; Singh et al.,
83 2016) was marked by genes encoding pigment cell transcription factors, general markers of
84 mesenchymal NC and factors associated with proliferation and migration but not pigment synthesis
85 (**Figure 2—figure supplement 3; Supplementary File 2—Table 1**). Some cells within this cluster
86 also expressed the zebrafish-specific embryonic NC marker *crestin*, which is generally down-
87 regulated at later developmental stages but is still expressed in a subset of presumptive progenitor
88 cells (Budi et al., 2011).

89 Beyond pigment cells and their presumptive precursors, other clusters were identifiable as
90 neurons, Schwann cells, other glia, and chromaffin cells. An additional cluster expressed markers
91 suggestive of proliferative, non-pigmentary progenitors, and one large cluster (“unknown”) was not
92 readily assignable to NC-derived populations described previously. Bioinformatic comparisons
93 across all clusters revealed distinct expression profiles of genes encoding ligands and receptors, cell
94 adhesion molecules, and products likely to have diverged in function after the teleost specific whole-
95 genome duplication (**Figure 2—figure supplement 4**).

96 The larva-to-adult transformation of zebrafish entails changes in a variety of traits including NC
97 derivatives (Parichy et al., 2009). In some instances cell types at different stages that are
98 superficially similar (e.g., larval vs. adult melanophores) can be distinguished by different genetic

101 requirements (Budi et al., 2008; Larson et al., 2010; Parichy et al., 1999), raising the possibility that
102 distinct gene expression programs regulate early larval and adult populations. If so, we predicted
103 that NC-derived cells isolated from middle larval–juvenile stages, during development of the adult
104 phenotype (i.e., **Figure 2a**), should form clusters distinct from cells that developed during embryonic
105 stages to form the embryonic–early larval (“EL”) phenotype. To test this idea, we isolated EL NC-
106 derived cells, which clustered in identifiable cell types similar to those of middle-larval juvenile stages
107 (**Figure 2—figure supplement 5A**). Combining profiles for cells at different stages failed to reveal
108 non-contiguous, life-stage specific clusters, although some EL cells occupied subsets of
109 transcriptomic space relative to their broader cell type (e.g., melanophores) (**Figure 2—figure**
110 **supplement 5B–D**). These data do not indicate markedly different transcriptomic programs of NC-
111 derived cell types across life stages, despite the existence of some stage-specific requirements for
112 particular genes and pathways.

113 Overall, our survey captured numerous NC-derived cell types, including abundant pigment cells
114 and progenitors, and revealed substantial variation in gene expression programs among them.
115

116 **Pigment cell sub-classes and gene expression dynamics across differentiation**

117 To understand the gene expression context in which TH impacts each pigment cell type, we
118 compared pigment cells and progenitors, the lineages of which have been described (Budi et al.,
119 2011; Mahalwar et al., 2014; McMenamin et al., 2014; Patterson and Parichy, 2019; Singh et al.,
120 2016) (**Figure 3A**). These analyses revealed subsets of melanophores and xanthophores (**Figure**
121 **3B**), consistent with differences in states of differentiation and morphogenetic behaviors (Eom et al.,
122 2015; Parichy et al., 2000b; Parichy and Spiewak, 2015). For example, cells of melanophore
123 subcluster 2 exhibited low levels of transcriptional activity and expressed fewer genes, suggesting a
124 more advanced state of differentiation, as compared to cells of melanophore 1 (**Figure 3—figure**
125 **supplement 1**). Likewise cells of xanthophore 1 had fewer transcripts and expressed fewer genes
126 than cells of xanthophore 2, suggesting they may represent undifferentiated, cryptic xanthophores
127 and actively differentiating populations, respectively (McMenamin et al., 2014).

128 Additional surveys of these data revealed new markers of xanthophore and iridophore lineages
129 (**Figure 3—figure supplements 2 and 3**), and cell-type specific expression of some previously
130 identified markers [e.g., *tyrp1b*, *aox5*, *tfec* (Lister et al., 2011; McMenamin et al., 2014)] (**Figure 3C**).
131 Expression of other genes was broader than might be expected from mutational or other analyses
132 (**Figure 3—figure supplement 4**); e.g., *mitfa*, encoding a transcription factor required for
133 melanophore fate specification (Lister et al., 1999) was expressed in melanophores and progenitors,
134 but also xanthophores (**Figure 3C**), consistent with prior reports (Eom et al., 2012; Parichy et al.,
135 2000b).

136 To characterize transcriptional dynamics through lineage maturation, we pseudotemporally
137 ordered cells (Qiu et al., 2017a, 2017b; Trapnell et al., 2014), yielding a differentiation trajectory with
138 each pigment cell type arising from a common progenitor (**Figure 3D**). This topology differed from
139 lineage relationships (**Figure 3A**), but was consistent with similarity of EL and mid-larval/juvenile
140 gene expression programs (**Figure 2—figure supplement 5D**). Branch expression analysis
141 modeling (BEAM) (Qiu et al., 2017a) confirmed that genes known to function in specification (e.g.,
142 *mitfa* in melanophores) were expressed early in pseudotime whereas genes associated with
143 differentiation [e.g., *dct*, encoding a melanin synthesis enzyme (Kelsh et al., 2000b)] were expressed
144 late (**Figure 3E; Figure 3—figure supplement 5A**). These analyses revealed dynamics of dozens
145 of genes potentially identifying discrete processes in lineage-specific maturation (**Supplementary**
146 **File 2—Table 2**) as well as broader trends. For example, transcripts per cell declined in
147 melanophores but not iridophores, consistent with an expectation of reduced RNA abundance as
148 melanophores—but not iridophores—exit the cell cycle with maturation (**Figure 3—figure**
149 **supplement 5B**) (Budi et al., 2011; Darzynkiewicz et al., 1980; McMenamin et al., 2014; Spiewak et
150 al., 2018).

151

152 **TH-independence of pigment cell fate specification and absence of lineage-specific restraints**
153 **on developmental progress**

154 Resolution of pigment cell states through their development allowed us to test if TH functions in fate
155 specification (**Figure 1B-i**). If so, the excess melanophores and missing xanthophores of hypothyroid
156 fish should reflect biases on specification of multipotent progenitors, or the transdifferentiation (Lewis
157 et al., 2019; Niu, 1954) of initially specified cells. Such alterations should be evident in reduced-
158 dimension transcriptomic space as strong skew in the apportionment of cells between branches or
159 abnormal paths in the cellular trajectory, respectively. Yet, euthyroid and hypothyroid trajectories
160 were topologically equivalent. Moreover, pigment cell progenitors were not depleted in hypothyroid
161 fish as might occur were these cells being allocated inappropriately as melanophores (**Figure 4A–**
162 **D**).

163 Through a second model—lineage discordance—TH could have opposite effects on cells already
164 committed to particular fates, selectively amplifying one cell type while simultaneously repressing
165 amplification of the other (**Figure 1B-ii**). For example, TH could promote differentiation of
166 xanthoblasts to xanthophores, but prevent differentiation of melanoblasts to melanophores.
167 Alternatively, TH could be a survival factor in the xanthophore lineage but a pruning factor in the
168 melanophore lineage. Terminal phenotypes of both hypothyroid and hyperthyroid mutant fish are
169 consistent with such effects (McMenamin et al., 2014). If TH has discordant effects between
170 lineages, we predicted that hypothyroid fish should exhibit a strong depletion of xanthophores from
171 the end of their branch of the trajectory, whereas melanophores should be strongly over-represented
172 near the tip of their branch. Yet, empirical distributions of pigment cell states in hypothyroid fish were
173 all biased towards earlier steps in pseudotime, sometimes severely (**Figure 4E**). Indeed, prior
174 analyses showed that addition of exogenous TH to hypothyroid cells *ex vivo* can promote
175 differentiation of unpigmented melanoblasts to melanophores (McMenamin et al., 2014), contrary to
176 the idea that TH specifically blocks melanophore development. Together these findings allow us to
177 reject a model in which TH regulation of pigment cell abundance in the adult fish occurs through
178 discordant effects on specific cellular processes across lineages.

179
180 **TH promotes a melanophore maturation program**

181 Having rejected both of our initial models (**Figure 1B**), we considered a third possibility, that TH
182 promotes the maturation of both lineages, but in distinct ways. For melanophores, inspection of
183 transcriptomic states and cellular phenotypes supported a role for TH in promoting maturation of this
184 lineage. Genes expressed during terminal differentiation of melanophores from euthyroid fish (e.g.,
185 *tfap2a*, *tyrp1b*) were expressed at lower levels in melanophores of hypothyroid fish, suggesting an
186 impediment to maturation in the absence of TH (**Figure 5A**).

187 To test further test the idea that TH promotes the maturation of melanophores, we examined
188 additional cellular phenotypes. Melanophores of juvenile euthyroid fish tended to be uniformly well-
189 melanized and stellate whereas melanophores of juvenile hypothyroid fish were variably melanized
190 and dendritic (**Figure 5B**), reminiscent of earlier stages of melanophore development in wild-type
191 (Eom et al., 2012; Parichy and Turner, 2003). Quantification of melanin content within individual cells
192 confirmed that melanophores of euthyroid fish are more heavily melanized than those of hypothyroid
193 fish (**Figure 5C**).

194 Prior analyses indicated that melanophores of euthyroid fish fail to divide whereas those of
195 hypothyroid fish continue to do so (McMenamin et al., 2014). These findings raised the possibility
196 that melanophores of euthyroid fish might exhibit signs of cellular senescence or other indications of
197 proliferative cessation not observed in melanophores of hypothyroid fish. Human nevus
198 melanocytes, and melanophores of teleost melanoma models, exhibit senescent or senescent-like
199 phenotypes and can be multinucleated (Leikam et al., 2015, 2008; Regneri et al., 2019; Savchenko,
200 1988). Accordingly, we asked whether similar attributes were evident for zebrafish stripe
201 melanophores. When plated *ex vivo*, some stripe melanophores exhibited senescence-associated β-

galactosidase (SA- β -gal) activity (**Figure 5—figure supplement 1A**) although we were unable to score such staining reliably, precluding comparisons across TH conditions.

SA- β -gal staining results from lysosomal β -gal activity and both β -gal activity and lysosome number increase in aging cells (Kurz et al., 2000; Lee et al., 2006). We therefore quantified lysosome-specific Lysotracker labeling (**Figure 5—figure supplement 1B and F**) of melanophores by fluorescence activated cell sorting *tyrp1b:palm-mCherry+* melanophores. Lysosomal contents of melanophores from euthyroid fish were greater than melanophores from hypothyroid fish (**Figure 5—figure supplement 1C**). Measurements of forward scatter (FSC-A) also suggested that melanophores from juvenile euthyroid fish were larger than melanophores from hypothyroid fish (**Figure 5—figure supplement 1D**), though FSC-A can be influenced by cell-size independent factors as well (Tzur et al., 2011)).

Finally we examined multinucleation, a condition linked to increased cell survival and size (Orr-Weaver, 2015; Usui et al., 2018). In euthyroid fish, ~20% of melanophores were binucleate near the onset of adult melanophore differentiation but >50% were binucleate by juvenile stages, confirming an overall increase in binucleation with somatic stage and melanophore age (**Figure 5—figure supplement 1E**). In stage-matched comparisons for TH status, ~70% of melanophores from euthyroid fish were binucleated, whereas only ~25% of melanophores from hypothyroid fish were in this state (**Figure 5D and E**).

Collectively, our observations and those of McMenamin et al. (2014) suggest a model in which TH drives melanophores into a terminally differentiated state of increased melanization, larger size and lysosomal content, binucleation, and proliferative cessation.

TH promotes carotenoid-dependent xanthophore re-pigmentation during adult development

We next examined TH functions specific to the xanthophore lineage. Most adult xanthophores develop directly from EL xanthophores that lose their pigment and then reacquire it late in adult pattern formation (**Figure 3A**) (McMenamin et al., 2014). Because xanthophores of hypothyroid fish persist, albeit in a cryptic state, we predicted that TH effects should be less pervasive in these cells than in melanophores that develop *de novo* from transit amplifying cells originating from multipotent progenitors. Indeed, fewer genes were expressed differentially between TH backgrounds in xanthophore than melanophore lineages (3.6% vs. 9%; **Figure 6A**). Prominent among these were several loci implicated in, or plausibly associated with, the processing of yellow/orange carotenoids (**Figure 6B and C; Figure 6—figure supplement 1**), dietarily derived pigments that contribute to xanthophore coloration (Schartl et al., 2016; Toews et al., 2017).

Differences in carotenoid gene expression suggested a corresponding pigmentation deficiency in xanthophores of hypothyroid fish that we confirmed by HPLC, histology, and transmission electron microscopy (**Figure 6D; Figure 6—figure supplement 2**). Among carotenoid genes, scavenger receptor B1 (*scarb1*) encodes a high density lipoprotein receptor essential for carotenoid accumulation in birds and invertebrates (Kiefer et al., 2002; Toomey et al., 2017) and we found it to be required in zebrafish for carotenoid deposition, though not cell persistence (**Figure 6—figure supplement 3A and B**). *scarb1* was expressed more highly in xanthophores of euthyroid than hypothyroid fish ($p=1.1\text{E-}10$) (**Figure 6B and E; Figure 6—figure supplement 1**) and exogenous TH was sufficient to rescue both expression and carotenoid deposition (**Figure 6F; Figure 6—figure supplement 3C**). Together these findings demonstrate an essential role for TH in carotenoid pigmentation and suggest that TH modulation of a suite of carotenoid pathway genes is required for cryptic xanthophores to re-pigment during adult pattern formation.

The distinct phases of xanthophore EL and adult pigmentation (McMenamin et al., 2014), and the TH-dependence of the latter, led us to ask whether mechanisms underlying coloration might be stage-specific. In contrast to the defect of adult xanthophore pigmentation in *scarb1* mutants, we found that 5 dpf larval xanthophores were indistinguishable from wild-type (**Figure 6—figure supplement 4A**). Conversely, mutants lacking xanthophore pigmentation at 5 dpf have normal adult xanthophores (Lister, 2019; Odenthal et al., 1996). Because two pigment classes—carotenoids and

pteridines—can contribute to xanthophore coloration, we hypothesized that visible colors at different stages depend on different pathways. Carotenoids were undetectable in euthyroid 5 dpf larvae, and carotenoid-related genes were expressed at lower levels in EL xanthophores than adult xanthophores (**Figure 6—figure supplement 4B and C**). By contrast, pteridine pathway genes tended to be expressed similarly across stages regardless of TH status, and were even moderately upregulated in hypothyroid xanthophores (**Figure 6C, Figure 6—figure supplement 4C**). Pteridine autofluorescence and pterinosomes were also indistinguishable between euthyroid and hypothyroid fish (**Figure 6—figure supplement 4D; Figure 6—figure supplement 2B**) despite the overt difference in xanthophore color with TH status [**Figure 1A**; (McMenamin et al., 2014)]. Together, these observations imply that TH induces new, carotenoid-based pigmentation, allowing transiently cryptic xanthophores to reacquire coloration during adult pattern development. TH therefore drives maturation of both xanthophores and melanophores yet has markedly different roles in each lineage.

Adult pigment cell maturation programs are gated by TH receptors

Finally, to understand how TH effects are transduced in pigment cell lineages, we evaluated roles for TH nuclear receptors (TRs) that classically activate target genes when ligand (T3) is present but repress gene expression when ligand is absent (Brent, 2012; Buchholz et al., 2003; Hörlein et al., 1995). Genes encoding each of the three zebrafish TRs (*thraa*, *thrab*, *thrb*) were expressed by melanophores and xanthophores, yet presumptive null alleles for each unexpectedly had pigment cell complements and patterns that resembled the wild type (**Figure 7A; Figure 7—figure supplement 1A–D**).

Given the absence of grossly apparent phenotypes for TR mutants, we hypothesized that instead of acting to promote maturation when T3 is present, TRs may function primarily to repress maturation when T3 is limiting. If so, we predicted that xanthophore development in hypothyroid fish should be rescued by mutation of TR. We therefore generated fish lacking TH and TRs. Loss of *thrab*, on its own or in conjunction with loss of *thraa*, partially restored the deposition of carotenoids in interstripe xanthophores; mutation of all three receptors fully rescued the number of carotenoid-containing xanthophores (**Figure 7B and C; Figure 7—figure supplement 1E and F**). TR receptor mutations likewise reduced the total numbers of melanophores in hypothyroid fish to levels indistinguishable from euthyroid fish (**Figure 7D**).

These findings suggest that repression by unliganded TRs contributes to pigment-associated phenotypes in hypothyroid fish, implying a function for TRs in repressing the repigmentation of xanthophores and terminal differentiation of melanophores until late stages in adult pigment pattern development. Nevertheless, roles for TRs are likely to be complex and outcomes of derepression dependent on context. For example, the simplest model of TR gating would predict that loss of TRs in euthyroid fish should result in the precocious maturation of pigment cells. Yet, we found no evidence for early pigmentation of xanthophores in euthyroid fish homozygous for *thrab* mutation (**Figure 7—figure supplement 1G**), suggesting essential roles for other factors present only at later stages (Patterson and Parichy, 2013).

Discussion

Our study provides insights into how TH coordinates local cellular events during the development of adult form. The stripes of adult zebrafish comprise three major classes of pigment cells that develop at specific stages and from distinct NC sublineages. Perturbations that affect the times of appearance, states of differentiation or morphogenetic behaviors of these cells can dramatically alter pattern by affecting total numbers of cells and the cascade of interactions normally required for spatial organization (Parichy and Spiewak, 2015; Patterson et al., 2014; Watanabe and Kondo, 2015). Fish lacking TH have gross defects in pigment cell numbers and pattern with ~two-fold the normal complement of melanophores and the simultaneous absence of visible xanthophores

(McMenamin et al., 2014). We show that this phenotype arises not because TH normally biases cell fate specification or has discordant effects on a particular cellular behavior that amplifies one cell type while repressing the other. Rather, our findings—combining discovery-based analyses of single-cell transcriptomic states with experiments to test specific cellular hypotheses—suggest a model whereby TH promotes maturation of both melanophores and xanthophores in distinct ways that reflect the developmental histories of these cells (**Figure 8**). Our study provides a glimpse into the diversity of cell states among post-embryonic NC-derivatives and illustrates how a single endocrine factor coordinates diverse cellular behaviors in a complex developmental process.

By sampling individual cell transcriptomes across NC-derived lineages, our study complements prior investigations of lineage relationships, morphogenetic behaviors, genetic requirements, and spatial and cell-type specific gene expression profiles (Eom et al., 2015; Irion et al., 2016; Johnson et al., 1995; Kelsh et al., 2017; McMenamin et al., 2014; Parichy and Spiewak, 2015; Singh et al., 2016, 2014). Multipotent progenitors that give rise to adult melanophores, some xanthophores, and iridophores are established in the embryo and reside within peripheral nerves as development progresses (Budi et al., 2011, 2008; Camargo-Sosa et al., 2019; Dooley et al., 2013a; Singh et al., 2016). As the adult pattern forms, some of these cells migrate to the hypodermis where they differentiate and integrate into dark stripes or light interstripes. The peripheral-nerve association of pigment cell progenitors in zebrafish is reminiscent of nerve-associated Schwann cell precursors that contribute to melanocytes of mammals and birds (Adameyko et al., 2009). Our collected cell-types, which include immature and mature glia, differentiating pigment cells, and presumptive progenitors of different types identify new candidate genes for promoting—and recognizing—distinct states of differentiation and morphogenetic activities, and will enable efforts to define how multipotent NC progenitors are maintained and recruited into particular lineages. That corresponding populations of embryonic and adult populations had largely overlapping transcriptomic states additionally highlights the intriguing problem of how specific pathways are deployed reiteratively across life cycle phases to achieve specific morphogenetic outcomes.

Our identification of a role for TH in the adult melanophore lineage illuminates how these cells develop normally and mechanisms that likely contribute to the supernumerary melanophores of hypothyroid fish. Melanoblasts derived from peripheral-nerve associated progenitors are proliferative during adult pigment pattern formation yet this activity largely ceases as the cells differentiate (Budi et al., 2011; McMenamin et al., 2014). Several lines of evidence suggest that TH promotes melanophore maturation to a terminally differentiated state: in the presence of TH, melanophores were more heavily melanized, larger, had greater lysosomal contents, and were more likely to be binucleated. TH similarly promotes the melanization of melanoblasts *ex vivo* and a cessation of proliferative activity *in vivo* (McMenamin et al., 2014). Our findings are broadly consistent with a role for TH in balancing proliferation and differentiation (Brent, 2012) and may be of clinical relevance, as human melanoma is associated with hypothyroidism and recurrent TH pathway mutations (Ellerhorst et al., 2003; Shah et al., 2006; Sisley et al., 1993). We suggest a model in which TH normally curtails expansion of the adult melanophore population by ensuring that cells cease to divide in a timely manner; in hypothyroid fish, the inappropriate retention of an immature state allows continued growth of the melanophore population during these post-embryonic stages. Whether TH induces a true cellular senescence and proliferative arrest, or whether cells at an apparently terminal state of differentiation remain competent to divide in specific conditions, will be interesting to learn.

TH promoted the terminal differentiation of xanthophores, but in a manner distinct from melanophores. We found far fewer TH-dependent genes in xanthophores than melanophores, likely reflecting the different developmental histories of these cells. In contrast to adult melanophores that arise from a transit-amplifying progenitor, most adult xanthophores develop directly from EL xanthophores that lose their pigment and then regain color late in adult pattern formation (McMenamin et al., 2014; Patterson et al., 2014) when TH levels are rising (Chang et al., 2012). The yellow-orange color of xanthophores can depend on pteridine pigments, carotenoid pigments, or both (Bagnara and Matsumoto, 2006; Granneman et al., 2017; Lister, 2019; Odenthal et al., 1996;

355 Ziegler, 2003). We showed that TH directly or indirectly regulates carotenoid-associated genes and
356 carotenoid deposition, allowing cryptic xanthophores to reacquire visible pigmentation. TH did not
357 similarly influence pteridine pathway genes. These observations suggest that TH mediates a
358 transition from pteridine-dependent pigmentation at embryonic/early larval stages to carotenoid-
359 dependent pigmentation of the same cells in the adult. Consistent with the notion of TH-mediated
360 pigment-type switching, TH-dependent *scarb1* was required for carotenoid accumulation during adult
361 pattern formation, yet mutants lacked an embryonic/early larval xanthophore phenotype. Conversely,
362 mutants with pteridine and color deficiencies in embryonic/early larval xanthophores have normally
363 pigmented adult xanthophores (Lister, 2019; Odenthal et al., 1996). In xanthophores at post-
364 embryonic stages, then, TH drives a state of terminal differentiation from a developmental program
365 that is relatively more advanced than that of progenitor-derived melanophores. That cryptic
366 xanthophores appear poised to re-differentiate likely explains the smaller proportion of genes that
367 were TH-dependent in these cells as compared to melanophores.

368 Finally, our study provides clues to likely roles for TRs during adult pigment pattern formation. TR
369 mutants lacked overt pigmentation defects yet allowed for rescues of both melanophore and
370 xanthophore defects in hypothyroid fish, suggesting that unliganded TRs normally repress
371 maturation of these lineages. Loss of TRs similarly allows the survival of congenitally hypothyroid
372 mice (Flamant et al., 2002; Flamant and Samarut, 2003). TRs may therefore prevent the
373 inappropriate activation of gene expression programs required for lineage maturation when TH levels
374 are low, as is thought to occur during amphibian metamorphosis (Choi et al., 2015; Shi, 2013).
375 Although we detected pigment cell expression of each TR locus, our analyses cannot indicate
376 whether TH acts directly on pigment cells through TR activities that are autonomous to these
377 lineages. A plausible alternative would be that TH acts on stromal or other cell types in which TRs
378 might be expressed and might exert similarly repressive effects when unliganded. Indeed, stromal
379 cells of the hypodermis (Lang et al., 2009) and also iridophores (Frohnhofer et al., 2013; Patterson
380 and Parichy, 2013) regulate melanophore and xanthophore numbers during adult pigment pattern
381 formation, and we observed striking differences in iridophore maturation depending on TH status.
382 On-going efforts seek to distinguish between these possibilities. Results of the current study,
383 however, represent a useful first step in understanding how globally available signals can control
384 fine-grained patterning of cells within this complex adult trait.

385
386
387
388
389
390

391 **Materials and methods**392 **Key resources**

Reagent type (species) or resource	Designation	Source or reference	Identifiers	Additional information
gene (<i>Danio rerio</i>)	bco1	this paper	NCBI_Reference_Sequence: NM_001328495.1	Amplified from cDNA
gene (<i>Danio rerio</i>)	bco2b	this paper	NCBI_Reference_Sequence: NM_001040312.1	Amplified from cDNA
gene (<i>Danio rerio</i>)	bscl2l	this paper	NCBI_Reference_Sequence: NM_001013553.2	Amplified from cDNA
gene (<i>Danio rerio</i>)	slc2a11b	this paper	NCBI_Reference_Sequence: NM_001114430.1	Amplified from cDNA
gene (<i>Danio rerio</i>)	slc22a7a	this paper	NCBI_Reference_Sequence: M_001083861.1	Amplified from cDNA
gene (<i>Danio rerio</i>)	wu:fc46h12	this paper	NCBI_Reference_Sequence: NM_001291347.1	Amplified from cDNA
gene (<i>Danio rerio</i>)	alx4a	this paper	NCBI_Reference_Sequence: XM_001340930	Amplified from cDNA
gene (<i>Danio rerio</i>)	alx4b	this paper	NCBI_Reference_Sequence: NM_001310078.1	Amplified from cDNA
gene (<i>Danio rerio</i>)	crip2	this paper	NCBI_Reference_Sequence: NM_001005968.1	Amplified from cDNA
gene (<i>Danio rerio</i>)	defbl1	this paper	NCBI_Reference_Sequence: NM_001081553.1	Amplified from cDNA
strain, strain background (<i>Danio rerio</i>)	Tg(tg:nVenus-v2a-nfnB)	PMID:25170046	NA	NA
strain, strain background (<i>Danio rerio</i>)	WT(ABb)	PMID:23737760	NA	NA
strain, strain background (<i>Danio rerio</i>)	Tg(aox5:palmEGFP)wp.rt22	PMID:25170046	NA	NA
strain, strain background (<i>Danio rerio</i>)	Tg(tyrp1b:palm-mCherry)wp.rt11	PMID:25170046	NA	NA
strain, strain background (<i>Danio rerio</i>)	Tg(-28.5Sox10:Cre)zf384	Gift. PMID:23155370	NA	NA
strain, strain background (<i>Danio rerio</i>)	Tg(-3.5ubi:loxP-eGFP-loxP-mCherry)cz1701	Gift. PMID:21138979	NA	NA
strain, strain background (<i>Danio rerio</i>)	Tg(tuba8l3:nEosFP)vp.rt17	this paper	NA	NA

strain, strain background (Danio rerio)	<i>thraa</i> ^{vp33rc1}	this paper	NA	NA
strain, strain background (Danio rerio)	<i>thrab</i> ^{vp31rc1}	this paper	NA	NA
strain, strain background (Danio rerio)	<i>thrb</i> ^{vp34rc1}	this paper	NA	NA
strain, strain background (Danio rerio)	<i>scarb1</i> ^{vp32rc1}	this paper	NA	NA
strain, strain background (Danio rerio)	<i>tyr</i> ^{vp35rc1}	this paper	NA	NA
antibody	anti-Dig-AP, sheep polyclonal Fab fragments	Millipore-Sigma	SKU_millipore-sigma:11093274910	1:5000 overnight at 4°C
antibody	anti-GFP rabbit polyclonal antibody	Thermo Fisher	CatalogNo_A-11122	1:1000 overnight at 4°C
commercial assay or kit	Lysotracker Far Red	Thermo Fisher	CatalogNo_L12492	75 nM
commercial assay or kit	Vybrant DyeCycle Violet stain	Thermo Fisher	CatalogNo_V35003	5 µM
commercial assay or kit	Senescence associated β-Galactosidase Staining Kit	Cell Signaling Technologies	CatalogNo_9860	NA
chemical compound, drug	Metronidazole	Acros Organics	CatalogNo_210341000	NA
chemical compound, drug	Oil Red O	Millipore-Sigma	CatalogNo_3125-12	5 mM
software, algorithm	Cellranger	10X Genomics	v2.0.2	
software, algorithm	Monocle	NA	v2.9.0 and v2.99.1	https://github.com/cole-trapnell-lab/monocle-release.git

395

396

397

Staging, rearing and stocks

398 Staging followed (Parichy et al., 2009) and fish were maintained at ~28.5 °C under 14:10 light:dark
 399 cycles. All thyroid-ablated (Mtz-treated) and control (DMSO-treated) *Tg(tg:nVenus-v2a-nfnB)* fish
 400 were kept under TH-free conditions and were fed only *Artemia*, rotifers enriched with TH-free
 401 Algamac (Aquafauna), and bloodworms. Fish stocks used were: wild-type AB^{wp} or its derivative
 402 WT(ABb) (Eom et al., 2015); *Tg(tg:nVenus-v2a-nfnB)*^{wp.rt8}, *Tg(aox5:palmEGFP)*^{wp.rt22},
 403 *Tg(tyrp1b:palm-mCherry)*^{wp.rt11} (McMenamin et al., 2014); *csf1ra*^{4blue} (Parichy et al., 1999); *Tg(-*
 404 *28.5Sox10:Cre)*^{zf384} (Kague et al., 2012); *Tg(-3.5ubi:loxP-EGFP-loxP-mCherry)*^{cz1701} (Mosimann et
 405 al., 2011); *tuba8l3:nEosFP*^{vp.rt17}, *thrab*^{vp31rc1}, *thraa*^{vp33rc1}, *thrb*^{vp34rc1}, *scarb1*^{vp32rc1} and *tyr*^{vp35rc1} (this
 406 study). Mutants and transgenic lines were maintained in the WT(ABb) genetic background. Fish
 407 were anesthetized prior to imaging with MS222 and euthanized by overdose of MS222. All

procedures involving live animals followed federal, state and local guidelines for humane treatment and protocols approved by Institutional Animal Care and Use Committees of University of Virginia and University of Washington.

Nitroreductase-mediated cell ablation

To ablate thyroid follicles of *Tg(tg:nVenus-2a-nfnB)*, we incubated 4 day post-fertilization (dpf) larvae for 8 h in 10 mM Mtz with 1% DMSO in E3 media, with control larvae incubated in 1% DMSO in E3 media. For all thyroid ablations, treated individuals were assessed for loss of nuclear-localizing Venus (nVenus) the following day. Ablated thyroid glands fail to regenerate (McMenamin et al., 2014) and absence of regeneration in this study was confirmed by continued absence of nVenus expression.

Mutant and transgenic line production

For CRISPR/Cas9 mutagenesis, 1-cell stage embryos were injected with 200 ng/ μ l sgRNAs and 500 ng/ μ l Cas9 protein (PNA Bio) using standard procedures (Shah et al., 2015). Guides were tested for mutagenicity by Sanger sequencing and injected fish were reared through adult stages at which time they were crossed to *Tg(tg:nVenus-v2a-nfnB)* to generate heterozygous F1s from which single allele strains were recovered. CRISPR gRNA targets (excluding protospacer adjacent motif) are included in **Supplementary File 2—Table 7**. Mutant alleles of *scarb1* and TR loci are provided in **Figure 6—figure supplement 3** and **Figure 7—figure supplement 1**, respectively. The melanin free *tyr^{vp,r34c1}* allele generated for analyses of melanophore lysosomal content exhibits a 4 nucleotide deletion beginning at position 212 that leads to novel amino acids and a premature stop codon (H71QEWTIESDGL*).

For F0 *thrb* mutagenesis analysis in the *thraa; thrb* mutant background, chemically synthesized Alt-R® CRISPR-Cas9 sgRNAs targeting the *thrb* site and Cas9 protein (Alt-R® S.p. Cas9 nuclease, v.3) were obtained from Integrated DNA Technologies (IDT). RNPs were prepared as recommended and ~1 nl was injected into the cytoplasm of one-cell stage embryos.

To label nuclei of adult melanophores, BAC CH73-199E17 containing the *puma* gene *tuba8l3* (Larson et al., 2010) was recombineered to contain nuclear-localizing photoconvertible fluorophore EosFP using standard methods (Sharan et al., 2009; Suster et al., 2011).

Imaging

Images were acquired on: Zeiss AxioObserver inverted microscopes equipped with Axiocam HR or Axiocam 506 color cameras; a Zeiss AxioObserver inverted microscope equipped with CSU-X1 laser spinning disk (Yokogawa) and Orca Flash 4.0 camera (Hamamatsu Photonics); or a Zeiss LSM 880 scanning laser confocal microscope with Fast Airyscan and GaAsP detectors. Images were corrected for color balance and adjusted for display levels as necessary with conditions within analyses treated identically.

Cell counts

Melanophores and xanthophores were counted within regions defined dorsally and ventrally by the margins of the primary stripes, anteriorly by the anterior margin of the dorsal fin, and posteriorly by five myotomes from the start. Only hypodermal melanophores were included in analysis; dorsal melanophores and those in scales were excluded. Mature xanthophores were counted by the presence of autofluorescent carotenoid with associated yellow pigment. Cell counts were made using ImageJ. Individual genotypes of fish assessed were confirmed using PCR or Sanger sequencing.

In situ hybridization

In situ hybridization (ISH) probes and tissue were prepared as described (Quigley et al., 2004). Probes were hybridized for 24 hr at 66°C. Post-hybridization washes were performed using a

459 BioLane HTI 16Vx (Intavis Bioanalytical Instruments), with the following parameters: 2x SSCT 3 × 5
460 min, 11 × 10 min at 66°C; 0.2x SSCT 10 × 10 min; blocking solution [5% normal goat serum
461 (Invitrogen), 2 mg/mL BSA (RPI) in PBST] for 24 hr at 4 °C; anti-Dig-AP, Fab fragments (1:5000 in
462 blocking solution, Millipore-Sigma) for 24 hr at 4 °C; PBST 59 × 20 min. AP staining was performed
463 as described (Quigley et al., 2004).

464

465 **Pigment analyses**

466 Xanthophore pigments were examined by imaging autofluorescence in eGFP and DAPI spectral
467 ranges for carotenoids and pteridines respectively. For imaging pteridines, fish were euthanized and
468 treated with dilute ammonia to induce autofluorescence (Odenthal et al., 1996).

469 For analyses of carotenoid contents by HPLC we pooled three skin samples from each genotype
470 and condition (Mtz-treated or control) into two separate samples. We homogenized the tissue in a
471 glass dounce homogenizer with 1 ml of 0.9% sodium chloride and quantified the protein content of
472 each sample with a bicinchoninic acid (BCA) assay (23250, Thermo). We then extracted carotenoids
473 by combining the homogenates with 1 ml methanol, 2 ml distilled water, and 2 ml of hexane:*tert*-
474 methyl butyl ether (1:1 vol:vol), separated the fractions by centrifuging, collected the upper solvent
475 fraction, and dried it under a stream of nitrogen. We saponified these extracts with 0.2 M NaOH in
476 methanol at room temperature for four hours following the protocol described in (Toomey and
477 McGraw, 2007). We extracted the saponified carotenoids from this solution with 2 ml of hexane:*tert*-
478 methyl butyl ether (1:1 vol:vol) and dried the solvent fraction under a stream of nitrogen. We
479 resuspended the saponified extracts in 120 µl of methanol:acetonitrile 1:1 (vol:vol) and injected 100
480 µl of this suspension into an Agilent 1100 series HPLC fitted with a YMC carotenoid 5.0 µm column
481 (4.6 mm × 250 mm, YMC). We separated the pigments with a gradient mobile phase of
482 acetonitrile:methanol:dichloromethane (44:44:12) (vol:vol:vol) through 11 minutes, a ramp up to
483 acetonitrile:methanol:dichloromethane (35:35:30) for 11-21 minutes and isocratic conditions through
484 35 minutes. The column was warmed to 30°C, and mobile phase was pumped at a rate of 1.2 ml
485 min⁻¹ throughout the run. We monitored the samples with a photodiode array detector at 400, 445,
486 and 480 nm, and carotenoids were identified and quantified by comparison to authentic standards (a
487 gift of DSM Nutritional Products, Heerlen, The Netherlands). Analyses of 5 dpf wild-type and *csf1ra*
488 mutants used only larval heads where xanthophores are abundant in the wild type; other procedures
489 were the same as for later stages.

490

491 **Immunohistochemistry and Oil-red-O staining**

492 Skins of *Tg(aox5:palmEGFP)* euthyroid and hypothyroid zebrafish (8.6–10.4 SSL) were dissociated
493 and plated at low density in L-15 medium (serum free) on collagen-coated, glass bottom dishes
494 (Mattek) for 5 h. Cells were then fixed with freshly prepared 4% PFA for 15 m, rinsed with PBST
495 (0.1%), blocked (5% goat serum, 1% BSA, 1X PBS), then incubated at 4°C overnight with rabbit anti-
496 GFP primary antibody (ThermoFisher). Stained cells were rinsed 3X with 1X PBS and fixed again
497 with 4% PFA for 30 minutes. Cells were then rinsed twice with ddH₂O, washed with 60%
498 isopropanol for 5 min, and then dried completely. Cells were incubated with filtered, Oil Red O
499 solution (5 mM in 60% isopropanol) for 10 min, and rinsed 4X with ddH₂O before imaging (Koopman
500 et al., 2001). All GFP+ cells were imaged across two plates per condition and were scored for
501 presence or absence of red staining.

502

503 **Melanophore maturation assays**

504 For assaying senescence of melanophores *ex vivo*, skins from euthyroid and hypothyroid fish (*n*=3
505 each, 11 SSL) were cleared of scales, dissociated and plated on glass-bottom, collagen coated
506 dishes (MatTek) in L-15 medium (Gibco) and incubated overnight at 28°C. Cells were then rinsed
507 with dPBS, fixed with 4% PFA and stained using a Senescence β-Galactosidase Staining Kit (Cell
508 Signaling Technologies, cat. #9860) according to manufacturer's instructions (Ceol et al., 2011;
509 Dimri et al., 1995). Staining was carried out for 48 h at pH 6 prior to imaging.

To assay cell state as measured by lysosomal content (Kurz et al., 2000; Lee et al., 2006) of melanophores by FACS, skins from euthyroid and hypothyroid *Tg(tyrp1b:palm-mCherry;tuba8l3:nEOS)*, *tyr* fish lacking melanin ($n=12$ each) were dissociated and resuspended 1% BSA / 5% FBS / dPBS. Cells were incubated for 1 h with Lysotracker (75 nM) (ThermoFisher, L12492) and Vybrant DyeCycle Violet stain (5 μ M) (ThermoFisher, V35003) shaking at 500 rpm, 28°C. Without washing, cells were FAC sorted. Single transgene controls and wild type cells were used to adjust voltage and gating. Prior to analysis of fluorescence levels, single cells were isolated by sequentially gating cells according to their SSC-A vs. FSC-A, FSC-H vs FSC-W and SSC-H vs SSC-W profiles according to standard flow cytometry practices. Intact live cells were then isolated by excluding cells with low levels of DyeCycle violet staining (DAPI-A). As expected these cells express a wide range of our *tuba8l3:nlsEosFP* transgene as determined by levels of green fluorescence (FITC-A). Melanophores were isolated by identifying cells with high fluorescence in the FITC-A and mCherry-A channels which describe expression of the *tuba8l3:nlsEosFP* and *tyrp1b:palm-mCherry* transgenes. Lastly, lysosomal content of melanophores was determined by the median fluorescence intensity of the lysosomal marker, Lysotracker Deep Red (APC-A). The data were collected on a FACS ARIA using FACSDiva version 8 software (BD Biosciences) and analyzed using FlowJo v10.

Melanin content was measured from brightfield images in Fiji. All image quantifications were performed using the base processing and analysis functions in ImageJ. Images were aligned and centered on the horizontal myoseptum and cropped to 2500 x 1500 pixels around dorsal and ventral stripes. Images were segmented based on red channel intensity using “Auto Local Threshold” with parameters “method=Sauvola radius=50”. To account for close or overlapping melanophores, particles were further segmented using watershed segmentation. Particles larger than 25 pixels and not touching an edge were used for subsequent analyses.

Transmission electron microscopy

Fish were euthanized then fixed in sodium cacodylate buffered 4% glutaraldehyde overnight at 4°C. Trunk regions were dissected then tissue stained in 2% osmium tetroxide for 30 minutes, washed, and then stained in 1% uranyl acetate overnight at 4°C. Samples were dehydrated with a graded ethanol series then infiltrated with a 1:1 propylene oxide:Durcupan resin for 2 hours followed by fresh Durcupan resin overnight and flat embedded prior to polymerization. Blocks were thin sectioned on a Leica EM UC7 and sections imaged on a JEOL 1230 transmission electron microscope.

Tissue dissociations and FACS

Trunks or skins of staged, post-embryonic zebrafish (7.2–11.0 SSL) were dissected ($n=8$ per replicate) and enzymatically dissociated with Liberase (Sigma-Aldrich cat. 5401119001, 0.25 mg/mL in dPBS) at 25°C for 15 min followed by manual trituration with a flame polished glass pipette for 5 min. Cell suspensions were then filtered through a 70 μ m Nylon cell strainer to obtain a single cell suspension. Liberated cells were re-suspended in 1% BSA / 5% FBS in dPBS and DAPI (0.1 μ g/mL, 15 min) before FACS purification. All plastic and glass surfaces of cell contact were coated with 1% BSA in dPBS before to use. Prior to sorting for fluorescence levels, single cells were isolated by sequentially gating cells according to their SSC-A vs. FSC-A, FSC-H vs FSC-W and SSC-H vs SSC-W profiles according to standard flow cytometry practices. Cells with high levels of DAPI staining were excluded as dead or damaged. Cells from wild-type and *Tg(ubi:switch)* zebrafish without Cre were used as negative control to determine gates for detection of mCherry and GFP fluorescence, then cells from *Tg(sox10:Cre; ubi:switch)* zebrafish were purified according to these gates. NC-derived cells were isolated by identifying cells with high fluorescence in the mCherry-A channel which describes expression of the *ubi:loxP-EGFP-loxP-mCherry* transgene after permanent conversion to *ubi:mCherry* after exposure to Sox10:Cre (see **Figure 2—figure supplement 1C**). All samples were kept on ice except during Liberase incubation, and sorted chilled.

RT-PCR

561 Skin tissue from stage-matched fish was dissociated as above and melanophores and xanthophores
562 were FAC sorted for the presence *aox5:palmeGFP* or *tyrp1b:palm-mCherry*, respectively. RNA was
563 extracted from pools of 1000 cells using the RNAqueous-Micro kit (Thermo Fisher, cat. AM1912).
564 Full length cDNA was synthesized with Superscript III reverse transcriptase (Thermo Fisher, cat.
565 #18080093). Amplifications were 40 cycles with Q5 DNA polymerase (NEB, M0492), 38 cycles at
566 94°C, 30 s; 67°C, 20 s; 72°C, 20 s. For primer sequences (*actb1*, *thraa*, *thrab*, *thrb*), see
567 **Supplementary File 2—Table 7.**

568

569 **Single cell collection, library construction and sequencing**

570 Whole-trunks or skins were collected from stage-matched *Tg(tg:nVenus-2a-nfnB)* euthyroid and
571 hypothyroid siblings, dissociated, and *sox10:Cre:mCherry+* cells isolated by FACS.
572 We replicated the experiment three times. For each replicate, we collected cells from euthyroid and
573 hypothyroid fish at 7.2 SSL, 8.6 SSL, and 9.6 SSL (mid-larval, 6–10 fish per stage, per replicate) and
574 sorted equal numbers of mCherry+ cells from each group into a single sample. Cells were pelleted
575 and resuspended in 0.04% ultrapure BSA (ThermoFisher Scientific). Representing a terminal stage
576 of pigment pattern development, we also collected mCherry+ cells from one sample within each
577 replicate of 11 SSL (juvenile, 5 fish per condition) euthyroid and hypothyroid fish. To capture cells
578 representing the EL pigment pattern, we collected mCherry+ cells from 5 dpf larvae (50 fish). In each
579 experiment, we ran parallel euthyroid and hypothyroid samples (fish were siblings). For each
580 sample, we targeted 2000–4000 cells for capture using the Chromium platform (10X Genomics) with
581 one lane per sample. Single-cell mRNA libraries were prepared using the single-cell 3' solution V2 kit
582 (10X Genomics). Quality control and quantification assays were performed using a Qubit fluorometer
583 (Thermo Fisher) and a D1000 ScreenTape Assay (Agilent). Libraries were sequenced on an Illumina
584 NextSeq 500 using 75-cycle, high output kits (read 1: 26 cycles, i7 Index: 8 cycles, read 2: 57
585 cycles). Each sample was sequenced to an average depth of 150 million total reads. This resulted in
586 an average read depth of ~40,000 reads/cell after read-depth normalization.

587

588 **scRNA-Seq data processing**

589 We found that for many genes, annotated 3' UTRs in the Ensembl 93 zebrafish reference
590 transcriptome were shorter than true UTR lengths observed empirically in pileups of reads mapped
591 to the genome. This led to genic reads being counted as intergenic. To correct for this bias in
592 aligning reads to the transcriptome, we extended all 3' UTR annotations by 500 bp. In rare cases,
593 UTR extension resulted in overlap with a neighboring gene and in these instances we manually
594 truncated the extension to avoid such overlap. We built a custom zebrafish STAR genome index
595 using gene annotations from Ensembl GRCz11 with extended 3' UTRs plus manually annotated
596 entries for mCherry transcript, filtered for protein-coding genes (with Cell Ranger *mkgtf* and *mkref*
597 options). Final cellular barcodes and UMIs were determined using Cell Ranger 2.0.2 (10X
598 Genomics) and cells were filtered to include only high-quality cells. Cell Ranger defaults for selecting
599 cell-associated barcodes versus barcodes associated with empty partitions were used. All samples
600 were aggregated (using 10X Cell Ranger pipeline “cellranger aggr” option), with intermediary depth
601 normalization to generate a gene-barcode matrix containing ~25,000 barcoded cells and gene
602 expression counts.

603

604 **UMAP visualization and clustering**

605 We used Uniform Manifold Approximation and Projection (UMAP) (McInnes et al., 2018) to project
606 cells in two or three dimensions and performed louvain clustering (Blondel et al., 2008) using the
607 *reduceDimension* and *clusterCells* functions in Monocle (v.2.99.1) using default parameters (except
608 for, *reduceDimension*: *reduction_method*=UMAP, *metric*=cosine, *n_neighbors*=30, *mid_dist*=0.5;
609 *clusterCells*: *res*=1e-3, *k*=15). We assigned clusters to cell types based on the detection of published
610 marker genes. Cells isolated from euthyroid and hypothyroid fish were combined to maintain
611 consistency of analysis and for comparisons between groups. Batch correction methods were not

used between the two groups or across samples because we did not observe sample-specific separation or clustering in UMAP space. Cells with more than 15,000 UMIs were discarded as possible doublets. All genes were given as input to Principal Components Analysis (PCA). The top 30 principal components (high-loading, based on the associated scree plot) were then used as input to UMAP for generating either 2D or 3D projections of the data. For, subclustering of pigment cell clusters (melanophores, iridophores, xanthophores, and pigment progenitors) we subsetted the data set and again applied UMAP dimensionality reduction and louvain clustering.

Differential expression analysis to determine cell-type markers

To identify genes expressed cell-type specifically, we used the principalGraphTest function in Monocle3 (v.2.99.1) with default parameters (Cao et al., 2019). This function uses a spatial correlation analysis, the Moran's I test, to assess spatially restricted gene expression patterns in low dimensional space. We selected markers by optimizing for high specificity, expression levels and effect sizes within clusters (For extended list of cell-type specific genes, see **Supplementary File 2—Table 1**).

Trajectory analysis

The top 800 highly dispersed genes (**Supplementary File 2—Table 5**) within euthyroid pigment cells (melanophores, xanthophores, iridophores, and pigment progenitors) were chosen as feature genes to resolve pseudotemporal trajectories using the setOrderingFilter, reduceDimension, and orderCells functions in Monocle (v2.9.0) using default parameters with the exception of setting max_components = 3 and num_dim = 10 to generate the trajectory in 3D with the top 10 PCs (high-loading based on scree plot) during dimensionality reduction.

Branched Expression Analysis Modeling (BEAM)

After running trajectory analysis on pigment cells, we used the BEAM function in Monocle (v.2.9.0) with default settings (except, branch_point = 3) to determine differentially expressed genes between trajectory branches. To generate the BEAM heatmap for the three pigment cell trajectory branches, we used the plot_multiple_branches_heatmap function with default settings (except assigning branch 1, 5, and 6 to iridophores, melanophores, and xanthophores, respectively; and num_clusters = 6). Genes were selected by significance levels for the three-branch BEAM analysis with additional significant genes added from the melanophore and iridophore two-branch analysis for more even distribution of genes across lineages ($q < 6.0E-11$ for all genes, except for *pax3a* (starred, $q=0.03$) which is a positive indicator of early pseudotime for all lineages).

Differential expression analysis across pseudotime

To determine differentially expressed genes over pseudotime that were TH-dependent, we filtered the data set for genes expressed in at least 5 cells and performed differential expression analysis using a full model of sm.ns(Pseudotime, df=3)*condition and a reduced model of sm.ns(Pseudotime, df=3).

Development and analysis of pathway signature scores

Gene sets for signature scores were selected using gene ontology (terms and gene sets from zfin.org; cell-cycle, unfolded protein response, AP-1 transcription factor complex members) or manual curation based on literature when required (carotenoid, pteridine, melanin) (see **Supplementary File 2—Table 4**). Signature scores were calculated by generating z-scores (using scale()) of the mean of expression values (log transformed, size factor normalized) from genes in a given set.

Statistics

662 Parametric, non-parametric and multiple logistic regression analyses were performed using JMP
663 14.0 (SAS Institute, Cary, NC) or *R* [version 3.5.0] (R Core Team, 2017). For parametric analyses,
664 residuals were assessed for normality and homoscedasticity to meet model assumptions and no
665 transformations were found to be warranted.

666
667 **Data availability**
668 Data is available on GEO via accession GSE131136.
669

670 **Code availability**
671 Monocle is available through GitHub (<https://github.com/cole-trapnell-lab/monocle-release.git>).
672
673
674
675

- 676 **Acknowledgments**
677 For assistance we thank D. Jackson, D. Huang, E. Bain, B. McCluskey, D.S. Eom, D. Raible, A.
678 Fulbright, A. Leith, A. Schwindling, T. Linbo, D. White, and E. Parker. **Funding:** Supported by NIH
679 R35 GM122471 (DMP); NIH T32 GM007067 (LMS); NIH P30 EY001730 (Core Grant for Vision
680 Research); NIH DP2 HD088158 (CT); Paul G. Allen Frontiers Group - Allen Discovery Center grant
681 (CT); W.M. Keck Foundation Grant (CT); Alfred P. Sloan Foundation Research Fellowship (CT); NIH
682 EY024958, EY025196, and EY026672 (JCC).
- 683
684 **Competing interests**
685 Authors declare no competing interests.
686

687 **References**

- 688 Adameyko I, Lallemand F, Aquino JB, Pereira JA, Topilko P, Müller T, Fritz N, Beljajeva A, Mochii M, Liste I,
689 Usoskin D, Suter U, Birchmeier C, Ernfors P. 2009. Schwann cell precursors from nerve innervation are a
690 cellular origin of melanocytes in skin. *Cell* **139**:366–379.
- 691 Arduini BL, Bosse KM, Henion PD. 2009. Genetic ablation of neural crest cell diversification. *Development*
692 **136**:1987–1994.
- 693 Atchley WR, Hall BK. 1991. A model for development and evolution of complex morphological structures. *Biol
694 Rev Camb Philos Soc* **66**:101–157.
- 695 Bagnara JT, Matsumoto J. 2006. Comparative Anatomy and Physiology of Pigment Cells in Nonmammalian
696 Tissues In: Nordlund JJ, Boissy RE, Hearing VJ, King RA, Oetting WS, Ortonne J-P, editors. *The
697 Pigmentary System*. Oxford, UK: Blackwell Publishing Ltd. pp. 11–59.
- 698 Bagnara JT, Taylor JD, Hadley ME. 1968. The dermal chromatophore unit. *J Cell Biol* **38**:67–79.
- 699 Barrallo-Gimeno A, Holzschuh J, Driever W, Knapik EW. 2004. Neural crest survival and differentiation in
700 zebrafish depends on mont blanc/tfap2a gene function. *Development* **131**:1463–1477.
- 701 Baxter LL, Watkins-Chow DE, Pavan WJ, Loftus SK. 2018. A curated gene list for expanding the horizons of
702 pigmentation biology. *Pigment Cell Melanoma Res*. doi:10.1111/pcmr.12743
- 703 Becht E, McInnes L, Healy J, Dutertre C-A, Kwok IWH, Ng LG, Ginhoux F, Newell EW. 2018. Dimensionality
704 reduction for visualizing single-cell data using UMAP. *Nat Biotechnol*. doi:10.1038/nbt.4314
- 705 Beirl AJ, Linbo TH, Cobb MJ, Cooper CD. 2014. oca2 Regulation of chromatophore differentiation and number
706 is cell type specific in zebrafish. *Pigment Cell Melanoma Res* **27**:178–189.
- 707 Blondel VD, Guillaume J-L, Lambiotte R, Lefebvre E. 2008. Fast unfolding of communities in large networks.
708 *arXiv [physics.soc-ph]*.
- 709 Braasch I, Brunet F, Wolff J-N, Schartl M. 2009. Pigmentation pathway evolution after whole-genome
710 duplication in fish. *Genome Biol Evol* **1**:479–493.
- 711 Braasch I, Peterson SM, Desvignes T, McCluskey BM, Batzel P, Postlethwait JH. 2015. A new model army:
712 Emerging fish models to study the genomics of vertebrate Evo-Devo. *J Exp Zool B Mol Dev Evol* **324**:316–
713 341.
- 714 Brent GA. 2012. Mechanisms of thyroid hormone action. *J Clin Invest* **122**:3035–3043.
- 715 Brown DD, Cai L. 2007. Amphibian metamorphosis. *Dev Biol* **306**:20–33.
- 716 Buchholz DR, Hsia S-CV, Fu L, Shi Y-B. 2003. A dominant-negative thyroid hormone receptor blocks
717 amphibian metamorphosis by retaining corepressors at target genes. *Mol Cell Biol* **23**:6750–6758.
- 718 Budi EH, Patterson LB, Parichy DM. 2011. Post-embryonic nerve-associated precursors to adult pigment cells:
719 genetic requirements and dynamics of morphogenesis and differentiation. *PLoS Genet* **7**:e1002044.
- 720 Budi EH, Patterson LB, Parichy DM. 2008. Embryonic requirements for ErbB signaling in neural crest
721 development and adult pigment pattern formation. *Development* **135**:2603–2614.
- 722 Camargo-Sosa K, Colanesi S, Müller J, Schulte-Merker S, Stemple D, Patton EE, Kelsh RN. 2019. Endothelin
723 receptor Aa regulates proliferation and differentiation of Erb-dependent pigment progenitors in zebrafish.
724 *PLoS Genet* **15**:e1007941.
- 725 Cao J, Spielmann M, Qiu X, Huang X, Ibrahim DM, Hill AJ, Zhang F, Mundlos S, Christiansen L, Steemers FJ,
726 Trapnell C, Shendure J. 2019. The single-cell transcriptional landscape of mammalian organogenesis.
727 *Nature* **566**:496–502.
- 728 Ceol CJ, Houvras Y, Jane-Valbuena J, Bilodeau S, Orlando DA, Battisti V, Fritsch L, Lin WM, Hollmann TJ,
729 Ferré F, Bourque C, Burke CJ, Turner L, Uong A, Johnson LA, Beroukhim R, Mermel CH, Loda M, Ait-Si-
730 Ali S, Garraway LA, Young RA, Zon LI. 2011. The histone methyltransferase SETDB1 is recurrently
731 amplified in melanoma and accelerates its onset. *Nature* **471**:513–517.
- 732 Chang J, Wang M, Gui W, Zhao Y, Yu L, Zhu G. 2012. Changes in thyroid hormone levels during zebrafish
733 development. *Zoolog Sci* **29**:181–184.
- 734 Chinenov Y, Kerppola TK. 2001. Close encounters of many kinds: Fos-Jun interactions that mediate
735 transcription regulatory specificity. *Oncogene* **20**:2438–2452.
- 736 Choi J, Suzuki K-IT, Sakuma T, Shewade L, Yamamoto T, Buchholz DR. 2015. Unliganded thyroid hormone
737 receptor α regulates developmental timing via gene repression in *Xenopus tropicalis*. *Endocrinology*
738 **156**:735–744.
- 739 Coller HA, Sang L, Roberts JM. 2006. A new description of cellular quiescence. *PLoS Biol* **4**:e83.
- 740 Curran K, Lister JA, Kunkel GR, Prendergast A, Parichy DM, Raible DW. 2010. Interplay between Foxd3 and
741 Mitf regulates cell fate plasticity in the zebrafish neural crest. *Dev Biol* **344**:107–118.

- 742 D'Agati G, Beltre R, Sessa A, Burger A, Zhou Y, Mosimann C, White RM. 2017. A defect in the mitochondrial
743 protein Mpv17 underlies the transparent casper zebrafish. *Dev Biol* **430**:11–17.
- 744 Darzynkiewicz Z, Traganos F, Melamed MR. 1980. New cell cycle compartments identified by multiparameter
745 flow cytometry. *Cytometry* **1**:98–108.
- 746 Dimri GP, Lee X, Basile G, Acosta M, Scott G, Roskelley C, Medrano EE, Linskens M, Rubelj I, Pereira-Smith
747 O. 1995. A biomarker that identifies senescent human cells in culture and in aging skin in vivo. *Proc Natl
748 Acad Sci U S A* **92**:9363–9367.
- 749 Djurdjević I, Kreft ME, Sušnik Bajec S. 2015. Comparison of pigment cell ultrastructure and organisation in the
750 dermis of marble trout and brown trout, and first description of erythrophore ultrastructure in salmonids. *J
751 Anat* **227**:583–595.
- 752 Dooley CM, Mongera A, Walderich B, Nüsslein-Volhard C. 2013a. On the embryonic origin of adult
753 melanophores: the role of ErbB and Kit signalling in establishing melanophore stem cells in zebrafish.
754 *Development* **140**:1003–1013.
- 755 Dooley CM, Schwarz H, Mueller KP, Mongera A, Konantz M, Neuhauss SCF, Nüsslein-Volhard C, Geisler R.
756 2013b. Slc45a2 and V-ATPase are regulators of melanosomal pH homeostasis in zebrafish, providing a
757 mechanism for human pigment evolution and disease. *Pigment Cell Melanoma Res* **26**:205–217.
- 758 Dutton KA, Pauliny A, Lopes SS, Elworthy S, Carney TJ, Rauch J, Geisler R, Haffter P, Kelsh RN. 2001.
759 Zebrafish colourless encodes sox10 and specifies non-ectomesenchymal neural crest fates. *Development*
760 **128**:4113–4125.
- 761 Ebisuya M, Briscoe J. 2018. What does time mean in development? *Development* **145**.
762 doi:10.1242/dev.164368
- 763 Ellerhorst JA, Cooksley CD, Broemeling L, Johnson MM, Grimm EA. 2003. High prevalence of hypothyroidism
764 among patients with cutaneous melanoma. *Oncol Rep* **10**:1317–1320.
- 765 Eom DS, Bain EJ, Patterson LB, Grout ME, Parichy DM. 2015. Long-distance communication by specialized
766 cellular projections during pigment pattern development and evolution. *eLife* **4**. doi:10.7554/eLife.12401
- 767 Eom DS, Inoue S, Patterson LB, Gordon TN, Slingwine R, Kondo S, Watanabe M, Parichy DM. 2012.
768 Melanophore migration and survival during zebrafish adult pigment stripe development require the
769 immunoglobulin superfamily adhesion molecule Igf11. *PLoS Genet* **8**:e1002899.
- 770 Eskova A, Chauvigné F, Maischein H-M, Ammelburg M, Cerdà J, Nüsslein-Volhard C, Irion U. 2017. Gain-of-
771 function mutations in Aqp3a influence zebrafish pigment pattern formation through the tissue environment.
772 *Development* **144**:2059–2069.
- 773 Fadeev A, Krauss J, Frohnhofer HG, Irion U, Nüsslein-Volhard C. 2015. Tight Junction Protein 1a regulates
774 pigment cell organisation during zebrafish colour patterning. *eLife* **4**. doi:10.7554/eLife.06545
- 775 Flament F, Poguet A-L, Plateroti M, Chassande O, Gauthier K, Streichenberger N, Mansouri A, Samarut J.
776 2002. Congenital Hypothyroid Pax8–/– Mutant Mice Can Be Rescued by Inactivating the TRα Gene. *Mol
777 Endocrinol* **16**:24–32.
- 778 Flament F, Samarut J. 2003. Thyroid hormone receptors: lessons from knockout and knock-in mutant mice.
779 *Trends Endocrinol Metab* **14**:85–90.
- 780 Frohnhofer HG, Krauss J, Maischein H-M, Nüsslein-Volhard C. 2013. Iridophores and their interactions with
781 other chromatophores are required for stripe formation in zebrafish. *Development* **140**:2997–3007.
- 782 Gans C, Northcutt RG. 1983. Neural crest and the origin of vertebrates: a new head. *Science* **220**:268–273.
- 783 Granneman JG, Kimler VA, Zhang H, Ye X, Luo X, Postlethwait JH, Thummel R. 2017. Lipid droplet biology
784 and evolution illuminated by the characterization of a novel perilipin in teleost fish. *eLife* **6**.
785 doi:10.7554/eLife.21771
- 786 Hamada H, Watanabe M, Lau HE, Nishida T, Hasegawa T, Parichy DM, Kondo S. 2014. Involvement of
787 Delta/Notch signaling in zebrafish adult pigment stripe patterning. *Development* **141**:318–324.
- 788 Higdon CW, Mitra RD, Johnson SL. 2013. Gene expression analysis of zebrafish melanocytes, iridophores,
789 and retinal pigmented epithelium reveals indicators of biological function and developmental origin. *PLoS
790 One* **8**:e67801.
- 791 Hirata M, Nakamura K-I, Kanemaru T, Shibata Y, Kondo S. 2003. Pigment cell organization in the hypodermis
792 of zebrafish. *Dev Dyn* **227**:497–503.
- 793 Hörlein AJ, Näär AM, Heinzel T, Torchia J, Gloss B, Kurokawa R, Ryan A, Kamei Y, Söderström M, Glass CK.
794 1995. Ligand-independent repression by the thyroid hormone receptor mediated by a nuclear receptor co-
795 repressor. *Nature* **377**:397–404.
- 796 Hultman KA, Bahary N, Zon LI, Johnson SL. 2007. Gene Duplication of the zebrafish kit ligand and partitioning
797 of melanocyte development functions to kit ligand a. *PLoS Genet* **3**:e17.

- 798 Ilicic T, Kim JK, Kolodziejczyk AA, Bagger FO, McCarthy DJ, Marioni JC, Teichmann SA. 2016. Classification
799 of low quality cells from single-cell RNA-seq data. *Genome Biol* **17**:29.
- 800 Inoue S, Kondo S, Parichy DM, Watanabe M. 2014. Tetraspanin 3c requirement for pigment cell interactions
801 and boundary formation in zebrafish adult pigment stripes. *Pigment Cell Melanoma Res* **27**:190–200.
- 802 Irion U, Frohnhofer HG, Krauss J, Colak Champollion T, Maischein H-M, Geiger-Rudolph S, Weiler C,
803 Nüsslein-Volhard C. 2014. Gap junctions composed of connexins 41.8 and 39.4 are essential for colour
804 pattern formation in zebrafish. *Elife* **3**:e05125.
- 805 Irion U, Singh AP, Nüsslein-Volhard C. 2016. The Developmental Genetics of Vertebrate Color Pattern
806 Formation: Lessons from Zebrafish. *Curr Top Dev Biol* **117**:141–169.
- 807 Iwashita M, Watanabe M, Ishii M, Chen T, Johnson SL, Kurachi Y, Okada N, Kondo S. 2006. Pigment pattern
808 in jaguar/obelix zebrafish is caused by a Kir7.1 mutation: implications for the regulation of melanosome
809 movement. *PLoS Genet* **2**:e197.
- 810 Johnson SL, Africa D, Walker C, Weston JA. 1995. Genetic control of adult pigment stripe development in
811 zebrafish. *Dev Biol* **167**:27–33.
- 812 Kague E, Gallagher M, Burke S, Parsons M, Franz-Odendaal T, Fisher S. 2012. Skeletogenic fate of zebrafish
813 cranial and trunk neural crest. *PLoS One* **7**:e47394.
- 814 Kaufman CK, Mosimann C, Fan ZP, Yang S, Thomas AJ, Ablain J, Tan JL, Fogley RD, van Rooijen E,
815 Hagedorn EJ, Ciarlo C, White RM, Matos DA, Puller A-C, Santoriello C, Liao EC, Young RA, Zon LI. 2016.
816 A zebrafish melanoma model reveals emergence of neural crest identity during melanoma initiation.
817 *Science* **351**:aad2197.
- 818 Kelsh RN, Dutton K, Medlin J, Eisen JS. 2000a. Expression of zebrafish fkd6 in neural crest-derived glia. *Mech
819 Dev* **93**:161–164.
- 820 Kelsh RN, Schmid B, Eisen JS. 2000b. Genetic analysis of melanophore development in zebrafish embryos.
821 *Dev Biol* **225**:277–293.
- 822 Kelsh RN, Sosa KC, Owen JP, Yates CA. 2017. Zebrafish adult pigment stem cells are multipotent and form
823 pigment cells by a progressive fate restriction process: Clonal analysis identifies shared origin of all
824 pigment cell types. *Bioessays* **39**. doi:10.1002/bies.201600234
- 825 Kiefer C, Sumser E, Wernet MF, Von Lintig J. 2002. A class B scavenger receptor mediates the cellular uptake
826 of carotenoids in Drosophila. *Proc Natl Acad Sci U S A* **99**:10581–10586.
- 827 Knight RD, Nair S, Nelson SS, Afshar A, Javidan Y, Geisler R, Rauch G-J, Schilling TF. 2003. lockjaw encodes
828 a zebrafish tfap2a required for early neural crest development. *Development* **130**:5755–5768.
- 829 Koopman R, Schaart G, Hesselink MK. 2001. Optimisation of oil red O staining permits combination with
830 immunofluorescence and automated quantification of lipids. *Histochem Cell Biol* **116**:63–68.
- 831 Krauss J, Astrinidis P, Frohnhofer HG, Walderich B, Nüsslein-Volhard C. 2013. transparent, a gene affecting
832 stripe formation in Zebrafish, encodes the mitochondrial protein Mpv17 that is required for iridophore
833 survival. *Biol Open* **2**:703–710.
- 834 Kurz DJ, Decary S, Hong Y, Erusalimsky JD. 2000. Senescence-associated (beta)-galactosidase reflects an
835 increase in lysosomal mass during replicative ageing of human endothelial cells. *J Cell Sci* **113** (Pt
836 20):3613–3622.
- 837 Lang MR, Patterson LB, Gordon TN, Johnson SL, Parichy DM. 2009. Basonuclin-2 requirements for zebrafish
838 adult pigment pattern development and female fertility. *PLoS Genet* **5**:e1000744.
- 839 Larson TA, Gordon TN, Lau HE, Parichy DM. 2010. Defective adult oligodendrocyte and Schwann cell
840 development, pigment pattern, and craniofacial morphology in puma mutant zebrafish having an alpha
841 tubulin mutation. *Dev Biol* **346**:296–309.
- 842 Lee BY, Han JA, Im JS, Morrone A, Johung K, Goodwin EC, Kleijer WJ, DiMaio D, Hwang ES. 2006.
843 Senescence-associated beta-galactosidase is lysosomal beta-galactosidase. *Aging Cell* **5**:187–195.
- 844 Leikam C, Hufnagel AL, Otto C, Murphy DJ, Mühlung B, Kneitz S, Nanda I, Schmid M, Wagner TU, Haferkamp
845 S, Bröcker E-B, Schartl M, Meierjohann S. 2015. In vitro evidence for senescent multinucleated
846 melanocytes as a source for tumor-initiating cells. *Cell Death & Disease*. doi:10.1038/cddis.2015.71
- 847 Leikam C, Hufnagel A, Schartl M, Meierjohann S. 2008. Oncogene activation in melanocytes links reactive
848 oxygen to multinucleated phenotype and senescence. *Oncogene* **27**:7070–7082.
- 849 Lewis VM, Saunders LM, Larson TA, Bain EJ, Sturiale SL, Gur D, Chowdhury S, Flynn JD, Allen MC, Deheyn
850 DD, Lee JC, Simon JA, Lippincott-Schwartz J, Raible DW, Parichy DM. 2019. Fate plasticity and
851 reprogramming in genetically distinct populations of Danio leucophores. *PNAS in revision*.
- 852 Lister JA. 2019. Larval but not adult xanthophore pigmentation in zebrafish requires GTP cyclohydrolase 2
853 (gch2) function. *Pigment Cell Melanoma Res*. doi:10.1111/pcmr.12783

- 854 Lister JA, Lane BM, Nguyen A, Lunney K. 2011. Embryonic expression of zebrafish MiT family genes tfe3b,
855 tfeb, and tfec. *Dev Dyn* **240**:2529–2538.
- 856 Lister JA, Robertson CP, Lepage T, Johnson SL, Raible DW. 1999. nacre encodes a zebrafish
857 microphthalmia-related protein that regulates neural-crest-derived pigment cell fate. *Development*
858 **126**:3757–3767.
- 859 Luo R, An M, Arduini BL, Henion PD. 2001. Specific pan-neural crest expression of zebrafish Crestin
860 throughout embryonic development. *Dev Dyn* **220**:169–174.
- 861 Mahalwar P, Walderich B, Singh AP, Nüsslein-Volhard C. 2014. Local reorganization of xanthophores fine-
862 tunes and colors the striped pattern of zebrafish. *Science* **345**:1362–1364.
- 863 Matsumoto J. 1965. Studies on fine structure and cytochemical properties of erythrophores in swordtail,
864 Xiphophorus helleri, with special reference to their pigment granules (Pterinosomes). *J Cell Biol* **27**:493–
865 504.
- 866 Maurus K, Hufnagel A, Geiger F, Graf S, Berking C, Heinemann A, Paschen A, Kneitz S, Stigloher C,
867 Geissinger E, Otto C, Bosserhoff A, Schartl M, Meierjohann S. 2017. The AP-1 transcription factor FOSL1
868 causes melanocyte reprogramming and transformation. *Oncogene* **36**:5110–5121.
- 869 McInnes L, Healy J, Saul N, Großberger L. 2018. UMAP: Uniform Manifold Approximation and Projection.
870 *JOSS* **3**:861.
- 871 McMenamin SK, Bain EJ, McCann AE, Patterson LB, Eom DS, Waller ZP, Hamill JC, Kuhlman JA, Eisen JS,
872 Parichy DM. 2014. Thyroid hormone-dependent adult pigment cell lineage and pattern in zebrafish.
873 *Science* **345**:1358–1361.
- 874 Minchin JEN, Hughes SM. 2008. Sequential actions of Pax3 and Pax7 drive xanthophore development in
875 zebrafish neural crest. *Dev Biol* **317**:508–522.
- 876 Mosimann C, Kaufman CK, Li P, Pugach EK, Tamplin OJ, Zon LI. 2011. Ubiquitous transgene expression and
877 Cre-based recombination driven by the ubiquitin promoter in zebrafish. *Development* **138**:169–177.
- 878 Nagao Y, Takada H, Miyadai M, Adachi T, Seki R, Kamei Y, Hara I, Taniguchi Y, Naruse K, Hibi M, Kelsh RN,
879 Hashimoto H. 2018. Distinct interactions of Sox5 and Sox10 in fate specification of pigment cells in
880 medaka and zebrafish. *PLoS Genet* **14**:e1007260.
- 881 Niu MC. 1954. Further studies on the origin of amphibian pigment cells. *J Exp Zool* **125**:199–220.
- 882 Nord H, Dennhag N, Muck J, von Hofsten J. 2016. Pax7 is required for establishment of the xanthophore
883 lineage in zebrafish embryos. *Mol Biol Cell* **27**:1853–1862.
- 884 Obika M. 1993. Formation of pterinosomes and carotenoid granules in xanthophores of the teleost Oryzias
885 latipes as revealed by the rapid-freezing and freeze-substitution method. *Cell Tissue Res* **271**:81–86.
- 886 Odenthal J, Rossnagel K, Haffter P, Kelsh RN, Vogelsang E, Brand M, van Eeden FJ, Furutani-Seiki M,
887 Granato M, Hammerschmidt M, Heisenberg CP, Jiang YJ, Kane DA, Mullins MC, Nüsslein-Volhard C.
888 1996. Mutations affecting xanthophore pigmentation in the zebrafish, Danio rerio. *Development* **123**:391–
889 398.
- 890 Orr-Weaver TL. 2015. When bigger is better: the role of polyploidy in organogenesis. *Trends Genet* **31**:307–
891 315.
- 892 Parichy DM, Elizondo MR, Mills MG, Gordon TN, Engeszer RE. 2009. Normal table of postembryonic zebrafish
893 development: staging by externally visible anatomy of the living fish. *Dev Dyn* **238**:2975–3015.
- 894 Parichy DM, Mellgren EM, Rawls JF, Lopes SS, Kelsh RN, Johnson SL. 2000a. Mutational analysis of
895 endothelin receptor b1 (rose) during neural crest and pigment pattern development in the zebrafish Danio
896 rerio. *Dev Biol* **227**:294–306.
- 897 Parichy DM, Ransom DG, Paw B, Zon LI, Johnson SL. 2000b. An orthologue of the kit-related gene fms is
898 required for development of neural crest-derived xanthophores and a subpopulation of adult melanocytes
899 in the zebrafish, Danio rerio. *Development* **127**:3031–3044.
- 900 Parichy DM, Rawls JF, Pratt SJ, Whitfield TT, Johnson SL. 1999. Zebrafish sparse corresponds to an
901 orthologue of c-kit and is required for the morphogenesis of a subpopulation of melanocytes, but is not
902 essential for hematopoiesis or primordial germ cell development. *Development* **126**:3425–3436.
- 903 Parichy DM, Spiewak JE. 2015. Origins of adult pigmentation: diversity in pigment stem cell lineages and
904 implications for pattern evolution. *Pigment Cell Melanoma Res* **28**:31–50.
- 905 Parichy DM, Turner JM. 2003. Temporal and cellular requirements for Fms signaling during zebrafish adult
906 pigment pattern development. *Development* **130**:817–833.
- 907 Patil C, Walter P. 2001. Intracellular signaling from the endoplasmic reticulum to the nucleus: the unfolded
908 protein response in yeast and mammals. *Curr Opin Cell Biol* **13**:349–355.
- 909 Patterson LB, Bain EJ, Parichy DM. 2014. Pigment cell interactions and differential xanthophore recruitment

- underlying zebrafish stripe reiteration and *Danio* pattern evolution. *Nat Commun* **5**:5299.
- Patterson LB, Parichy DM. 2019. Zebrafish pigment pattern formation: insights into the development and evolution of adult form. *Annual Review of Genetics* **53**, doi:10.1146/annurev-genet-112618-043741
- Patterson LB, Parichy DM. 2013. Interactions with iridophores and the tissue environment required for patterning melanophores and xanthophores during zebrafish adult pigment stripe formation. *PLoS Genet* **9**:e1003561.
- Qiu X, Hill A, Packer J, Lin D, Ma Y-A, Trapnell C. 2017a. Single-cell mRNA quantification and differential analysis with Census. *Nat Methods* **14**:309–315.
- Qiu X, Mao Q, Tang Y, Wang L, Chawla R, Pliner HA, Trapnell C. 2017b. Reversed graph embedding resolves complex single-cell trajectories. *Nat Methods* **14**:979–982.
- Quigley IK, Turner JM, Nuckels RJ, Manuel JL, Budi EH, MacDonald EL, Parichy DM. 2004. Pigment pattern evolution by differential deployment of neural crest and post-embryonic melanophore lineages in *Danio* fishes. *Development* **131**:6053–6069.
- Raposo G, Marks MS, Cutler DF. 2007. Lysosome-related organelles: driving post-Golgi compartments into specialisation. *Curr Opin Cell Biol* **19**:394–401.
- R Core Team. 2017. R: A Language and Environment for Statistical Computing.
- Regneri J, Klotz B, Wilde B, Kottler VA, Hausmann M, Kneitz S, Regensburger M, Maurus K, Götz R, Lu Y, Walter RB, Herpin A, Schartl M. 2019. Analysis of the putative tumor suppressor gene cdkn2ab in pigment cells and melanoma of Xiphophorus and medaka. *Pigment Cell Melanoma Res* **32**:248–258.
- Riabowol K, Schiff J, Gilman MZ. 1992. Transcription factor AP-1 activity is required for initiation of DNA synthesis and is lost during cellular aging. *Proc Natl Acad Sci U S A* **89**:157–161.
- Sachs LM, Buchholz DR. 2017. Frogs model man: In vivo thyroid hormone signaling during development. *Genesis* **55**. doi:10.1002/dvg.23000
- Savchenko I. 1988. Endomitosis in pigmented neoplasms of human skin. *Tsitol Genet* **22**:20–24.
- Schartl M, Larue L, Goda M, Bosenberg MW, Hashimoto H, Kelsh RN. 2016. What is a vertebrate pigment cell? *Pigment Cell Melanoma Res* **29**:8–14.
- Shah AN, Davey CF, Whitebirch AC, Miller AC, Moens CB. 2015. Rapid reverse genetic screening using CRISPR in zebrafish. *Nat Methods* **12**:535–540.
- Shah M, Orengo IF, Rosen T. 2006. High prevalence of hypothyroidism in male patients with cutaneous melanoma. *Dermatol Online J* **12**:1.
- Sharan SK, Thomason LC, Kuznetsov SG, Court DL. 2009. Recombineering: a homologous recombination-based method of genetic engineering. *Nat Protoc* **4**:206–223.
- Sheets L, Ransom DG, Mellgren EM, Johnson SL, Schnapp BJ. 2007. Zebrafish melanophilin facilitates melanosome dispersion by regulating dynein. *Curr Biol* **17**:1721–1734.
- Shi Y-B. 2013. Chapter Ten - Unliganded Thyroid Hormone Receptor Regulates Metamorphic Timing via the Recruitment of Histone Deacetylase Complexes In: Rougvie AE, O'Connor MB, editors. *Current Topics in Developmental Biology*. Academic Press. pp. 275–297.
- Shi Y-B. 1999. Amphibian Metamorphosis: From Morphology to Molecular Biology. Wiley-Liss.
- Singh AP, Dinwiddie A, Mahalwar P, Schach U, Linker C, Irion U, Nüsslein-Volhard C. 2016. Pigment Cell Progenitors in Zebrafish Remain Multipotent through Metamorphosis. *Dev Cell* **38**:316–330.
- Singh AP, Schach U, Nüsslein-Volhard C. 2014. Proliferation, dispersal and patterned aggregation of iridophores in the skin prefigure striped colouration of zebrafish. *Nat Cell Biol* **16**:607–614.
- Sisley K, Curtis D, Rennie IG, Rees RC. 1993. Loss of heterozygosity of the thyroid hormone receptor B in posterior uveal melanoma. *Melanoma Res* **3**:457–461.
- Spiewak JE, Bain EJ, Liu J, Kou K, Sturiale SL, Patterson LB, Diba P, Eisen JS, Braasch I, Ganz J, Parichy DM. 2018. Evolution of Endothelin signaling and diversification of adult pigment pattern in *Danio* fishes. *PLoS Genet* **14**:e1007538.
- Suster ML, Abe G, Schouw A, Kawakami K. 2011. Transposon-mediated BAC transgenesis in zebrafish. *Nat Protoc* **6**:1998–2021.
- Thisse C, Thisse B, Postlethwait JH. 1995. Expression of snail2, a second member of the zebrafish snail family, in cephalic mesendoderm and presumptive neural crest of wild-type and spadetail mutant embryos. *Dev Biol* **172**:86–99.
- Toews DPL, Hofmeister NR, Taylor SA. 2017. The Evolution and Genetics of Carotenoid Processing in Animals. *Trends Genet* **33**:171–182.
- Toomey MB, Lopes RJ, Araújo PM, Johnson JD, Gazda MA, Afonso S, Mota PG, Koch RE, Hill GE, Corbo JC, Carneiro M. 2017. High-density lipoprotein receptor SCARB1 is required for carotenoid coloration in birds.

- 966 *Proc Natl Acad Sci U S A* **114**:5219–5224.
967 Toomey MB, McGraw KJ. 2007. Modified saponification and HPLC methods for analyzing carotenoids from the
968 retina of quail: implications for its use as a nonprimate model species. *Invest Ophthalmol Vis Sci* **48**:3976–
969 3982.
970 Trapnell C, Cacchiarelli D, Grimsby J, Pokharel P, Li S, Morse M, Lennon NJ, Livak KJ, Mikkelsen TS, Rinn
971 JL. 2014. The dynamics and regulators of cell fate decisions are revealed by pseudotemporal ordering of
972 single cells. *Nat Biotechnol* **32**:381–386.
973 Tzur A, Moore JK, Jorgensen P, Shapiro HM, Kirschner MW. 2011. Optimizing optical flow cytometry for cell
974 volume-based sorting and analysis. *PLoS One* **6**:e16053.
975 Usui Y, Kondo S, Watanabe M. 2018. Melanophore multinucleation pathways in zebrafish. *Dev Growth Differ*
976 **60**:454–459.
977 Van de Putte T, Maruhashi M, Francis A, Nelles L, Kondoh H, Huylebroeck D, Higashi Y. 2003. Mice lacking
978 ZFHX1B, the gene that codes for Smad-interacting protein-1, reveal a role for multiple neural crest cell
979 defects in the etiology of Hirschsprung disease-mental retardation syndrome. *Am J Hum Genet* **72**:465–
980 470.
981 Watanabe M, Iwashita M, Ishii M, Kurachi Y, Kawakami A, Kondo S, Okada N. 2006. Spot pattern of leopard
982 Danio is caused by mutation in the zebrafish connexin41.8 gene. *EMBO Rep* **7**:893–897.
983 Watanabe M, Kondo S. 2015. Is pigment patterning in fish skin determined by the Turing mechanism? *Trends
984 Genet* **31**:88–96.
985 Williams JS, Hsu JY, Rossi CC, Artinger KB. 2018. Requirement of zebrafish pcdh10a and pcdh10b in
986 melanocyte precursor migration. *Dev Biol.* doi:10.1016/j.ydbio.2018.03.022
987 Zhang YM, Zimmer MA, Guardia T, Callahan SJ, Mondal C, Di Martino J, Takagi T, Fennell M, Garippa R,
988 Campbell NR, Bravo-Cordero JJ, White RM. 2018. Distant Insulin Signaling Regulates Vertebrate
989 Pigmentation through the Sheddase Bace2. *Dev Cell* **45**:580–594.e7.
990 Ziegler I. 2003. The pteridine pathway in zebrafish: regulation and specification during the determination of
991 neural crest cell-fate. *Pigment Cell Res* **16**:172–182.
992 Ziller C, Dupin E, Brazeau P, Paulin D, Le Douarin NM. 1983. Early segregation of a neuronal precursor cell
993 line in the neural crest as revealed by culture in a chemically defined medium. *Cell* **32**:627–638.

994

995 **Figure 1. TH dependent phenotypes and models for TH action.** (A) Euthyroid and hypothyroid zebrafish
996 [stage 10 (mm) standardized standard length (SSL) (Parichy et al., 2009); ~21 d post fertilization, dpf]. Insets,
997 yellow/orange xanthophores of euthyroid fish and absence of these cells in hypothyroid fish. (B) Models for TH
998 effects on alternative cell types derived from a common progenitor (P), by regulating: (i) cell fate specification;
999 or (ii) amplification and restraint of committed cell-types by differential effects on morphogenesis and
1000 differentiation.
1001

1002 **Figure 2. Single cell transcriptomic identification of post-embryonic NC-derived cell types.** (A) Cell-type
1003 assignments for clusters of cells ($n=16,150$) from euthyroid and hypothyroid fish. Cell types known to be of
1004 non-NC derivation are not shown (Figure 2—figure supplement 2D and E). (B) Known cell-type marker
1005 genes and new candidate markers (for cluster-specific genes, see Supplementary File 2—Table 1).

1006 **Figure 2—figure supplement 1. Experimental design and isolation of NC-derived cells from post-**
1007 **embryonic zebrafish.** (A) Fish transgenic for *sox10:cre* and *ubi:loxP-EGFP-loxP-mCherry* permanently and
1008 robustly expressed mCherry in NC-derived cells of both euthyroid and hypothyroid fish (Kague et al., 2012;
1009 Mosimann et al., 2011). At superficial layers, mCherry+ xanthophores (yellow arrowheads), melanophores (red
1010 arrowheads), and iridophores (blue dotted line) were apparent. At deeper layers, mCherry+ cells were found in
1011 dorsal root ganglia (magenta arrowheads) and other locations (e.g., mint arrowheads), potentially representing
1012 glia, neurons, progenitors and other cell types. mCherry+ cells of non-NC origin were evident as well (see
1013 Figure 2—figure supplement 2). Stage shown is 9.8 SSL (Parichy et al., 2009). (B) Single-cell RNA-Seq
1014 (scRNA-Seq) experimental design. To ensure that progenitors, cells at intermediate states of specification and
1015 commitment, and fully differentiated cells were captured, euthyroid and hypothyroid fish were collected at a
1016 range of stages encompassing adult pattern formation (7.2–9.8 SSL) and from juvenile fish (11 SSL) in which
1017 the first two adult stripes had fully formed. To compare transcriptomic signatures of NC-derived cells from
1018 embryonic–early larval and middle larval–juvenile stages, cells were additionally collected from euthyroid
1019 larvae at 5 dpf (3.5 SSL). (C) Representative FAC sort for NC-derived cells from post-embryonic skins and
1020 trunks. Single cells were isolated by sequentially gating cells according to their SSC-A vs. FSC-A, FSC-H vs.
1021 FSC-W, and SSC-H vs. SSC-W profiles according to standard flow cytometry practices. Cells with high levels
1022 of DAPI staining were excluded as dead or damaged. NC-derived cells were isolated by identifying cells with
1023 high fluorescence in the mCherry-A channel which describes expression of the *ubi:loxP-EGFP-loxP-mCherry*
1024 transgene after permanent conversion to *ubi:mCherry* after exposure to *sox10:Cre* (see Figure 2—figure
1025 supplement 1A).
1026

1027 **Figure 2—figure supplement 2. Population characteristics for full scRNA-Seq dataset from post-**
1028 **embryonic zebrafish.** (A) Percentages of cell types across samples (for details, see Supplementary File 2—
1029 **Table 3**). All cell types are represented in each sample in similar overall proportions. Colors correspond to cell
1030 types in (B–E). (B) Counts of cells by type captured from euthyroid and hypothyroid fish at post-embryonic
1031 stages (≥ 7.2 SSL). (C) Counts of unique molecular identifiers (UMI) and unique genes expressed, as well as
1032 fractions of mitochondrial reads by cell-type (shown are medians with boxes spanning interquartile ranges;
1033 vertical lines indicate farthest observations of data with outlier samples shown individually). Increased fractions
1034 of mitochondrially encoded genes may indicate broken cell (Illicic et al., 2016). Consistent with this idea,
1035 Schwann cells—many of which are expected to be damaged owing to their concentrically layered
1036 morphology—exhibited one of the largest overall proportions of UMIs derived from mitochondrial genes. (D)
1037 Two-dimensional UMAP representation of all post-embryonic cells (≥ 7.2 SSL) captured in scRNA-Seq that
1038 passed quality thresholds (22,613 cells, 13 combined samples). (E) Same cells as in D, with presumptive NC-
1039 derivatives shown in grey and presumptive non-NC derived cells highlighted by type.

1040 **Figure 2—figure supplement 3. Genes enriched in pigment progenitor clusters include known markers**
1041 **of embryonic NC cells.** Genes enriched in the pigment progenitor cluster compared to differentiated pigment
1042 cells included loci expressed in embryonic, migratory NC cells of zebrafish and other species (*crestin*, *sna12*,
1043 *foxd3*, *pax3a*, *vim*, *zeb2a*) (Kaufman et al., 2016; Kelsh et al., 2000a; Luo et al., 2001; Minchin and Hughes,

1044 2008; Thisse et al., 1995; Van de Putte et al., 2003; Ziller et al., 1983). Color indicates relative expression of
1045 each gene within individual cells (xan, xanthophores; mel, melanophores; irid, iridophores; prog, pigment
1046 progenitors).

1047
1048 **Figure 2—figure supplement 4. Distinct domains of gene expression across diverse NC derivatives. (A)**
1049 UMAP representation of major NC derivatives (left) with coordinate expression of two exemplar ligand–
1050 receptor gene pairs (middle and right). Xanthophores are known to express and require type III receptor
1051 tyrosine kinase (RTK) gene *colony stimulating factor 1 receptor a* (*csf1ra*) and to depend for their development
1052 on *csf1a* expressed by nearby iridophores (Parichy et al., 2000b; Patterson and Parichy, 2013). Melanophores
1053 require the type III RTK gene *kita* (Parichy et al., 1999) and ligand encoded by *kitlga*, expressed by skin
1054 (Hultman et al., 2007; Patterson and Parichy, 2013), but also pigment cells and progenitors revealed here by
1055 scRNA-Seq. **(B)** Pairs of cell adhesion molecules with distinct expression domains suggest differing
1056 morphogenetic requirements between pigment cell and other lineages (*cdh1* vs. *cdh2*), and for specific cell
1057 types [e.g., *cdh11* of iridophores, which form epithelium-like mats within adult interstripes (Singh et al., 2014);
1058 (Budi et al., 2011; Darzynkiewicz et al., 1980; McMenamin et al., 2014; Spiewak et al., 2018)]. **(C)** In teleosts,
1059 an ancient clade-specific genome duplication resulted in extra genes, allowing for subfunctionalization and
1060 retention of some paralogs (Braasch et al., 2015, 2009). scRNA-Seq revealed different degrees to which
1061 paralog expression has been partitioned across NC derived cell types. For example, proliferating progenitors
1062 and unknown (unk) cells were more likely to express receptor tyrosine kinase gene *erbb3b*, required for
1063 development of glia and adult melanophores (Budi et al., 2008), whereas Schwann cells and Schwann cell
1064 progenitors (SCP) were more likely to express *erbb3a*. Likewise, xanthophores express and require
1065 transcription factor genes *pax7a* and *pax7b* (Nord et al., 2016), but iridophores were also marked by *pax7a*
1066 expression, suggesting the possibility of functional significance to this cell type exclusive of *pax7b* activities (A–
1067 C, expression thresholds=1.)
1068

1069
1070 **Figure 2—figure supplement 5. Similarities and differences between EL and adult gene expression**
1071 **programs. (A)** UMAP representation of EL NC-derived cells ($n=1,466$) isolated from euthyroid 5 dpf fish (3.5
1072 SSL; prog, progenitor; SCP, Schwann cell precursors; PNS, non-enteric peripheral nervous system). **(B)** Mid-
1073 larval and juvenile NC-derived cells from euthyroid fish ($n=7,611$; from ≥ 7.2 SSL fish; sat, satellite). **(C)**
1074 Combined EL and euthyroid mid-larval/juvenile. **(D)** Comparison of EL (orange) and mid-larval/juvenile (blue)
1075 cell distributions revealed broadly overlapping domains of xanthophores in UMAP space, consistent with
1076 known derivation of most adult xanthophores from EL xanthophores (McMenamin et al., 2014) [and see Main
1077 text].
1078

1078 **Figure 3. Pigment cell subpopulations and dynamics of gene expression across pigment cell lineages.**
1079 **(A)** Established lineage relationships of embryonic (e) and post-embryonic pigment cells. Multipotent pigment
1080 cell progenitors (P) in the peripheral nervous system generate adult iridophores (I), melanophores (M) and
1081 some xanthophores (X). A few embryonic melanophores (M_e) persist whereas embryonic xanthophores (X_e)
1082 proliferate and lose their pigment to enter a cryptic phase (X_c), and then reacquire pigment late in pattern
1083 formation to form most adult xanthophores (McMenamin et al., 2014). **(B)** Sub-clusters of melanophores and
1084 xanthophores with distinct gene expression signatures. **(C)** Pigment cell clusters defined by markers for each
1085 cell-type. **(D-E)** Pseudotemporal ordering (D) and BEAM (E) revealed dynamics of gene expression over
1086 pseudotime for each pigment cell branch ($q<6.0\text{E-}11$ for all genes; except *pax3a* (starred, $q=0.03$), expressed
1087 as anticipated during early pseudotime in each branch.
1088

1089
1090 **Figure 3—figure supplement 1. Differences between melanophore and xanthophore sub-populations**
1091 **revealed distinct levels and types of transcriptional activity. (A)** Median transcript numbers (unique
1092 molecular identifiers, UMIs; upper plot) differed across pigment cell subpopulations. Reduced total RNA
content is associated with a G0 cell state (i.e., quiescence, replicative senescence, and/or terminal

1093 differentiation) (Coller et al., 2006; Darzynkiewicz et al., 1980); low median UMI counts in sub-clusters of
1094 melanophores and xanthophores (mel 2, xan 1) suggest alternative states within these differentiated cell
1095 populations. Mitochondrial read fraction (lower plot) was low and consistent across sub-clusters, suggesting
1096 that low median UMI counts (upper plot) were unlikely to reflect damage specifically incurred by particular cell
1097 types (Ilicic et al., 2016). **(B)** Both melanophore subclusters highly express genes associated with melanin
1098 synthesis, indicating that they are both represent true melanophores. However, cell clusters with lower median
1099 UMIs (mel 2, xan 1) exhibited gene expression trends indicative of curtailed transcriptional and translational
1100 activity, including reduced expression of AP-1 transcriptional complex members (AP1 TF signature score), and
1101 genes involved in unfolded protein response (UPR signature score), and proliferation (cell-cycle signature
1102 score) (Chinenov and Kerppola, 2001; Maurus et al., 2017; Patil and Walter, 2001; Riabowol et al., 1992) (for
1103 details of genes in signature scores, see **Supplementary File 2—Table 4**). **(C)** Melanophores and
1104 xanthophores in subclusters with lower total UMI counts (mel 2, xan 1) expressed fewer unique genes
1105 compared to cells in the other subcluster regardless of equivalent UMI counts, consistent with a more
1106 restricted gene expression profile of these populations (shaded areas indicate standard error bounds). **(D)**
1107 Differential expression of genes between pigment cell sub-clusters (xan1 vs. xan2; mel2 vs. mel1). These
1108 analyses revealed more genes, expressed at higher levels in xanthophore 2 compared to xanthophore 1, and
1109 in melanophore 1 compared to melanophore 2. These biases were consistent with xanthophore 2 and
1110 melanophore 1 representing more active cells, and xanthophore 1 and melanophore 2 representing less active
1111 cells. Genes compared were expressed by at least 5 cells in either cluster (\log_2 fold-change cutoff = 0.8, $P < 1e-3$;
1112 xanthophores = 160, 36; melanophores = 125, 39). **(E)** Melanophore and xanthophore subclusters were
1113 differentially distributed along trajectory branches in **Figure 3D**, consistent with xanthophore 2 and
1114 melanophore 2 representing cells at later steps of maturation as compared to xanthophore 1 and melanophore
1.
1115

1116
Figure 3—figure supplement 2. Xanthophore cluster-specific expression identifies novel xanthophore
1117 **markers.** **(A)** UMAP plots of pigment cells colored by expression of xanthophore cluster-enriched genes (*bco1*,
1118 *bco2b*, *bscl2l*, *slc2a11b*, *slc22a7a*, *wu:fc46h12*). **(B)** Expression in xanthophores of genes shown in A, as
1119 revealed by whole-mount *in situ* hybridization patterns corresponding to those of known xanthophore lineage
1120 markers and localization of differentiated and cryptic xanthophores (Hamada et al., 2014; Lang et al., 2009;
1121 McMenamin et al., 2014; Parichy et al., 2000b). Insets show at higher magnification blue-stained cells of
1122 xanthophore lineage. Bars at right indicate cell positions relative to anatomy of final pattern: solid black,
1123 melanophores in prospective stripe regions; dashed black, melanophores transiently located in prospective
1124 interstripe region; light yellow, xanthophores likely to remain cryptically (unpigmented) with stripes; orange,
1125 xanthophores likely to develop pigmentation in the interstripe.
1126

1127
Figure 3—figure supplement 3. Iridophore cluster-specific expression identifies novel iridophore
1128 **markers.** **(A)** UMAP plots of pigment cells colored by expression of iridophore cluster-specific genes (*alx4a*,
1129 *alx4b*, *crip2*, *defbl1*). **(B)** Whole-mount *in situ* hybridization of genes in A reveals patterns corresponding to
1130 previously described iridophore markers and locations (Lang et al., 2009; Patterson and Parichy, 2013;
1131 Spiewak et al., 2018). Insets, higher magnification views of blue-stained iridophores in the prospective
1132 interstripe (upper) and within or near prospective stripe (lower). Bars at right indicate cell positions relative to
1133 final pattern features: solid black, melanophores in prospective stripe regions; dashed black, melanophores in
1134 prospective interstripe; solid blue, dense iridophores of interstripe; dashed blue, sparse iridophores of stripe.
1135

1136
Figure 3—figure supplement 4. Genes identified as zebrafish pigmentation mutants often had
1137 **expression domains beyond affected cell types.** Mutations affecting a variety of pigmentary traits have
1138 been recovered or induced and affect pigment deposition, specification or morphogenesis of one or more
1139 pigment cell classes, and pattern at EL, adult or both stages (Arduini et al., 2009; Barrallo-Gimeno et al., 2004;
1140 Beirl et al., 2014; Budi et al., 2008; D’Agati et al., 2017; Dooley et al., 2013b; Dutton et al., 2001; Eskova et al.,
1141

1142 2017; Fadeev et al., 2015; Inoue et al., 2014; Irion et al., 2014; Iwashita et al., 2006; Knight et al., 2003;
1143 Krauss et al., 2013; Larson et al., 2010; Nagao et al., 2018; Parichy et al., 2000a; Sheets et al., 2007;
1144 Watanabe et al., 2006; Williams et al., 2018; Zhang et al., 2018). Shown are expression domains observed for
1145 affected genes in scRNA-Seq analyses of adult NC-derived cells (euthyroid and hypothyroid). Gene names are
1146 listed at upper right of each box, with corresponding mutant names indicated below for those loci identified in
1147 forward genetic screens (for mutants isolated independently in different screens more than one name is
1148 indicated). Logos at lower right of each panel are cell types reported to be affected. In some instances only EL
1149 phenotypes have been reported (e.g., *pcdh10a*). Red outlines around cell type logos indicates neomorphic
1150 alleles (*aqp3a*, *tuba8/3a*); dashed lines indicate effects that are known to be non-autonomous to the affected
1151 cell types (e.g., *erbb3b*). In many instances scRNA-Seq expression domains identified a more diverse array of
1152 cell types than would be expected from gross mutant phenotypes alone. For example, *slc45a2* is required for
1153 melanization of melanophores but detected at lower levels in xanthophores and iridophores, whereas *mpha* is
1154 required for melanosome dispersion but also expressed in xanthophores. Such instances raise the possibility
1155 of cell-type specific expression that is not functionally significant (e.g., if other pathway members are not
1156 themselves expressed), unanticipated functions that result in only subtle loss-of-function phenotypes not yet
1157 identified, or amelioration of functional deficiencies by cell-type specific mechanisms of genetic compensation.
1158 Conversely, genes not expressed in affected cell types suggest or support prior inferences of non-autonomous
1159 functions, or requirements in a common progenitor (*erbb3b*, *oca2*). Genes for some well-studied mutants [e.g.,
1160 *kita/sparse* (Johnson et al., 1995; Parichy et al., 1999)] were expressed at levels too low to be detected by
1161 scRNA-Seq.

1162
1163 **Figure 3—figure supplement 5. Dynamics of gene expression over pseudotime recapitulated distinct**
1164 **melanophore and iridophore differentiation programs. (A)** Expression of genes over pseudotime reflect
1165 predicted kinetics for melanophores and iridophores. Solid lines indicate smoothed expression curves for all
1166 cells in the branch. *mitfa* expression declined only marginally with melanophore differentiation yet decreased
1167 markedly with a transition from progenitor to iridophore as expected (Curran et al., 2010). *pax3a* was
1168 expressed in pigment progenitors (magenta) and decreased across pseudotime in melanophores, whereas
1169 expression of *tfec*, a transcription factor expressed in iridophores (Lister et al., 2011), increased over
1170 pseudotime. Melanin synthesis enzyme genes, *dct* and *tyrpb1b*, as well as *pmel*, encoding a melanosome-
1171 associated transmembrane protein, all increased over pseudotime in melanophores. In iridophores, *gpnmb*
1172 and *pnp4a* showed elevated expression late in pseudotime, as expected (Curran et al., 2010; Higdon et al.,
1173 2013). **(B)** Trends of total transcript UMI counts, scores of expressed cell-cycle (e.g. *ccnd1*, *pcna*), pigment cell
1174 transcription factors (e.g. *mitfa*, *tfec*, *pax7b*, *tfap2a*), and pigment synthesis-related genes (e.g. *impdh1b*, *gart*,
1175 and *atic* for purine processing in iridophores; *tyrpb1b*, *pmela*, and *tyr* for melanin synthesis in melanophores) in
1176 bins across pseudotime for melanophore and iridophore trajectory branches (for all score-associated genes,
1177 see **Supplementary File 2—Table 4**). Histograms indicate cell-type specific densities across pseudotime for
1178 each branch. For melanophores, total transcript number per cell decreased over pseudotime and expression
1179 levels of melanin synthesis genes increased. In iridophores, mRNA levels stayed relatively constant whereas
1180 expression of purine synthesis genes increased. The expression score for cell-cycle genes was greater for
1181 iridophores than melanophores at the terminal step of pseudotime ($P<0.0002$; Wilcoxon; pseudotime bin 8;
1182 $n=91$ iridophores, 319 melanophores), consistent with iridophores continuing to proliferate even after
1183 differentiation, and melanophores normally failing to do so (Budi et al., 2011; Darzynkiewicz et al., 1980;
1184 McMenamin et al., 2014; Spiewak et al., 2018).

1185
1186 **Figure 4. TH biased pigment cell lineages towards later steps of pseudotime. (A)** UMAP dimensionality
1187 reduction of euthyroid and hypothyroid pigment cells and pigment progenitors. Sub-clustering reveals two
1188 xanthophore and two melanophore clusters (indicated by different shades of yellow and grey, respectively). **(B)**
1189 Pigment cells colored by TH status. Euthyroid and hypothyroid cells generally intermix with some biases
1190 apparent within melanophore and iridophore clusters. **(C)** Percentages of each pigment cell class by TH-

status. Colors are consistent with other pigment cell plots. Of cells captured, a higher proportion of pigment cells from euthyroid fish were xanthophores and iridophores compared to those from hypothyroid fish. **(D)** Trajectories for euthyroid and hypothyroid pigment cells (plotted together, faceted by condition). Broad differences in trajectory topologies were not apparent between the two conditions. **(E)** Distributions of each pigment cell-type across pseudotime by condition. For each trajectory branch (mel, xan, irid) hypoTH cells were biased towards early pseudotime (Wilcoxon signed-rank tests, mel: $Z=-6.54$, $P<0.0001$, xan: $Z=-4.54$, $P<0.0001$, irid: $Z=-13.55$, $P<0.0001$). Median is indicated by red arrowhead and different colors demarcate quartiles over pseudotime.

Figure 5. TH promoted melanophore maturation by measures of transcriptomic state and cellular phenotype. (A) Gene expression differences between melanophores over pseudotime by TH-status ($q<1E-7$, genes expressed in >10% of melanophores). Heatmap is hierarchically clustered by row (method, Ward D2). The largest cluster (#3) contains 41% of the genes and represents loci expressed late in pseudotime of euthyroid melanophores but downregulated in hypothyroid melanophores [e.g. *tfap2a* and *tyrp1b*], identifying novel candidate genes for roles in melanophore maturation (see **Supplementary File 2—Table 6**, in which published melanophore-related genes are highlighted) (Baxter et al., 2018). **(B)** Euthyroid melanophores tended to be highly melanized and stellate whereas hypothyroid melanophores were variably melanized and often dendritic. **(C)** Quantification of melanin contents per cell, as estimated by area of pixels (px) having melanin following contraction of melanin granules in response to epinephrine (e.g., **Figure 1A**). Melanophores of euthyroid fish contained more melanin than those of hypothyroid fish ($F_{1,2710}=271.2$, $P<0.0001$), after controlling for individual variation among fish within TH conditions ($F_{10,2710}=8.5$, $P<0.0001$; sample sizes: $n=1180$ cells from 5 euthyroid fish, $n=1542$ cells from 5 hypothyroid fish). If planar areas of concentrated melanin granules are assumed spherical, then euthyroid melanophores had on average ~1.7x the total melanin content of hypothyroid melanophores. (Data in supplementary file **Figure 5—Source Data 1**.) **(D)** Fully differentiated melanophores of zebrafish are often binucleate (Usui et al., 2018). Left panel shows a binucleate stripe melanophore in a euthyroid fish (12 SSL). Right panel shows a mononucleate melanophore in a hypothyroid fish at the same stage. Magenta, membrane labeling of melanophores by *tyrp1b:palm-mCherry*. Blue, nuclei revealed by *tuba8l3:nEosFP*. **(E)** Euthyroid fish had proportionally more binucleate melanophores than hypothyroid fish ($\chi^2=230.3$, d.f.=1, $P<0.0001$) after controlling for a higher incidence of binucleation in developmentally more advanced fish overall (11.5–13 SSL; $\chi^2=5.5$, d.f.=1, $P<0.05$). Individual points indicate proportions of binucleate melanophores observed in dorsal stripes (circles) and ventral stripes (diamonds), which did not differ significantly ($P=0.8$; sample sizes: $n=383$ melanophores in 4 euthyroid fish, $n=706$ melanophores in 3 hypothyroid fish). (Data in supplementary file **Figure 5—Source Data 2**.)

Figure 5—figure supplement 1. Metrics of melanophore maturation in response to TH. **(A)** Melanophores plated ex vivo from fish at terminal stages of stripe development had diverse morphologies and some exhibited senescence-associated β -galactosidase staining (SA- β -gal; blue precipitate, upper panel), though relative intensities of staining were difficult to score, precluding a quantitative assessment. Xanthophores plated ex vivo did not exhibit SA- β -gal staining. **(B)** Lysosomes were revealed in *tyrp1b:palm-mCherry+* (magenta) melanophores by Lysotracker dye (cyan), which did not stain melanosomes (yellow) despite some similarities between these organelles (Raposo et al., 2007). Melanosomes were visualized in bright field and an inverted and pseudocolored overlay is shown here. **(C)** Lysosomal content revealed significantly greater normalized mean fluorescence intensity (MFI) of Lysotracker dye in melanophores from euthyroid fish as compared to hypothyroid fish (euthyroid, 20,423 melanophores from 10 fish; hypothyroid, 87,252 melanophores from 10 fish; $P<0.01$, Wilcoxon). **(D)** FSC-A values were higher for euthyroid compared to hypothyroid cells overall [$P<0.001$; cells are the same as in (C)], consistent with an overall difference in cell size. (C and D data in supplementary file **Figure 5—figure supplement 1 Source Data 1**.) **(E)** Euthyroid fish at a later stage of pattern formation exhibit a higher proportion of binucleate melanophores compared to those at earlier stages (early, 7.2 SSL: $n=153$ in 5 fish; late, 11 SSL: $n=477$ melanophores in 5 fish; $P<0.001$). (Data

1240 in supplementary file **Figure 5—figure supplement 1 Source Data 2.**) (**F**) Sequential FACS gating strategy
1241 (left to right) used in determining Lysotracker normalized MFI. For details, see Materials and Methods. (SSC,
1242 side scatter; FSC, forward scatter; W, width; H, height; A, area).

1243

1244 **Figure 6. TH promotes xanthophore maturation via *scarb1*-dependent carotenoid uptake.**

1245 (**A**) Proportions of differentially expressed genes in euthyroid and hypothyroid cells across pseudotime bins.
1246 Xanthophores expressed fewer TH-dependent genes than melanophores (expressed gene cutoff = 2% of bin
1247 expressing, DEGs are genes with $q < 0.05$ and fold change $> 1.5X$). Of 160 xanthophore DEGs and 519
1248 melanophore DEGs, only 58 were found to be overlapping. (**B**) TH-dependent expression of genes related to
1249 carotenoid pigmentation in xanthophores. Red bars: $q < 0.05$, \log_2 fold-change ≥ 2.0 . (**C**) Carotenoid pathway
1250 gene expression score was higher in xanthophore lineage cells of euthyroid fish compared to hypothyroid fish
1251 ($P=1.5E-15$, Wilcoxon). By contrast, pteridine pathway gene expression was marginally lower in cells from
1252 euthyroid fish ($P=0.01$). Box-and-whisker plots represent scores across groups (center line, median; box limits,
1253 upper and lower quartiles; whiskers, 1.5x interquartile range; points, outliers). (**D**) Carotenoids were detected
1254 by HPLC in skin containing xanthophores of euthyroid but not hypothyroid fish (11 SSL). (**E**) *scarb1* expression
1255 in euthyroid and hypothyroid zebrafish (10 SSL). (**F**) *scarb1* mutants lacked mature, yellow xanthophores (12
1256 SSL).

1257

1258 **Figure 6—figure supplement 1. Expression of multiple carotenoid-related genes in xanthophores are**
1259 **affected by TH.** UMAP plots of pigment cell clusters colored by expression of TH-dependent genes in
1260 xanthophores: *gstm.3* ($q=6.9E-99$, \log_2 fold-change = 4.3), *plin6* ($q=1.9E-13$, \log_2 fold-change=1.3), *scarb1*
1261 ($q=3.5E-11$, \log_2 fold-change=1.2).

1262

1263 **Figure 6—figure supplement 2. TH promotes development of lipid-filled carotenoid droplets in**
1264 **xanthophores.** (**A**) Carotenoid pigments are normally localized to lipid droplets, the presence of which can be
1265 revealed by Oil-red-O staining. Here, a proportion of *aox5:palmEGFP*+ xanthophores stained ex vivo from
1266 euthyroid fish ($n=112$ cells) contained lipid (red), whereas xanthophores from hypothyroid fish ($n=48$ cells)
1267 were never observed to have such lipid contents. (Incidence data in supplementary file **Figure 6—figure**
1268 **supplement 1 Source Data 1.**) (**B**) Ultrastructurally, carotenoids and lipids are detectable as electron-dense
1269 carotenoid vesicles (red circles) (Djurdjević et al., 2015; Granneman et al., 2017; Obika, 1993), which were
1270 observed in xanthophores from euthyroid but not hypothyroid fish. N, nucleus. P, pterinosome—the pteridine-
1271 containing organelle of xanthophores (Bagnara et al., 1968; Hirata et al., 2003; Matsumoto, 1965; Obika,
1272 1993).

1273

1274 **Figure 6—figure supplement 3. *scarb1* is specifically involved in xanthophore maturation and is**
1275 **induced by TH.** (**A**) Scarb1 protein alignment. Zebrafish *scarb1* mutants had a 105 bp, in-frame deletion in a
1276 conserved region of the protein. (**B**) *scarb1* mutants lacked mature, interstripe xanthophores but had normal
1277 stripes and *aox5:palmEGFP* expression, suggesting that patterning and unpigmented xanthophores were
1278 normal. (**C**) In hypothyroid fish treated with exogenous TH (T4), *scarb1* expression was rescued within ~1 d
1279 (upper) and carotenoid autofluorescence of xanthophores was recovered within ~2 d (lower).

1280

1281 **Figure 6—figure supplement 4. Xanthophores switch yellow pigmentation programs during the larval-**
1282 **to-adult transition.** (**A**) At 5 dpf, *scarb1* mutants had yellow larval xanthophores with wild-type levels of
1283 pteridines. (**B**) Carotenoids were not detectable in EL zebrafish (5 dpf, wild-type; compare to Fig. 3D); *csf1ra*
1284 mutants, which lack xanthophores, had HPLC profiles indistinguishable from wild-type. (**C**) Carotenoid and
1285 pteridine pathway signature scores for xanthophores in euthyroid EL and euthyroid and hypothyroid adult
1286 scRNA-Seq data sets. Box plots as in Fig. 3 with different letters above data indicating significant differences in
1287 *post hoc* comparisons (carotenoid, $P<2e-16$; pteridine, $P=0.01$; Tukey HSD). Pteridine signatures between EL,
1288 hypothyroid, and euthyroid xanthophores were more similar than carotenoid signatures. (**D**) Ammonia-induced

pteridine fluorescence was present in adult xanthophores of both euthyroid and hypothyroid fish (red arrowheads).

Figure 7. TH receptors repress developmental progression of pigment cell lineages. (A) In euthyroid fish, homozygous TR mutants singly and in combination resembled wild-type; shown is *thrab*. (B) Euthyroid fish wild-type for TRs exhibited numerous autofluorescing, carotenoid-containing xanthophores (upper left), whereas hypothyroid fish wild-type for TRs lacked nearly all of these cells (upper right). By contrast, hypothyroid fish mutant for TRs developed substantial complements of these cells. Shown here are representative individuals homozygous for *thrab* mutation (lower left) and homozygous *thrab* individuals with somatically induced mutations for *thraa* (*) as well as doubly *thraa* and *thrab* individuals with somatically induced mutations for *thrab* (*thrab**; lower right). Fish are 11.5 SSL. (C, D) Homozygous *thrab* mutation partially rescued numbers of pigmented xanthophores and more fully rescued numbers of melanophores in hypothyroid fish. Somatic mutagenesis of *thraa* in fish homozygous mutant for *thrab* mutants (*thrab thraa**) did not significantly enhance the rescue of xanthophore maturation or melanophore numbers. By contrast somatic mutagenesis of *thrab* in fish doubly homozygous mutant for *thraa* and *thrab* (*thrab thraa thrb**) rescued xanthophore maturation to wild-type levels in the absence of TH. Numbers of visible xanthophores and melanophores were not distinguishable between euthyroid fish wild-type or homozygous mutant for TR mutations either singly or in combination ($P>0.1$), and are shown combined here. Box plots as in **Figure 6C** with different letters above data indicating significant differences in *post hoc* comparisons (Tukey HSD, $P<0.05$). (Cell counts in supplementary file **Figure 7—Source Data 1**.)

Figure 7—figure supplement 1. Zebrafish TR gene expression and mutants. (A) RT-PCR for *thraa*, *thrab*, and *thrbc* in xanthophores and melanophores sorted by FACS for *aox5:palmEGFP* and *tyrp1b:palm-mCherry*, respectively. (B) Sanger sequencing of CRISPR/Cas9-induced mutant allele of *thrab* revealed a 13 bp deletion. (C) Schematic of Thrab wild-type and mutant proteins illustrating introduction of a novel amino acid followed by a premature stop codon at position 73. DBD, DNA binding domain; LBD, ligand binding domain. (D) Additional CRISPR/Cas9 mutant alleles for *thraa* and *thrbc* had phenotypes indistinguishable from wild-type or *thrab* (**Figure 7A**). (E) Xanthophore color phenotypes of euthyroid and hypothyroid wild-type fish, and rescue of xanthophore color in hypothyroid fish upon TR mutation (*thrab thraa thrb**). (F) HPLC revealed persisting carotenoids in hypothyroid fish mutant for *thrab* (boxed region), in contrast to the absence of detectable carotenoids in hypothyroid fish that were wild-type for *thrab* (**Figure 6D**). (G) Stage of first xanthophore appearance did not differ significantly ($P=0.7$) between euthyroid fish that were heterozygous or homozygous wild-type for *thrab* mutation.

Figure 8. Model of TH dependence in zebrafish pigment cell lineages. (A) Post-embryonic progenitor-derived, specified adult melanoblasts (Mb) that expand their population and differentiate to a state of proliferative cessation (McMenamin et al., 2014), binucleate state, and EL-derived cryptic xanthophores that redifferentiate as carotenoid-containing yellow/orange adult xanthophores. Disparate cell-type specific outcomes in fish lacking TH reflect differences in events required for maturation between sublineages. (B) TH-dependent lineage maturation involves a double negative gate, with essential repressive effects of unliganded TR.

Supplementary File 1. Interactive 3-dimensional UMAP representation of transcriptomic space. Cells are colored by type corresponding to **Figure 2A**.

Supplementary File 2—scRNA seq analyses.

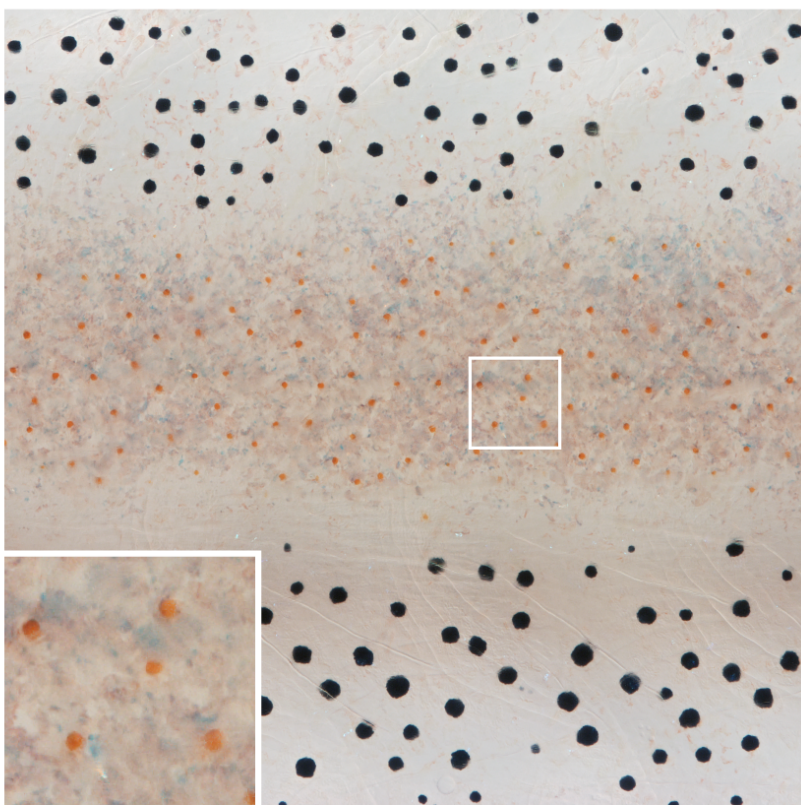
Table 1. Genes enriched in specific cell types from post-embryonic NC derivatives.

Table 2. Genes from BEAM analysis of pigment cell lineages. Genes corresponding to rows in Fig. 2e by cluster.

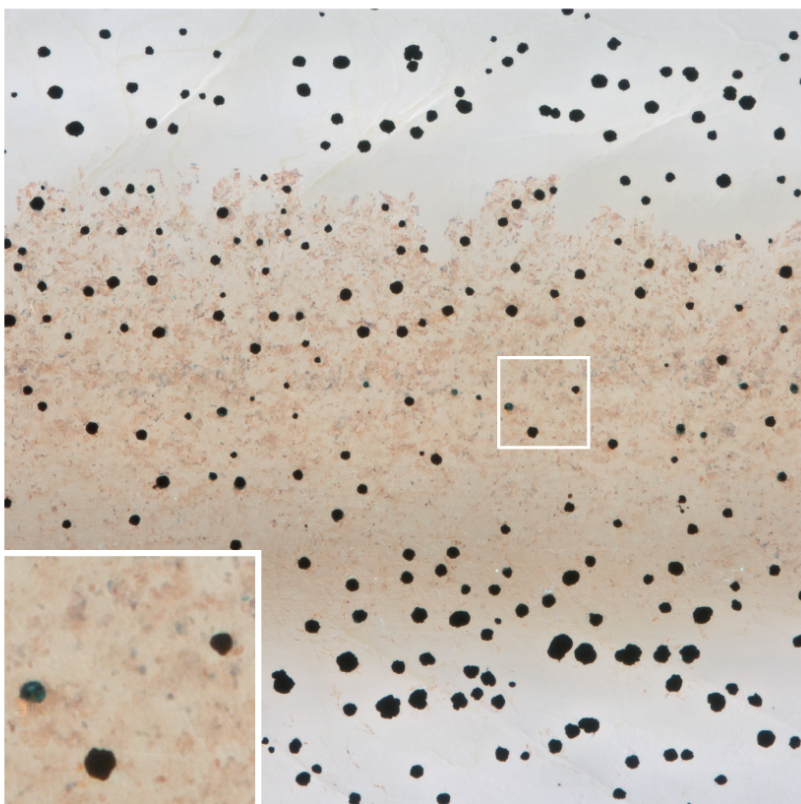
1338 Table 3. scRNA-seq sample information.
1339 Table 4. Signature score genes.
1340 Table 5. Ordering genes used as input for Monocle trajectory analysis.
1341 Table 6. TH-dependent genes over pseudotime in melanophores. Genes correspond to clusters in
1342 extended data figure 12. Highlighted genes are have published roles in melanophores (with associated
1343 PMIDs).
1344 Table 7. sgRNA and oligonucleotide sequences.
1345
1346 **Source Data 1.** Lysotracker FACS data corresponding to **Figure 5—figure supplement S1C and D.**
1347
1348 **Source Data 2.** Melanophore binucleation incidence data corresponding to **Figure 5—figure supplement**
1349 **S1E.**
1350
1351 **Source Data 3.** Melanin content data corresponding to **Figure 5C.**
1352
1353 **Source Data 4.** Melanophore binucleation incidence data corresponding to **Figure 5E.**
1354
1355 **Source Data 5.** Xanthophore lipid droplet incidence corresponding to **Figure 6—figure supplement 2A.**
1356
1357 **Source Data 6.** Counts for xanthophores and melanophores corresponding to **Figure 7C and D.**
1358
1359
1360
1361

A

euthyroid



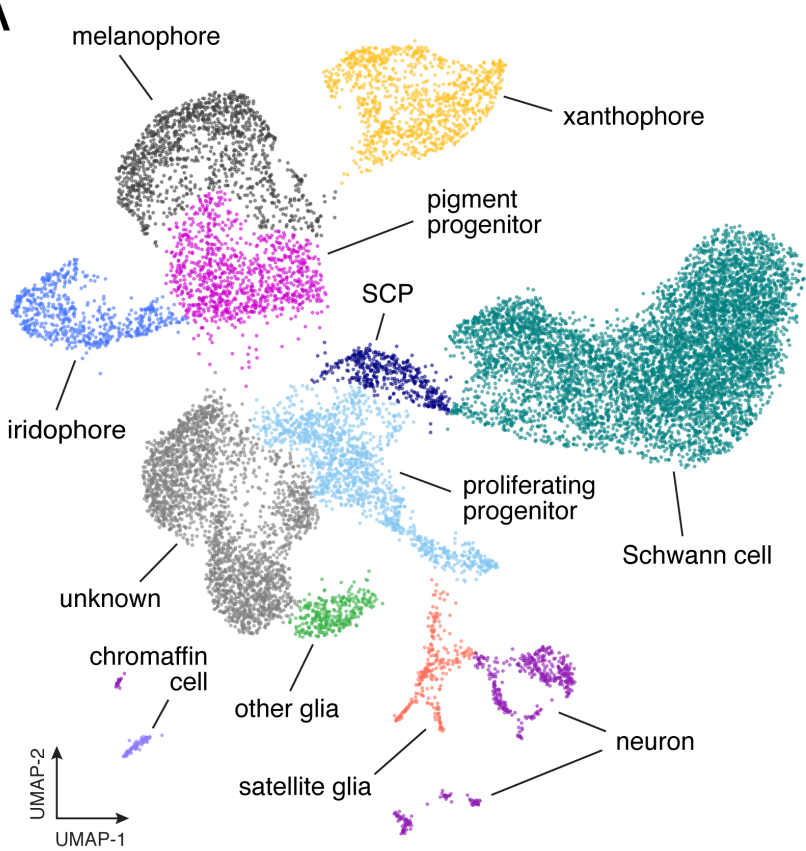
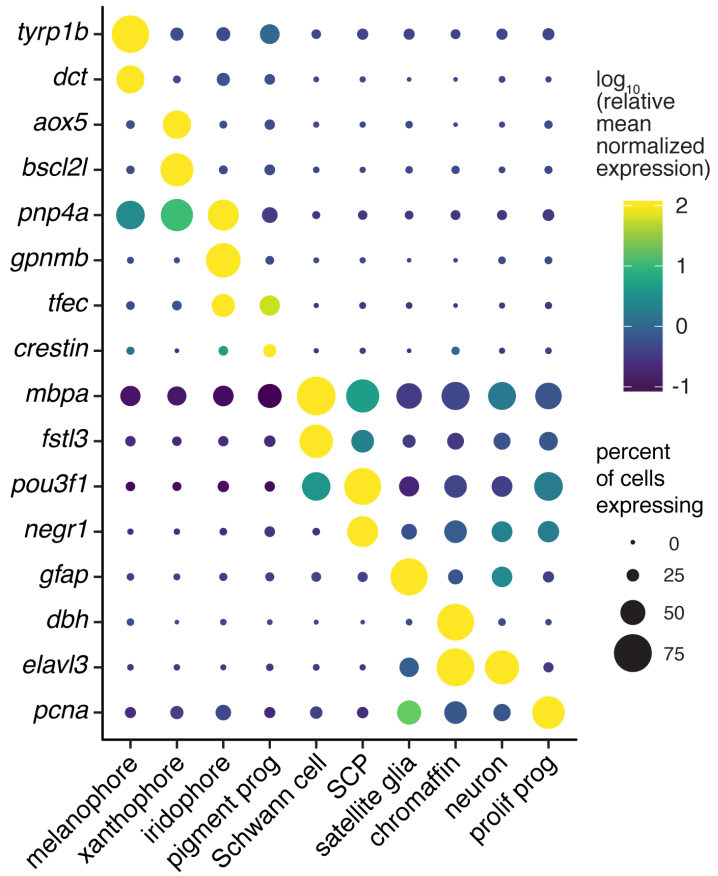
hypothyroid

**B**

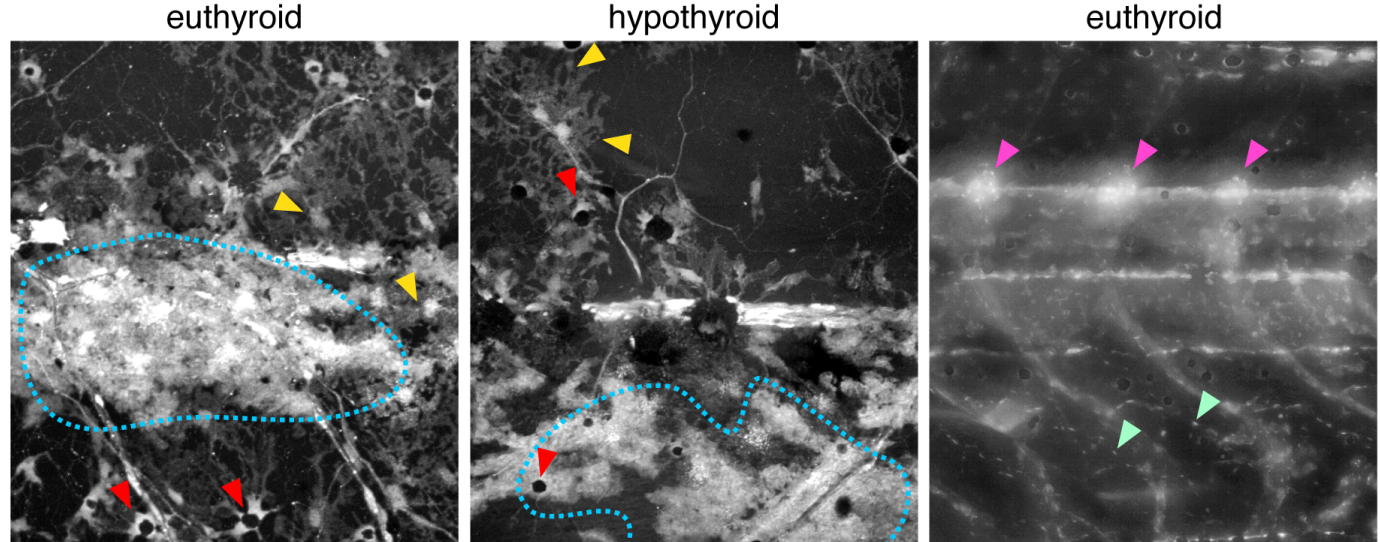
(i) specification bias



(ii) lineage discordance

A**B**

A

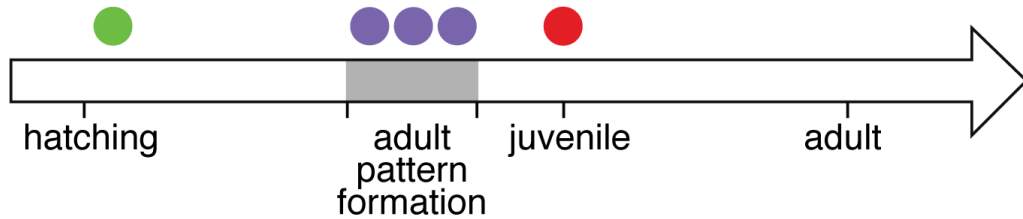


B

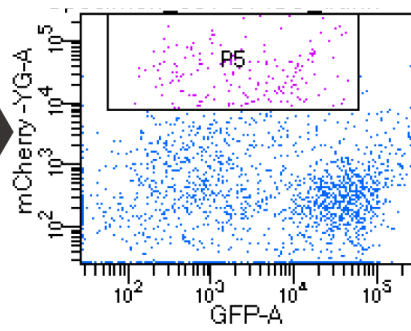
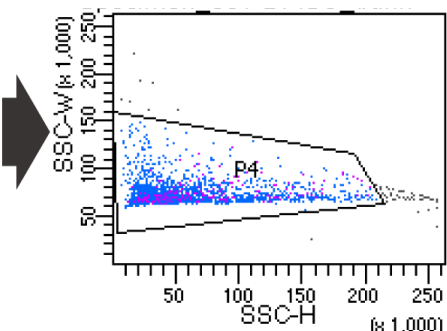
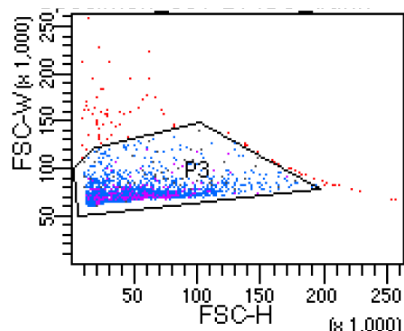
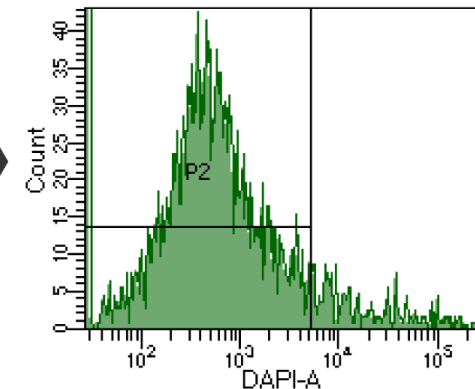
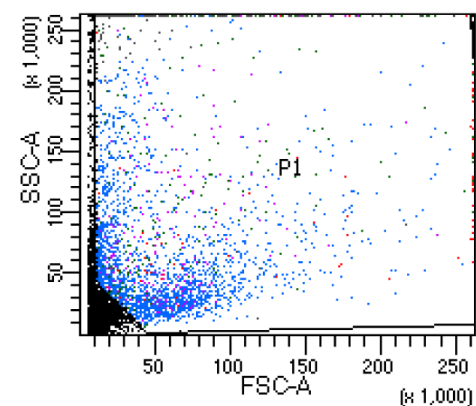
euthyroid	✓				
hypothyroid	—	✓	✓	—	—
~ age (dpf)	5	12–25	28	60+	
stage (SSL)	3.5	7.2–9.6	11	20+	

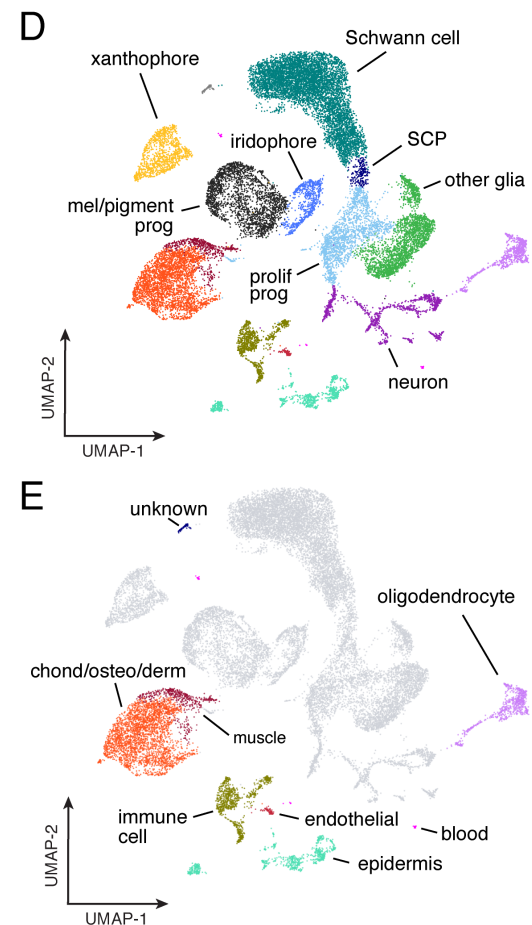
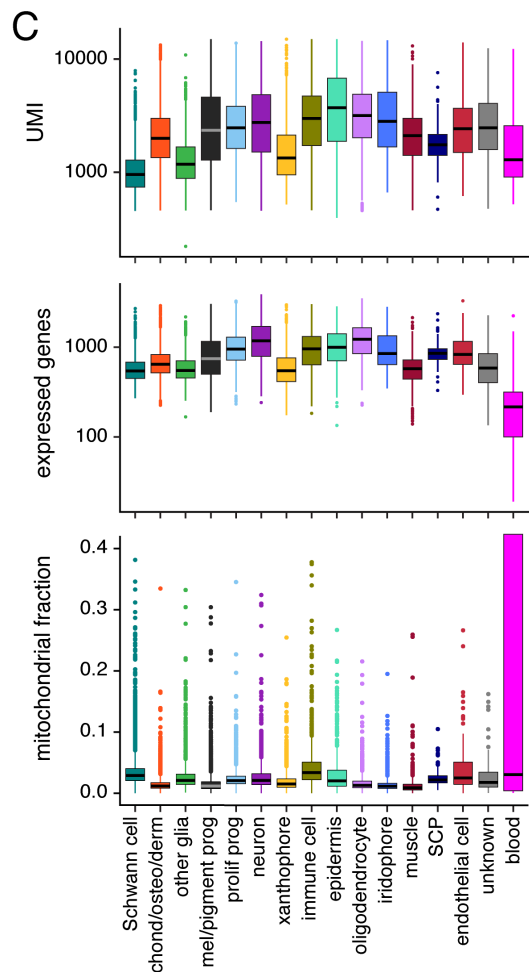
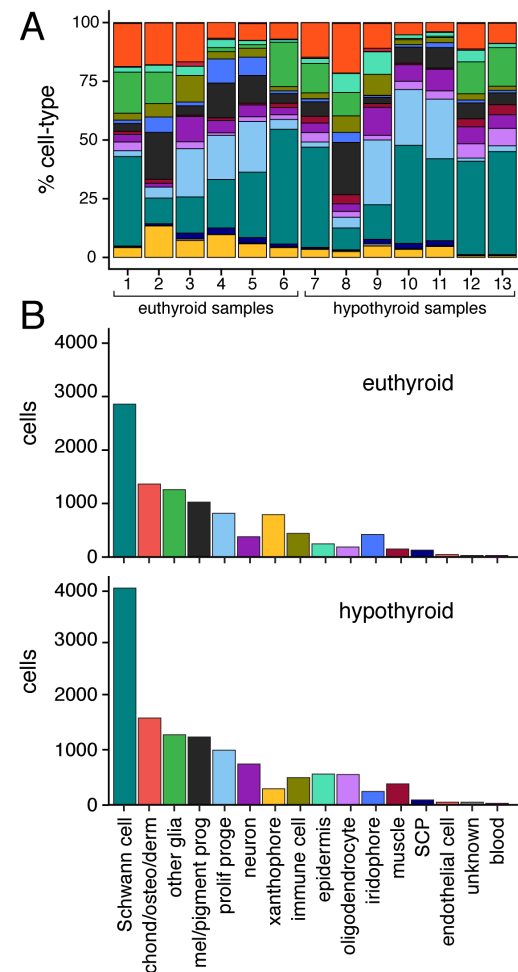


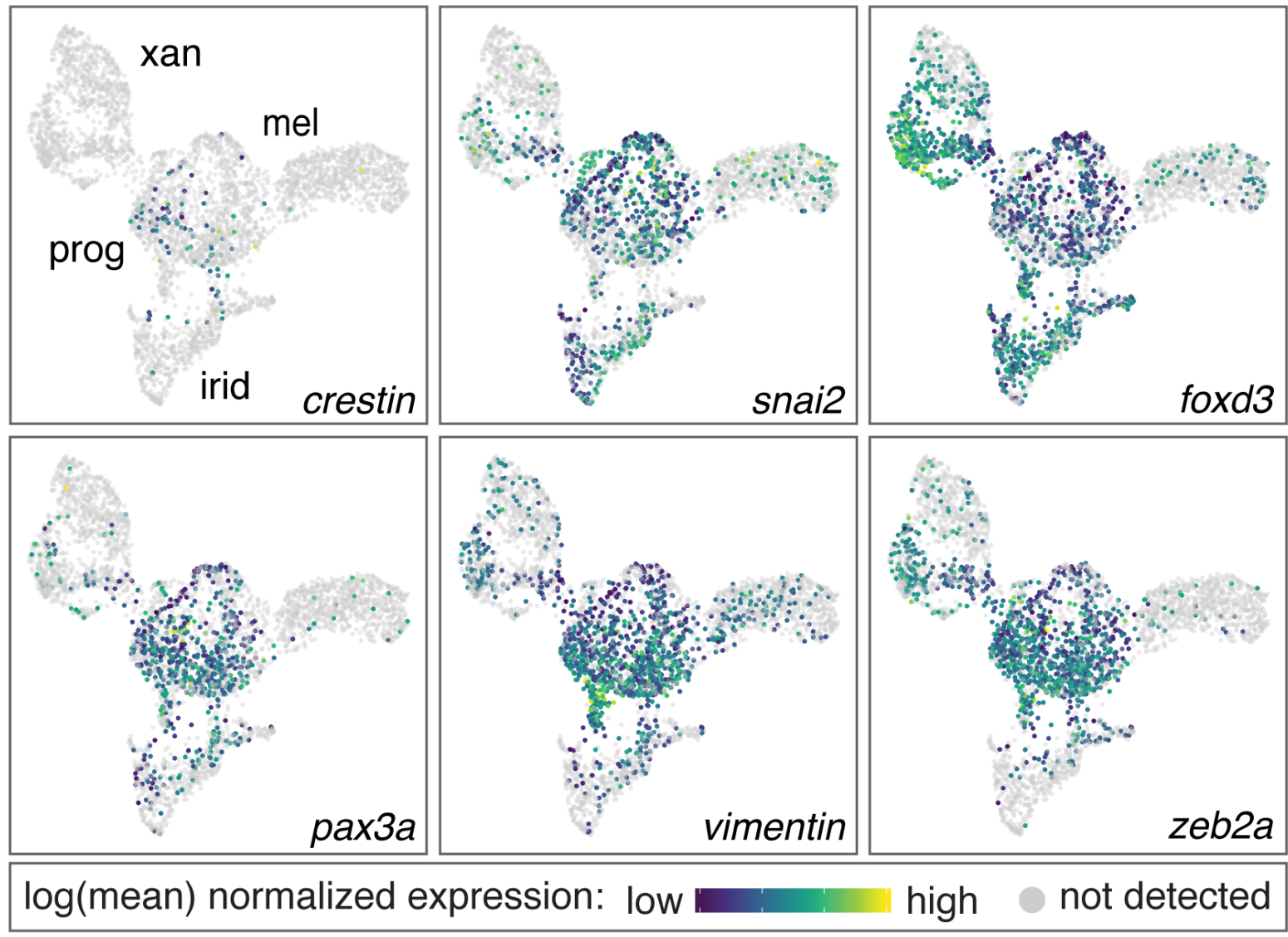
sampling

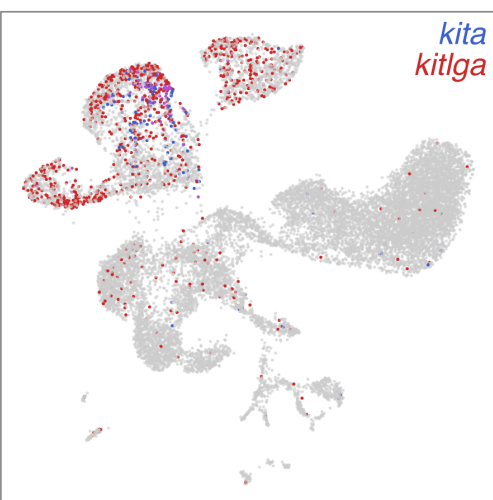
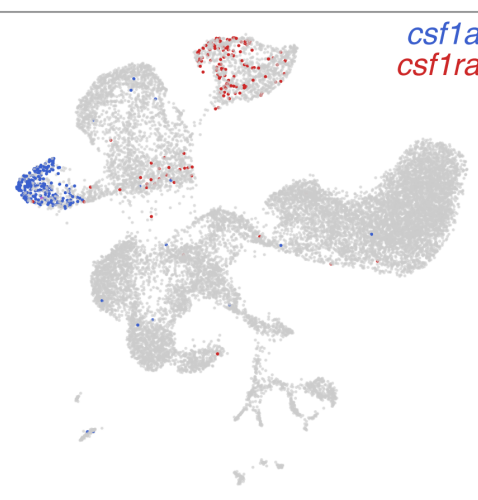
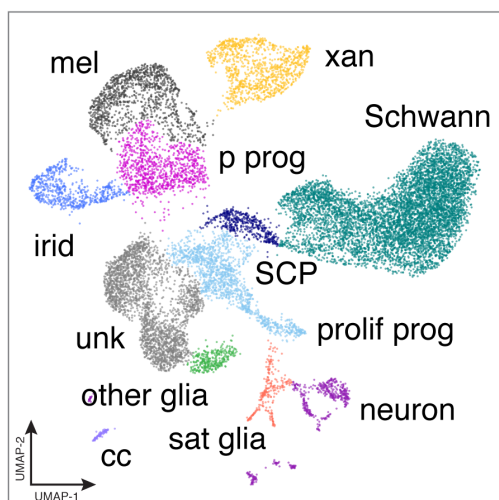
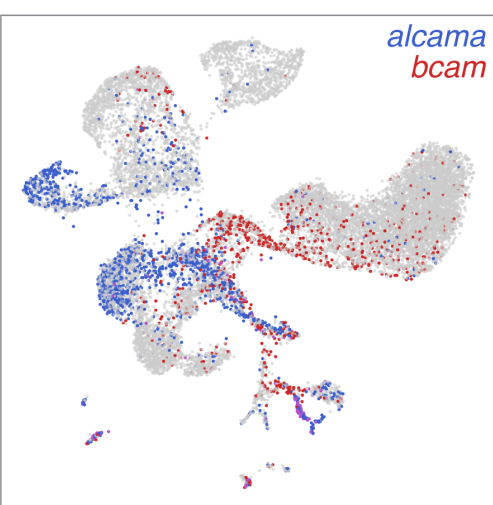
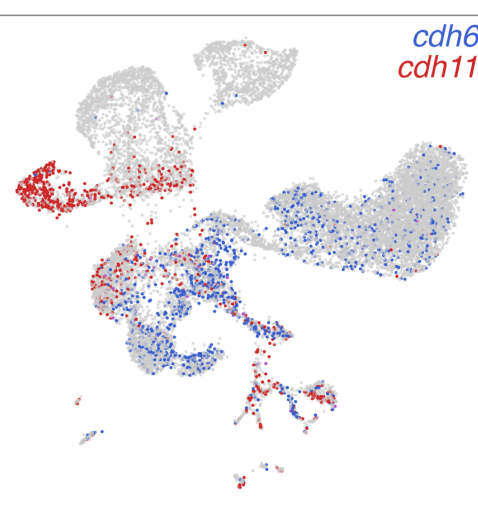
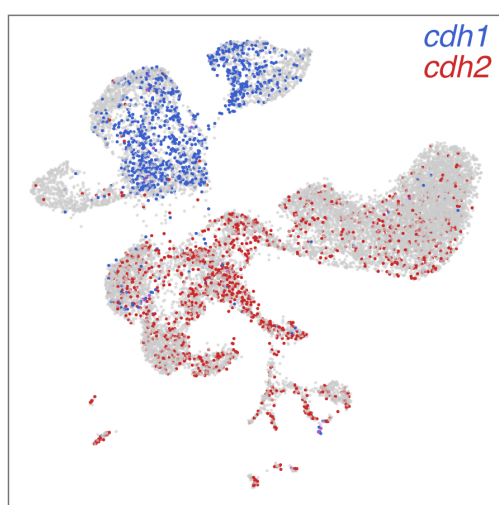
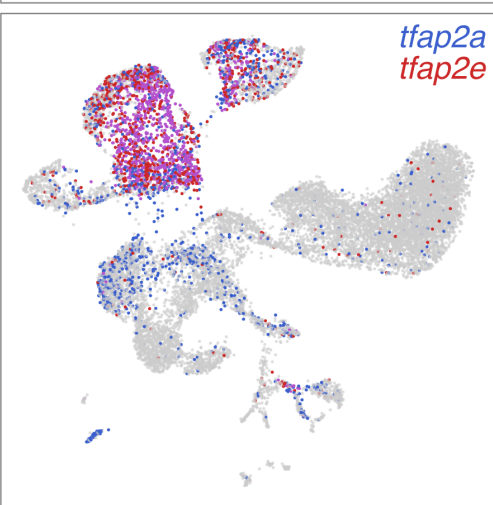
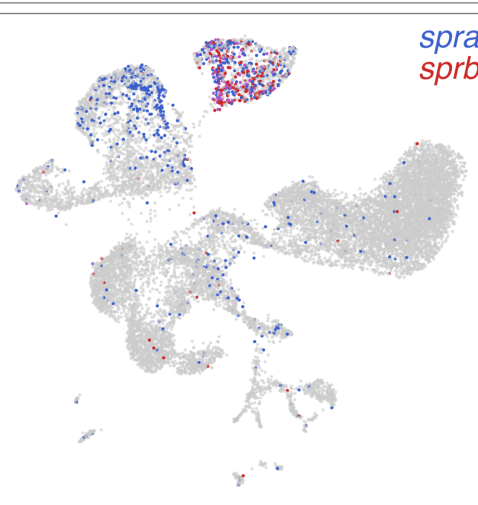
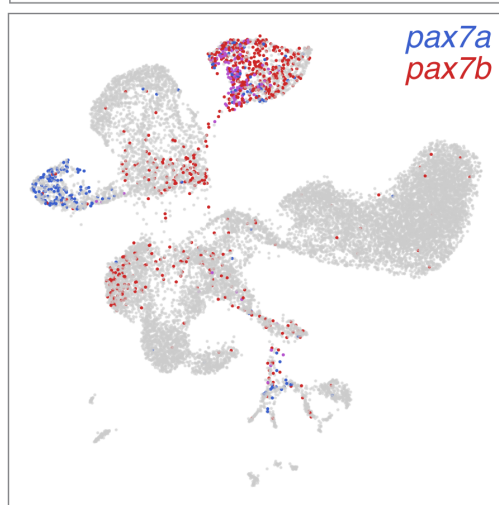
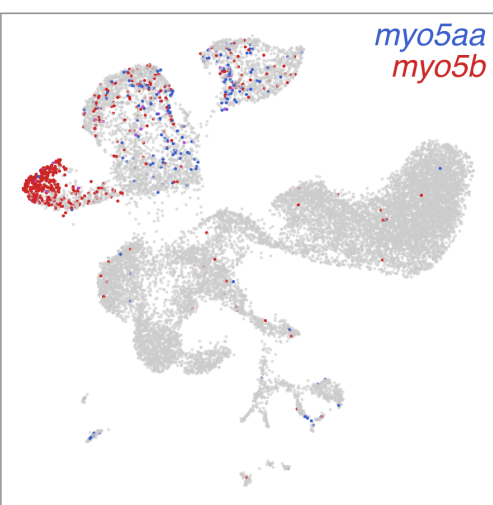
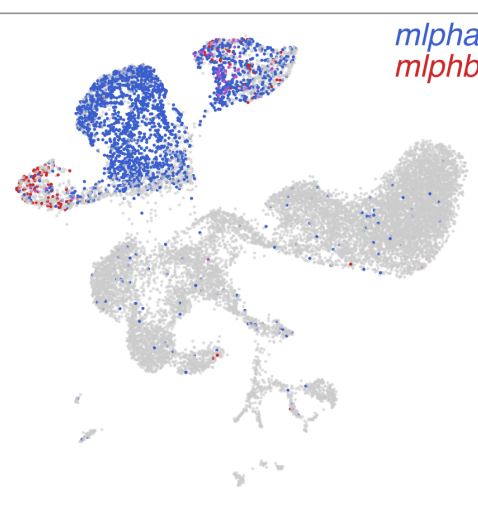
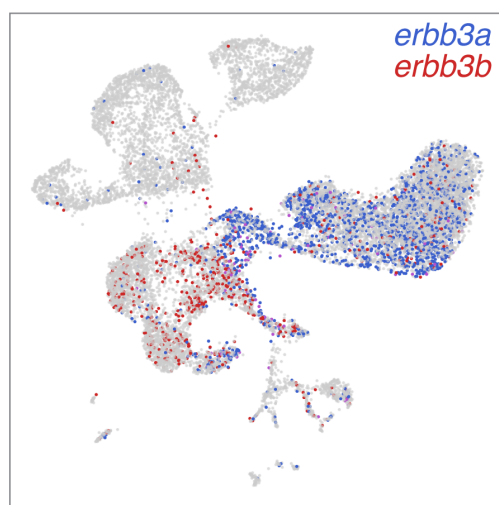


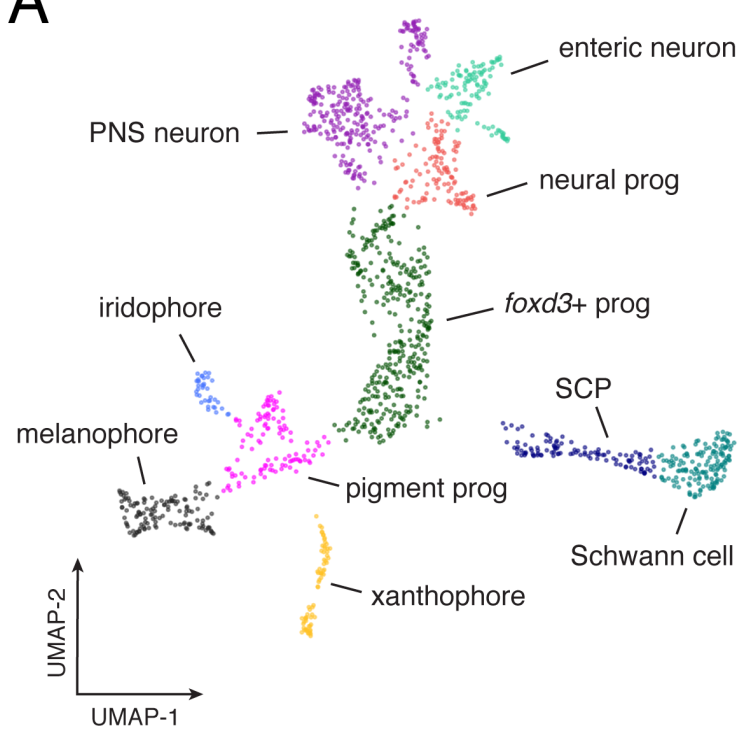
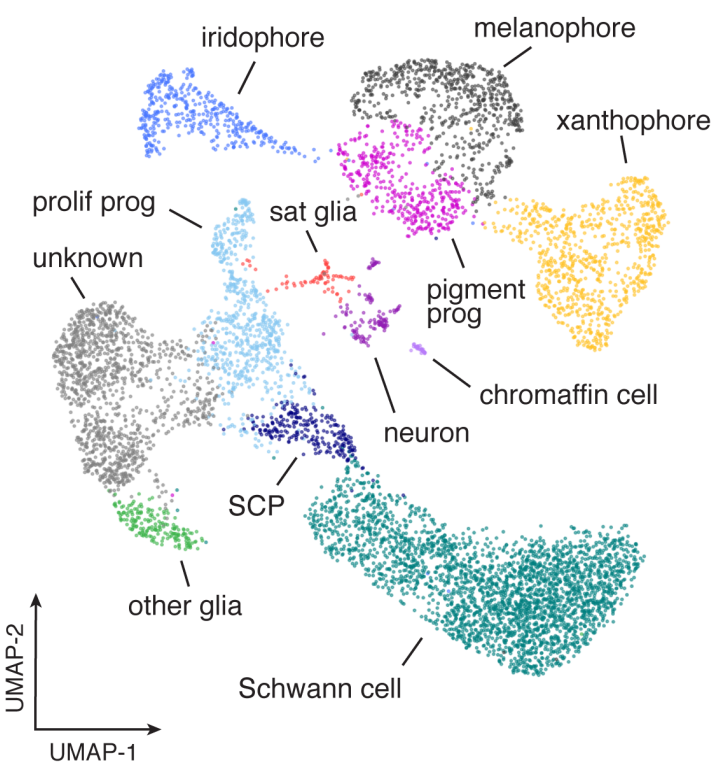
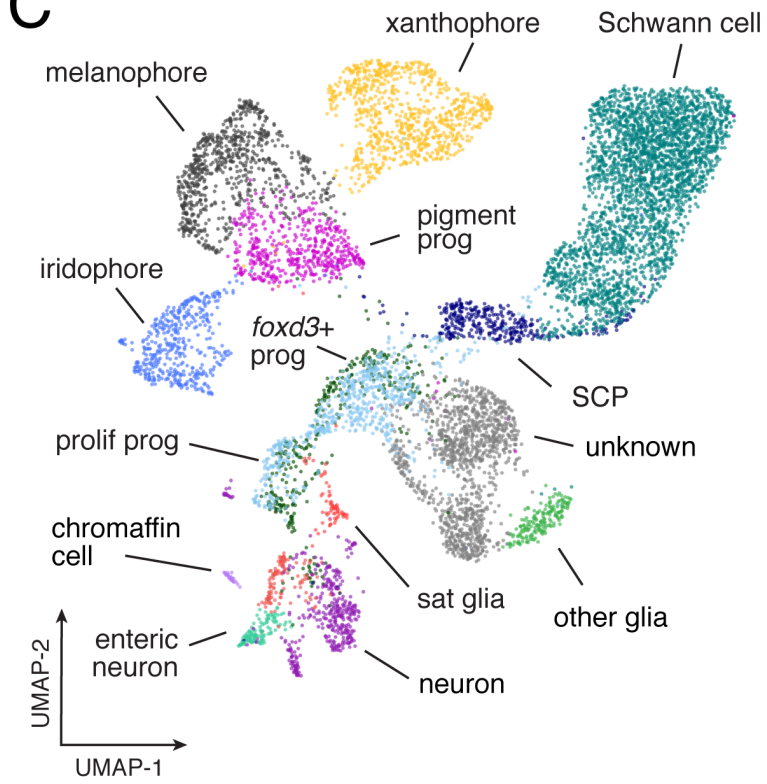
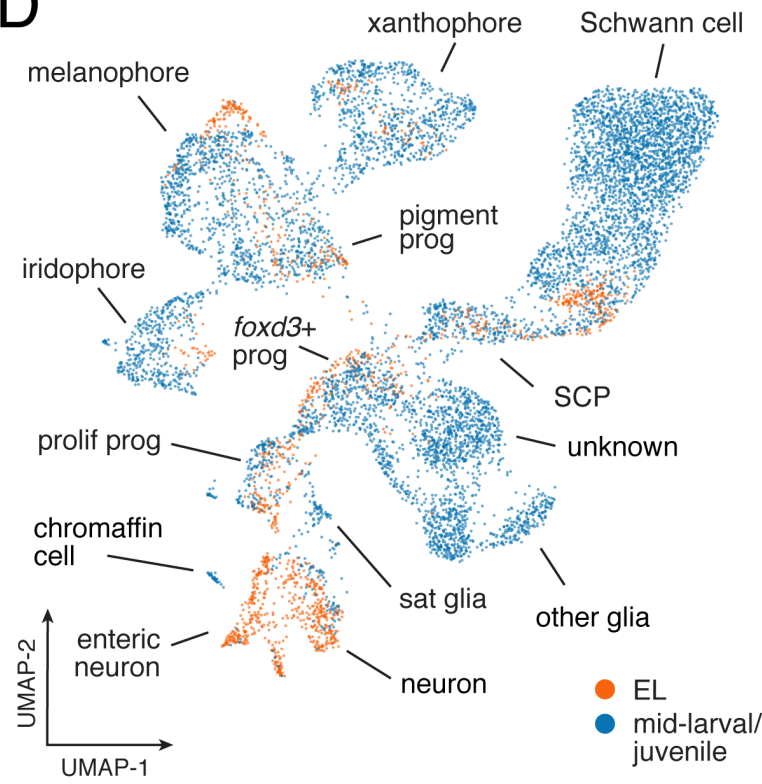
C

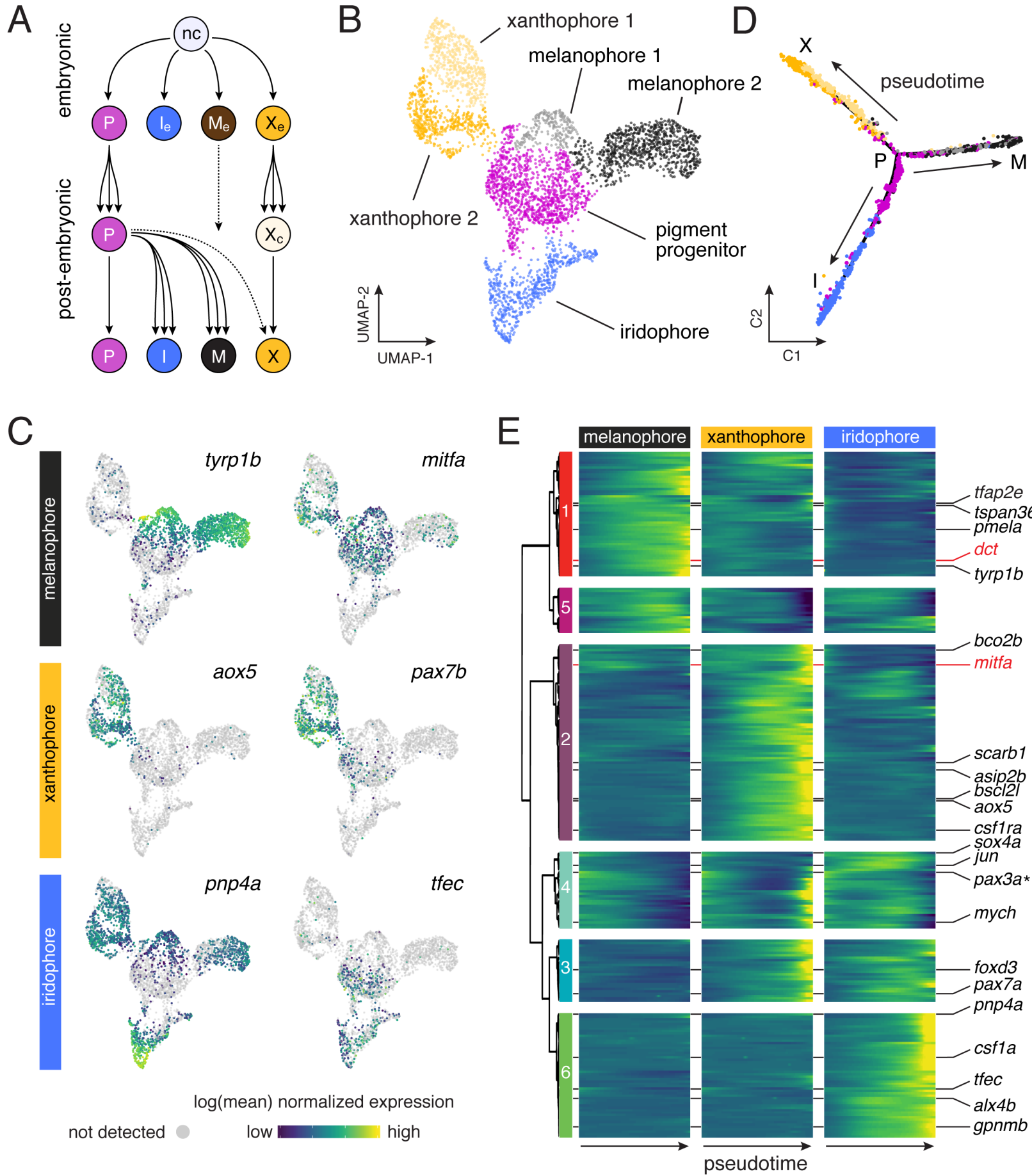


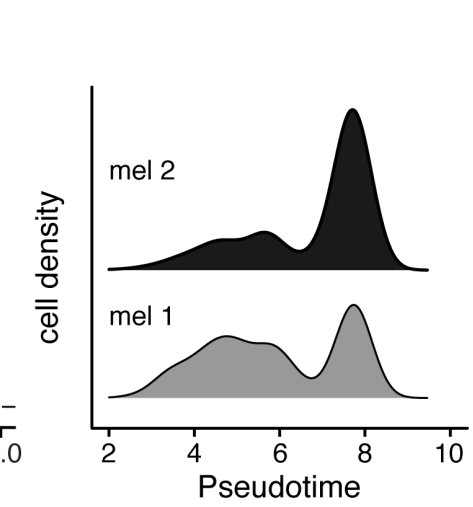
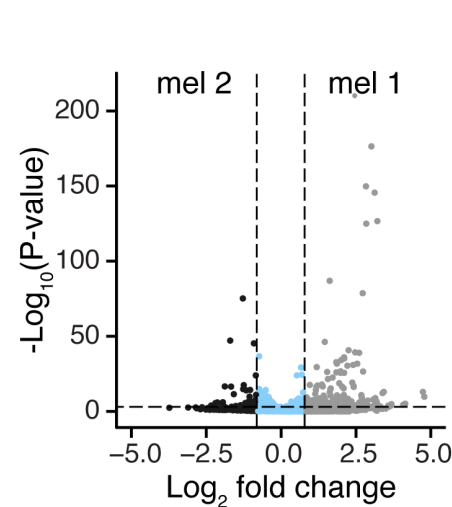
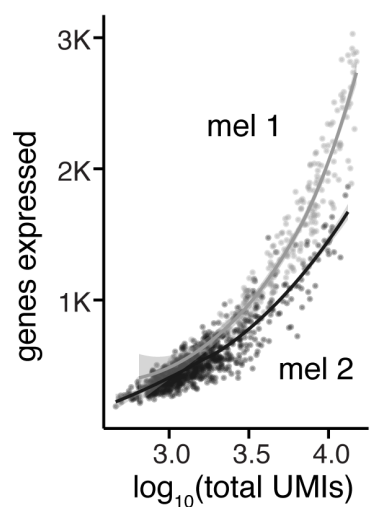
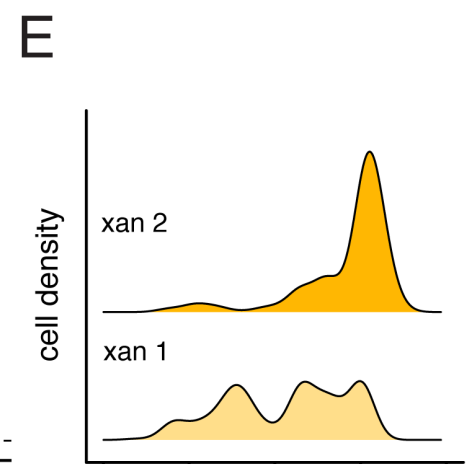
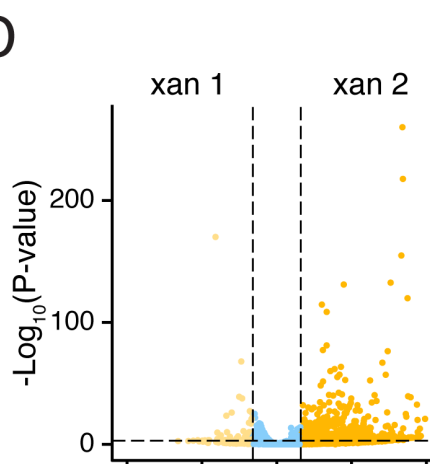
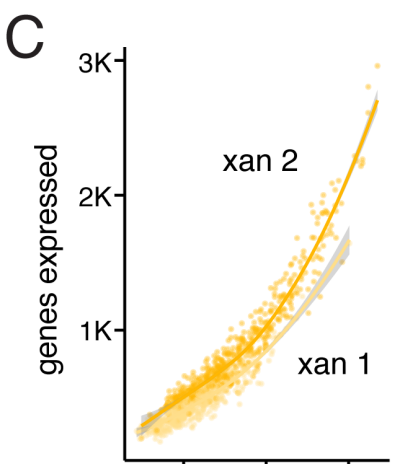
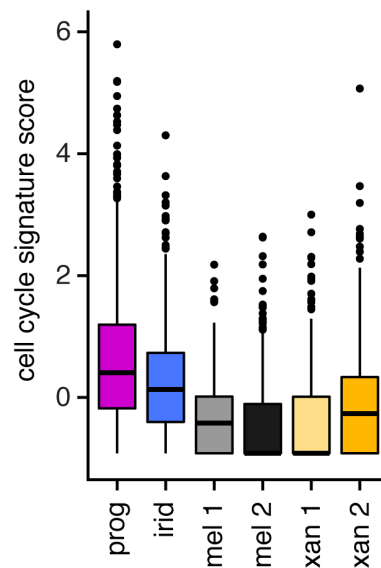
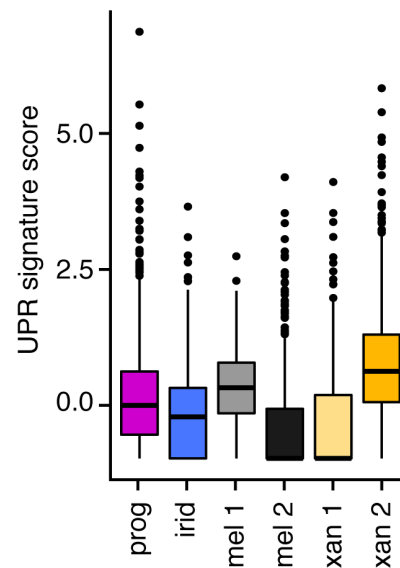
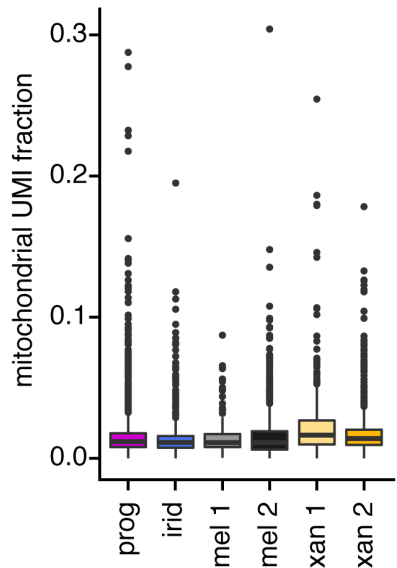
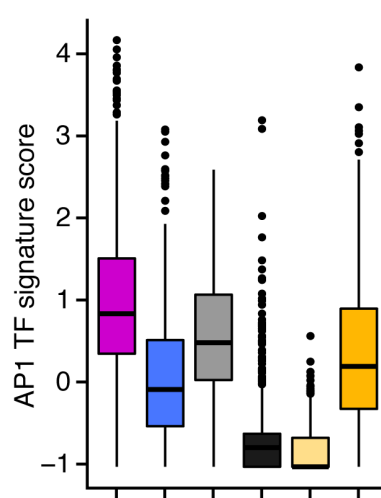
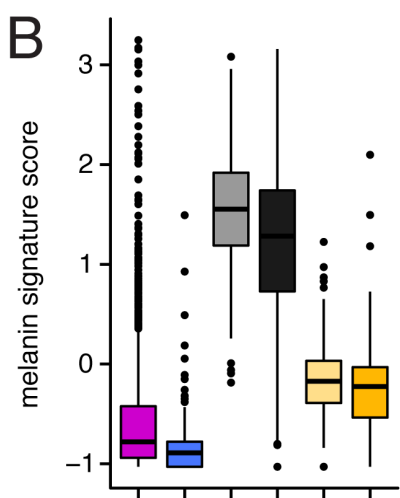
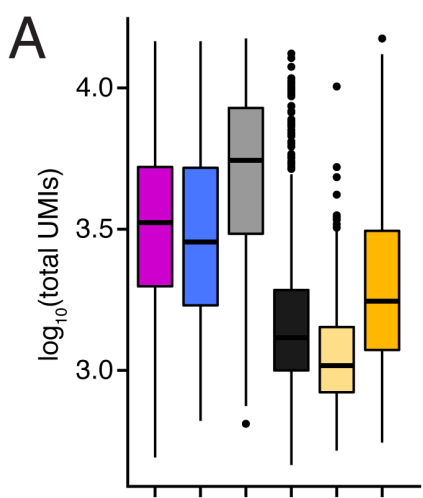




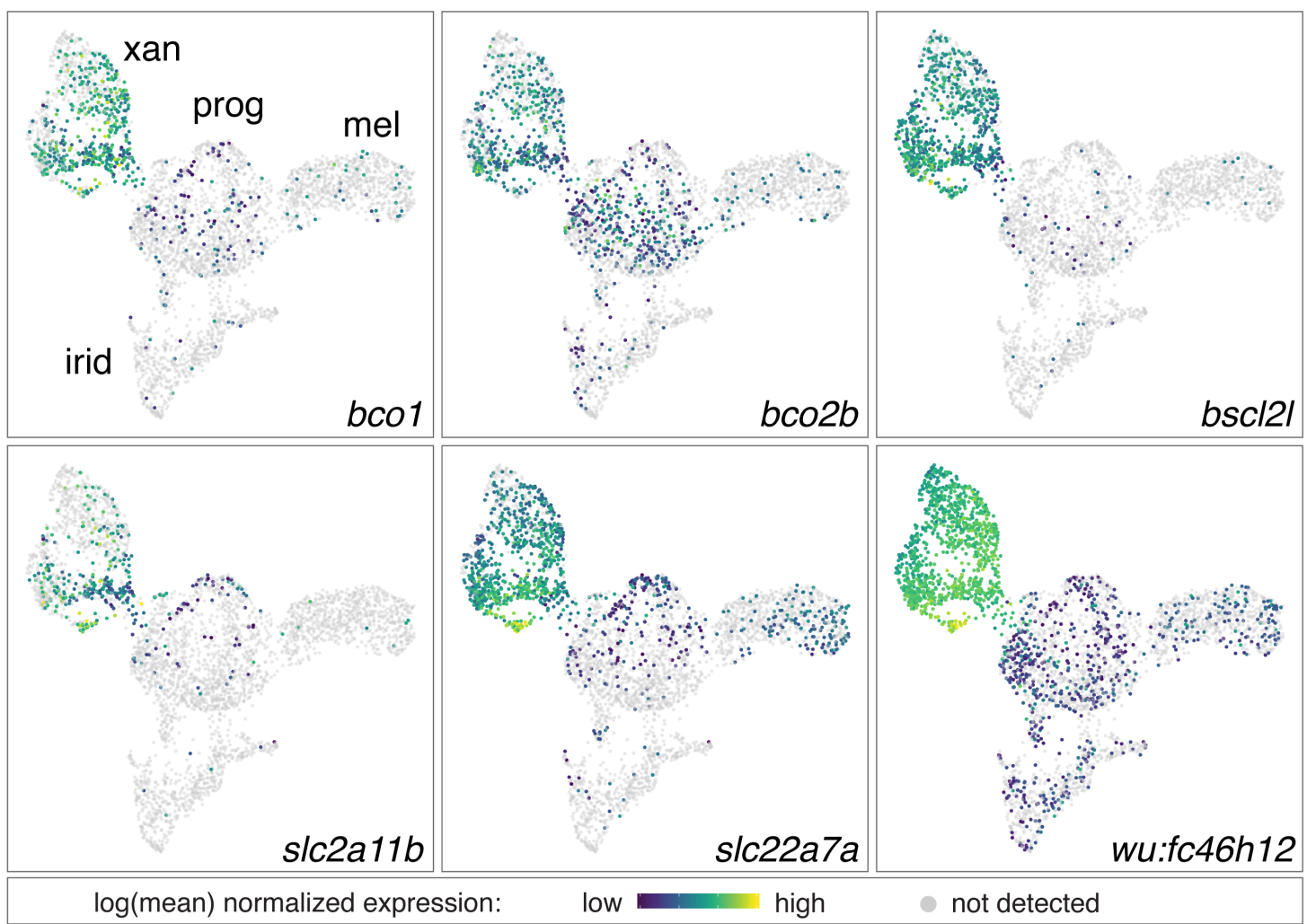
A**B****C**

A**B****C****D**



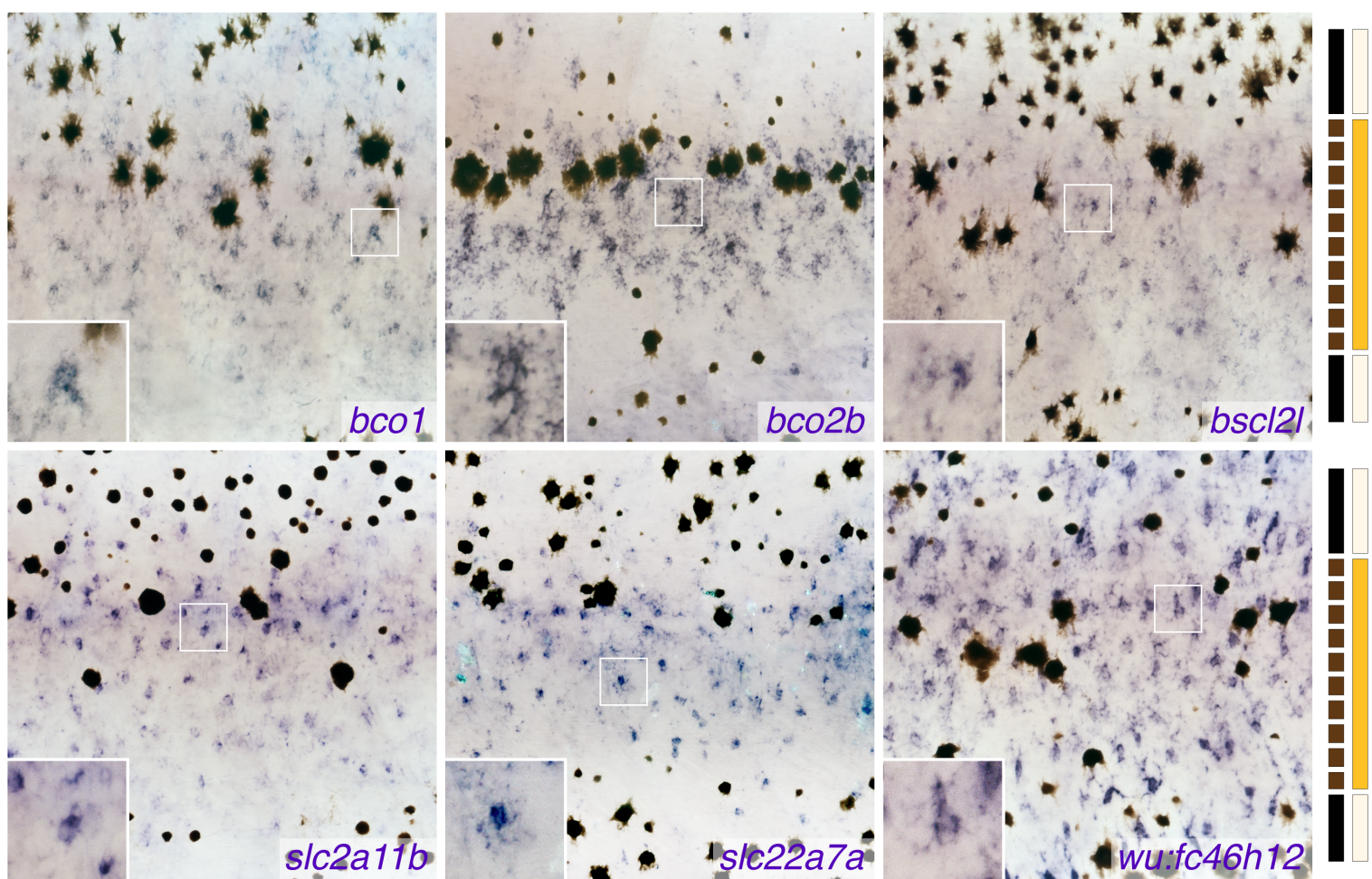


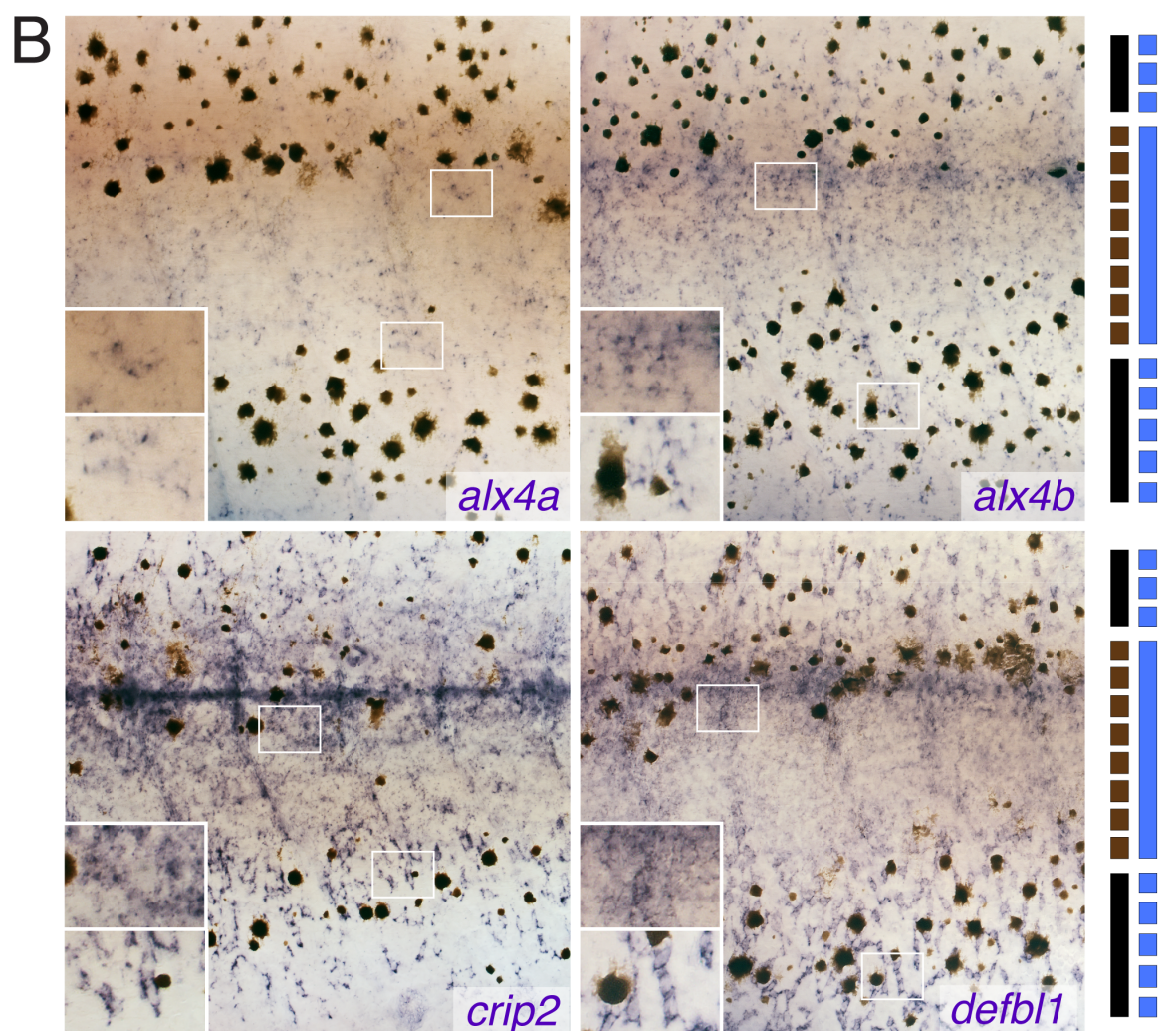
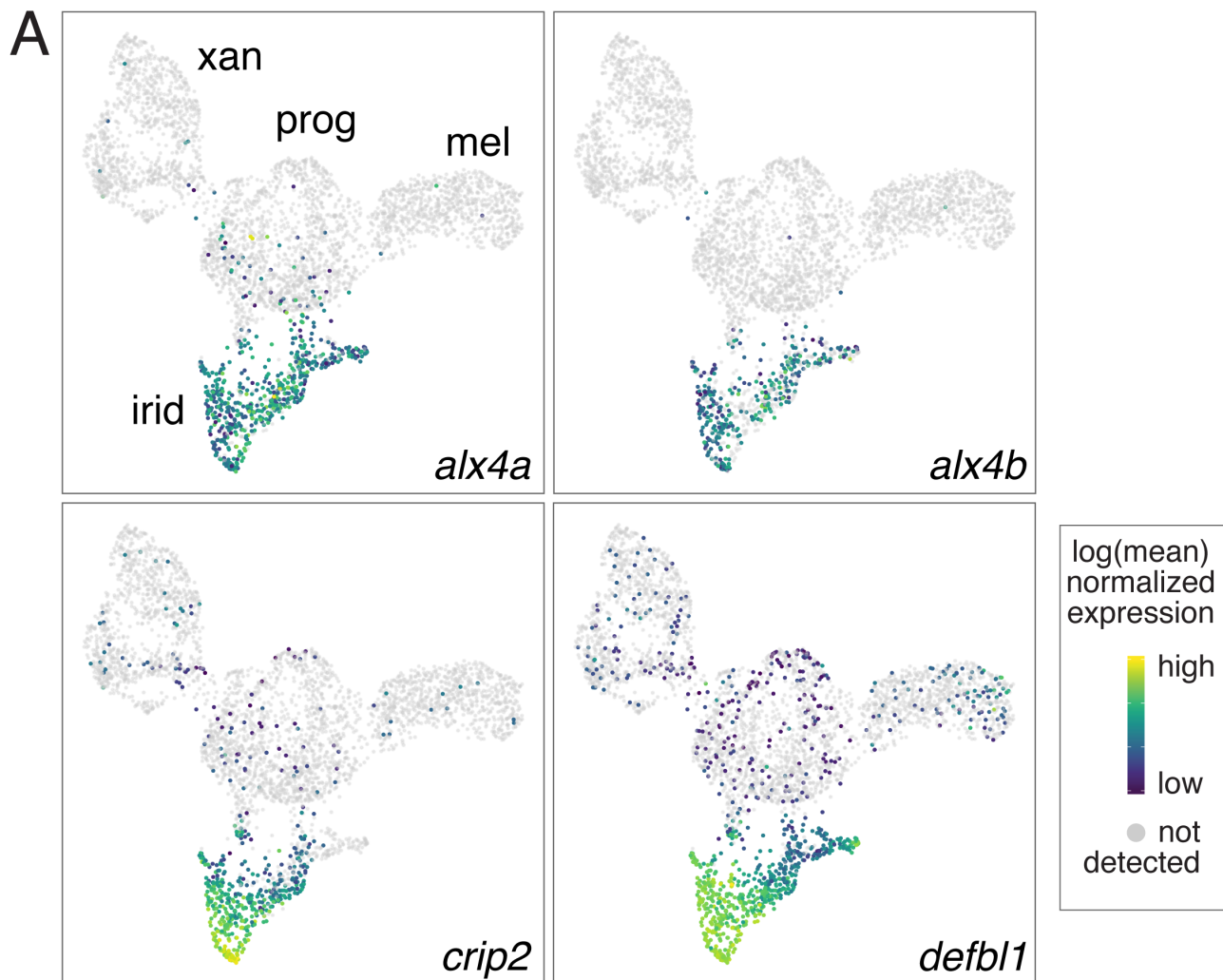
A

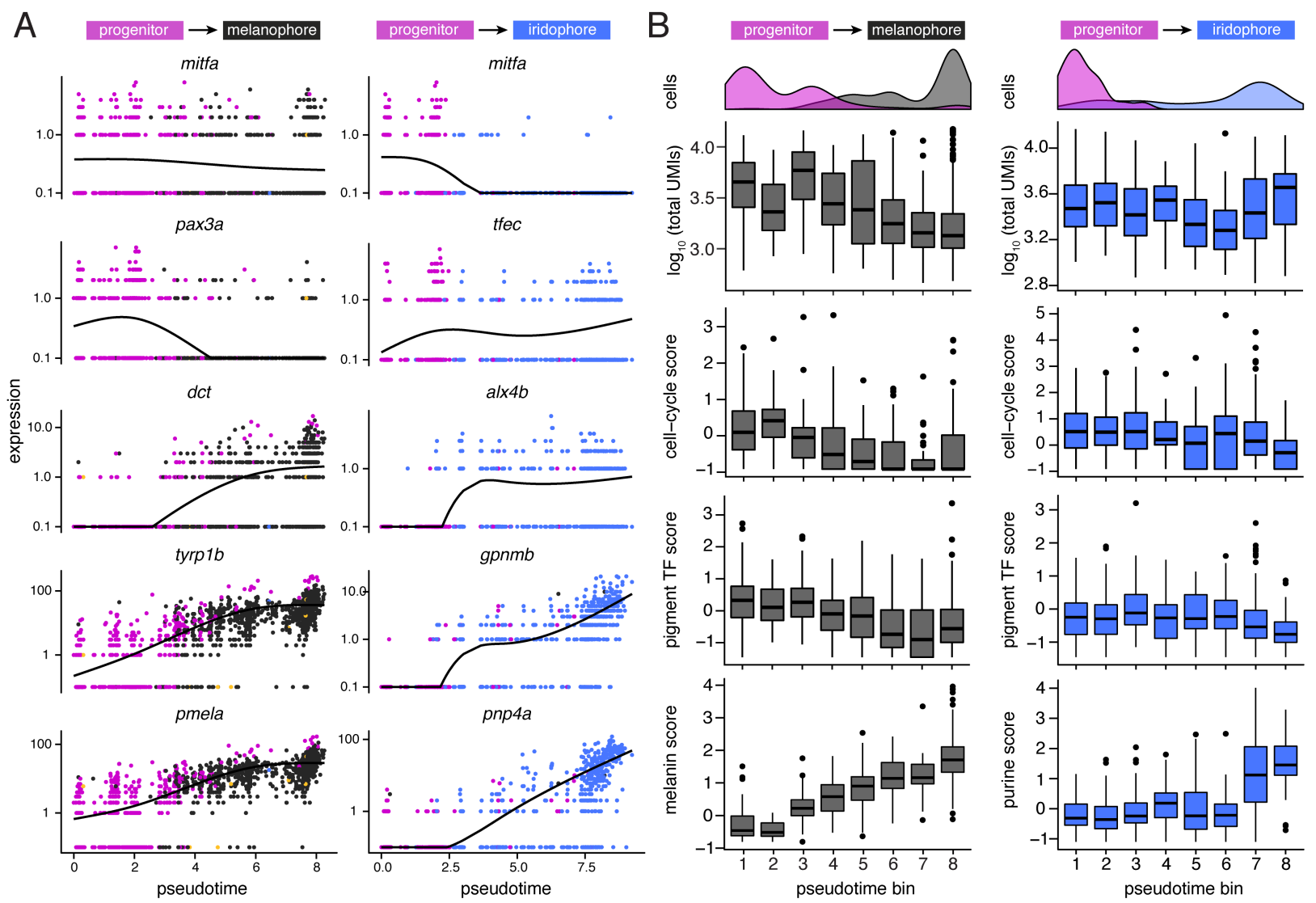


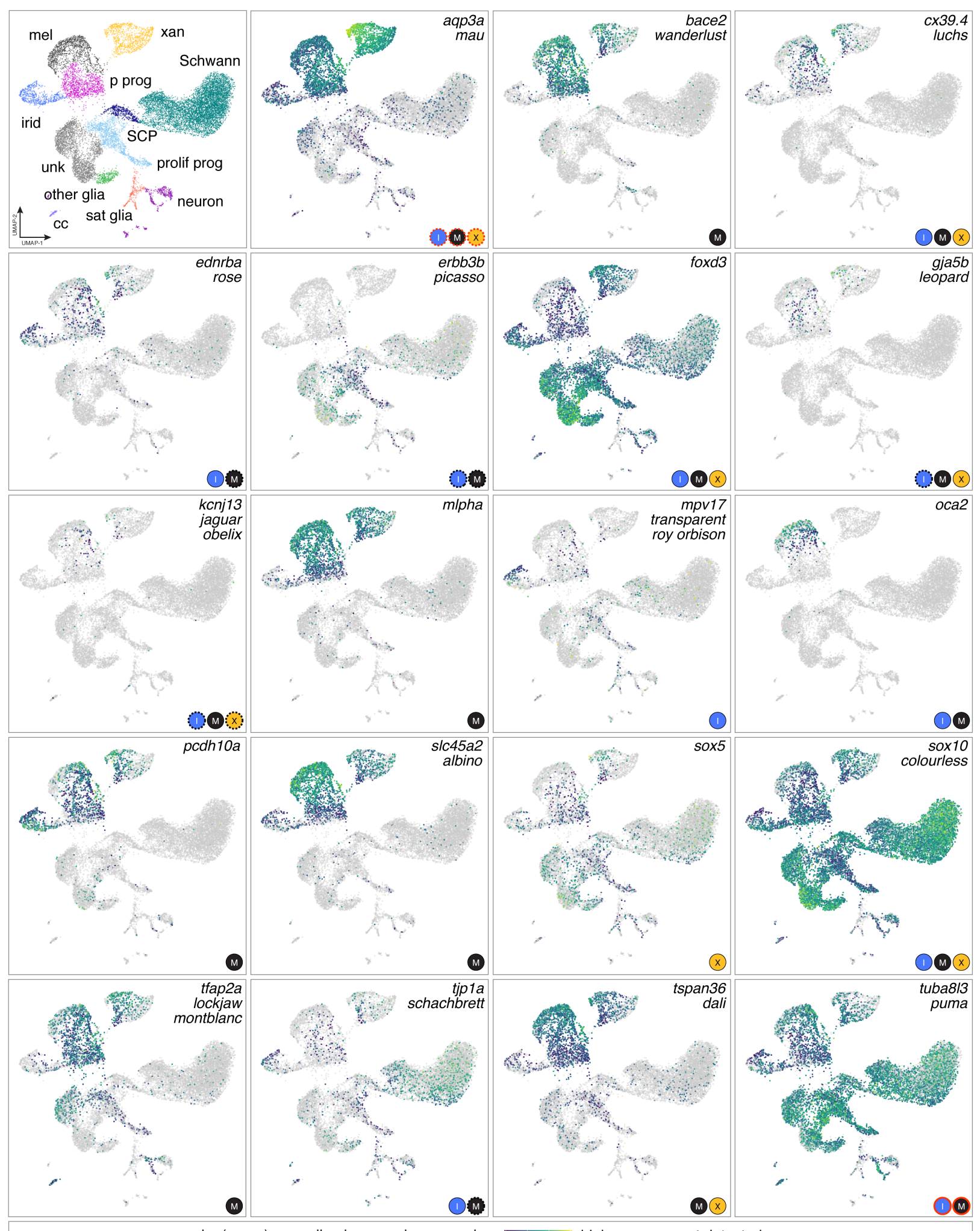
log(mean) normalized expression: low high ● not detected

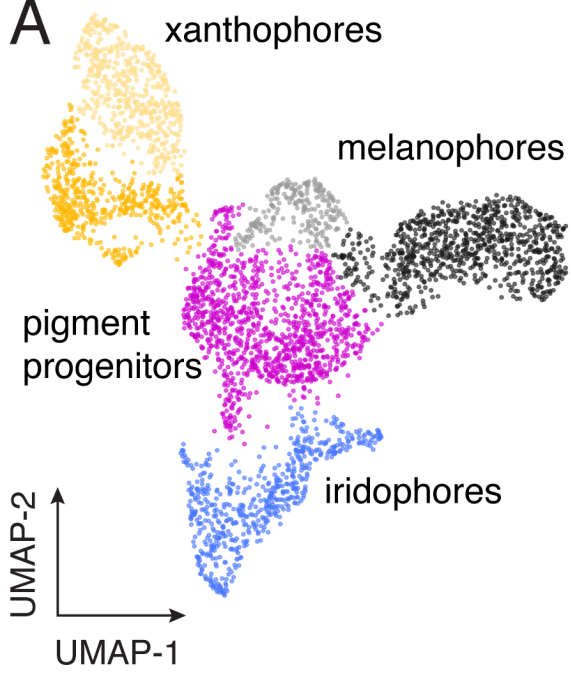
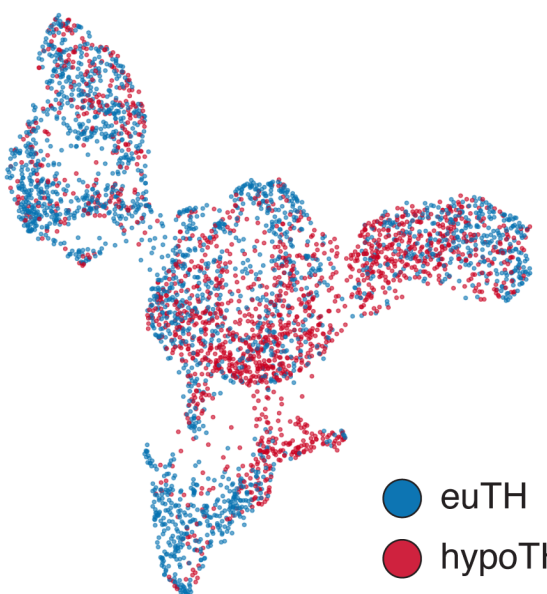
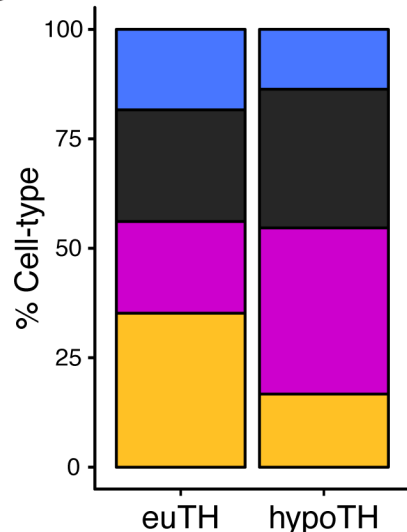
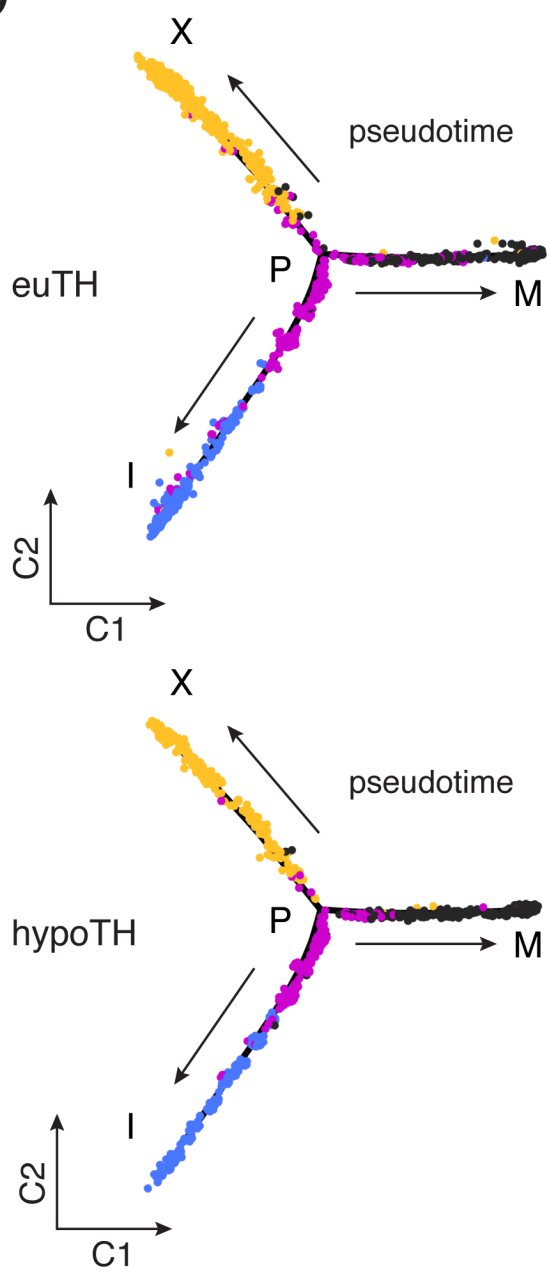
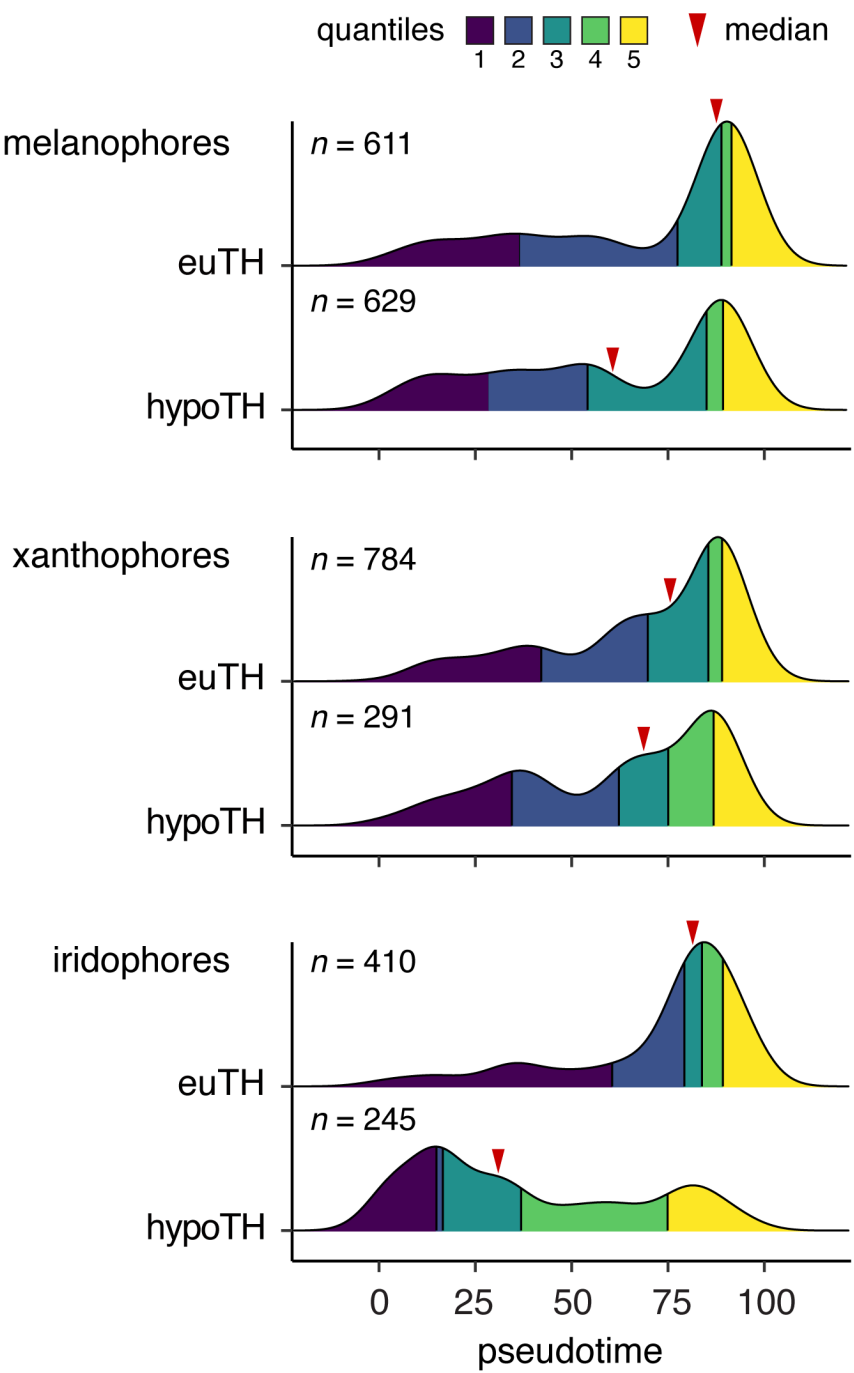
B

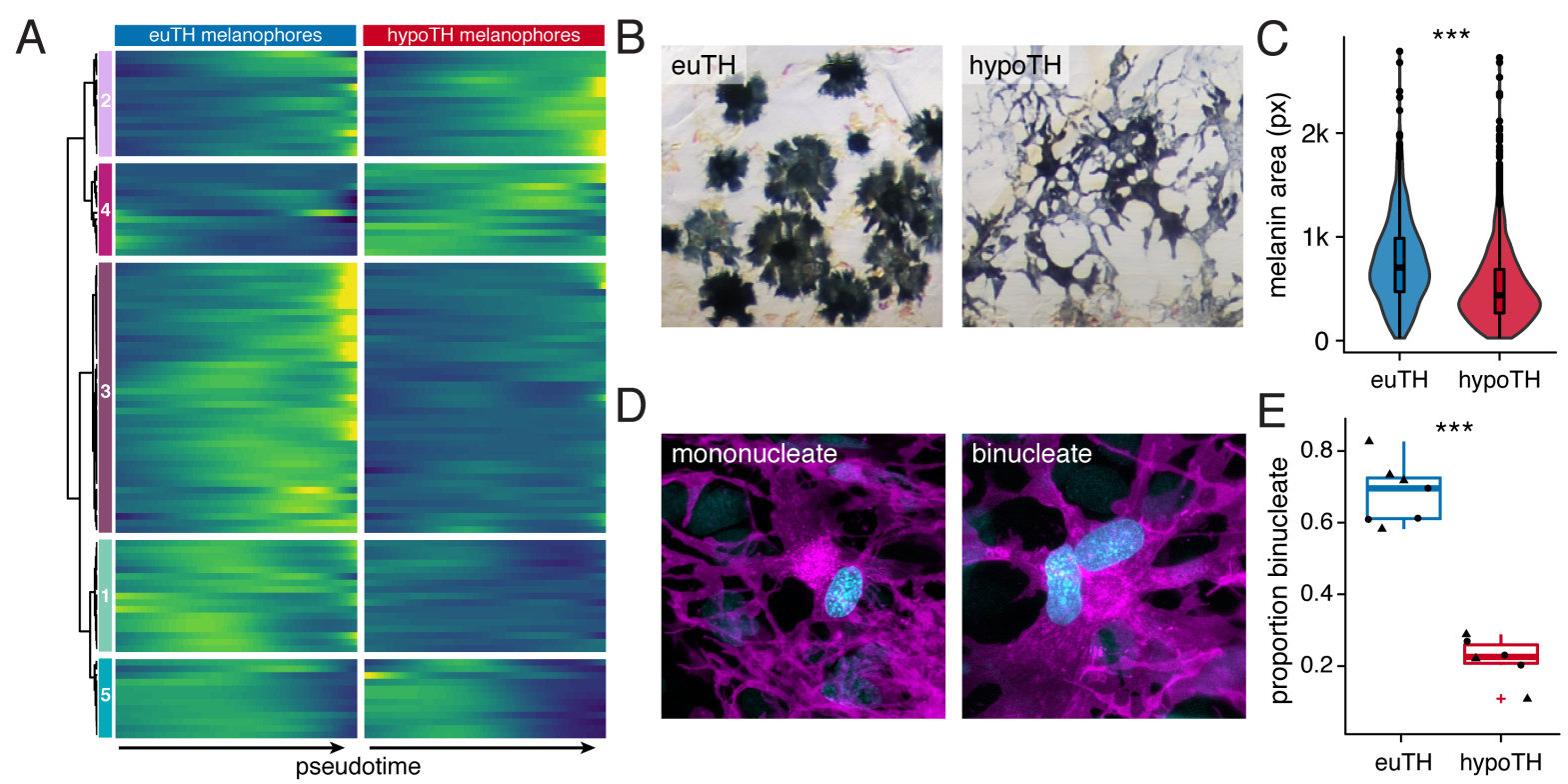


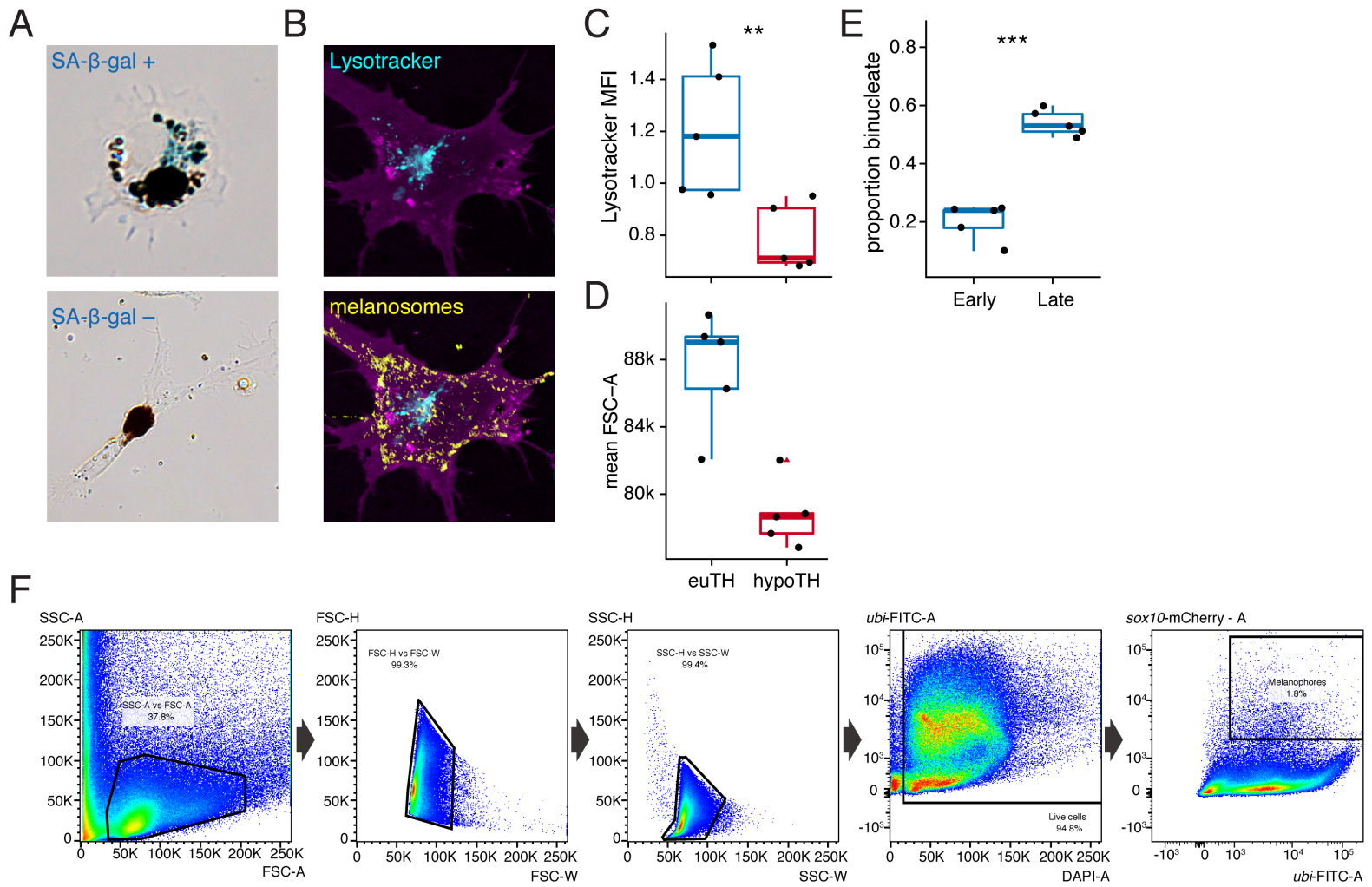


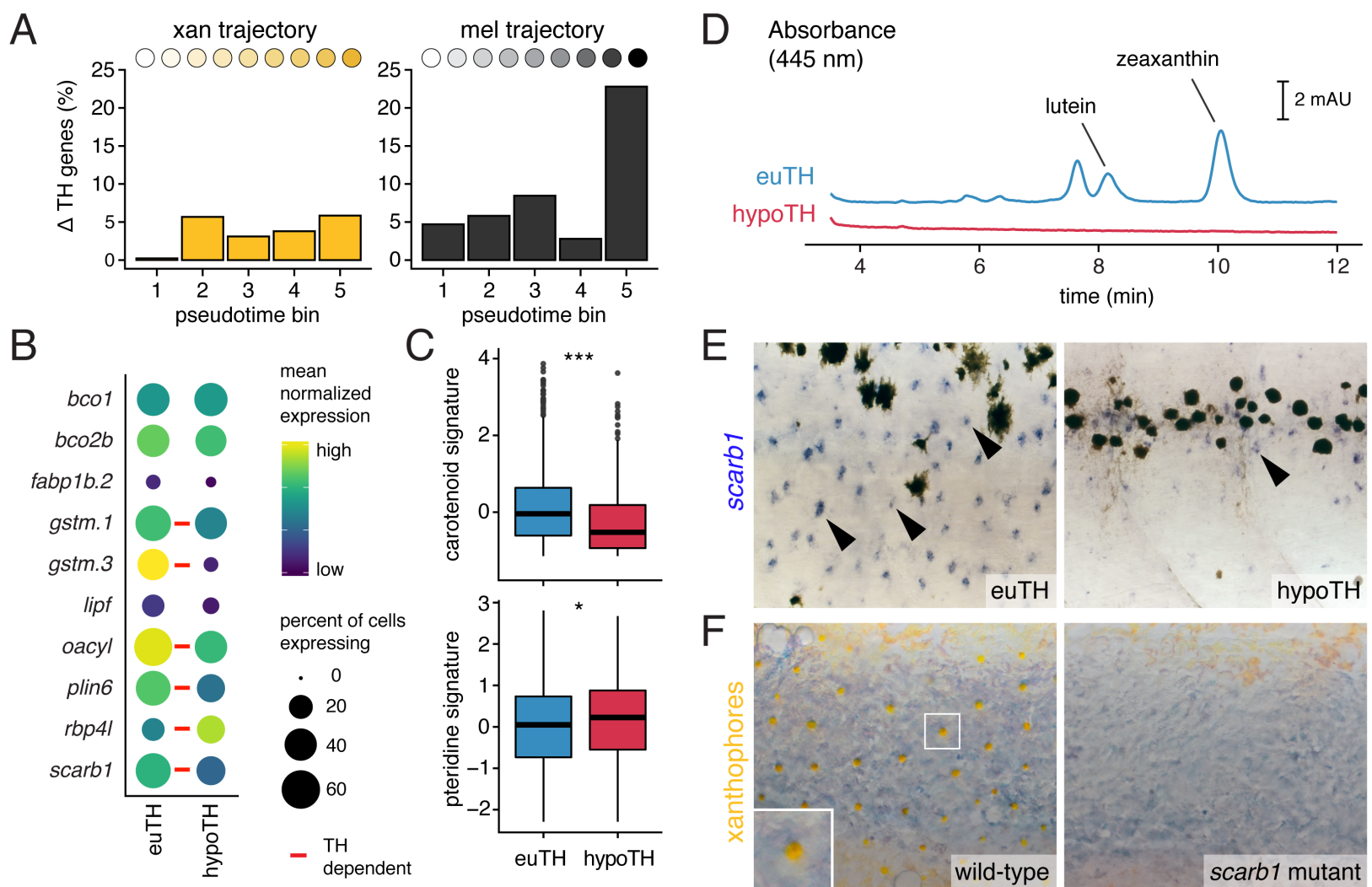


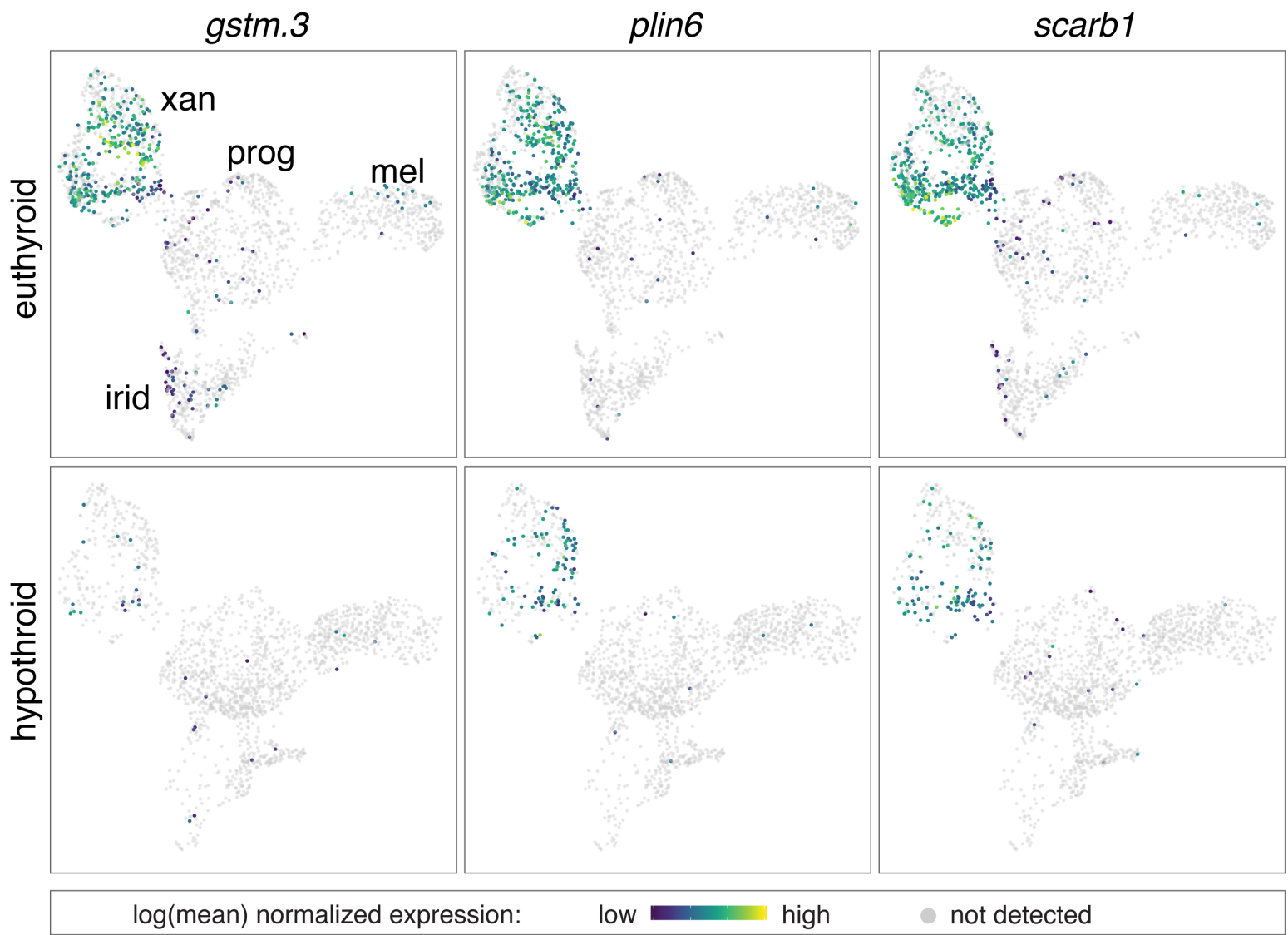


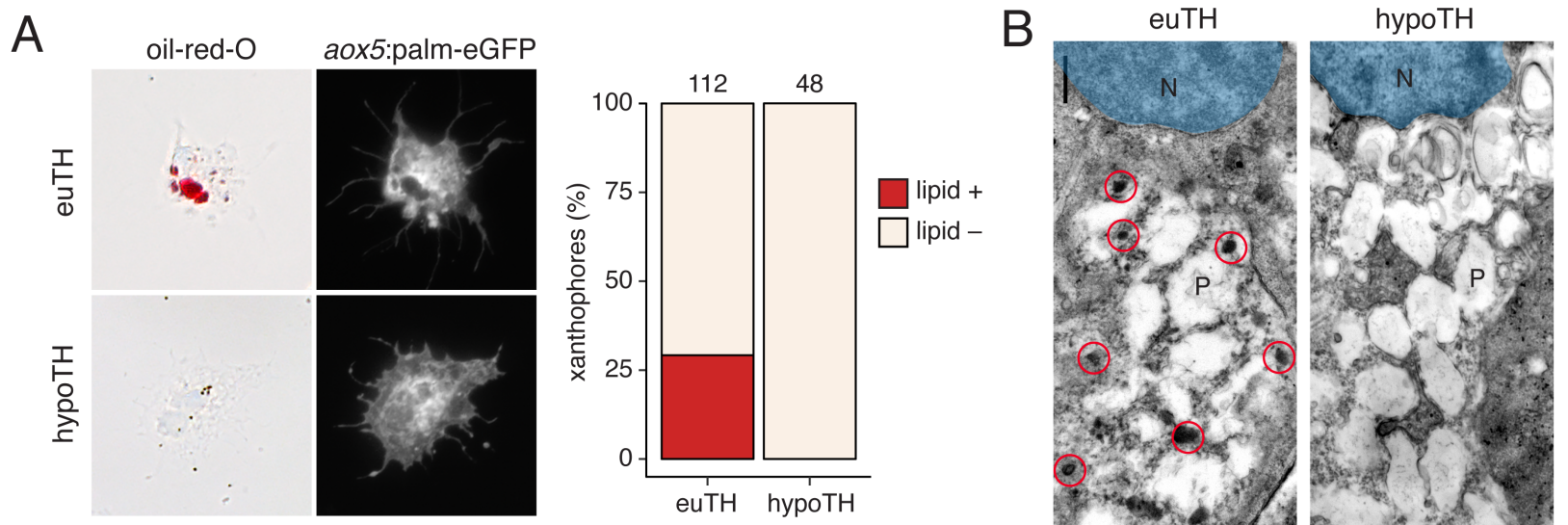
A**B****C****D****E**











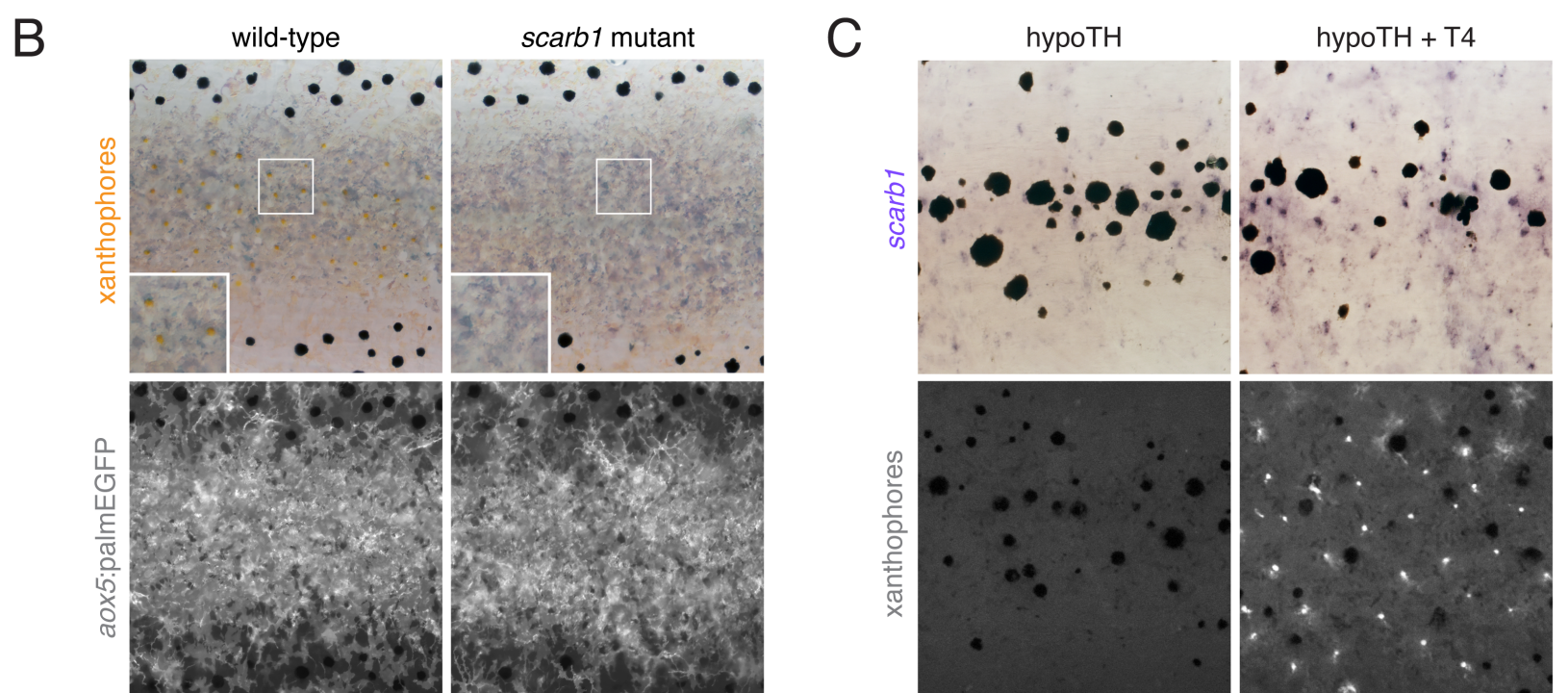
A

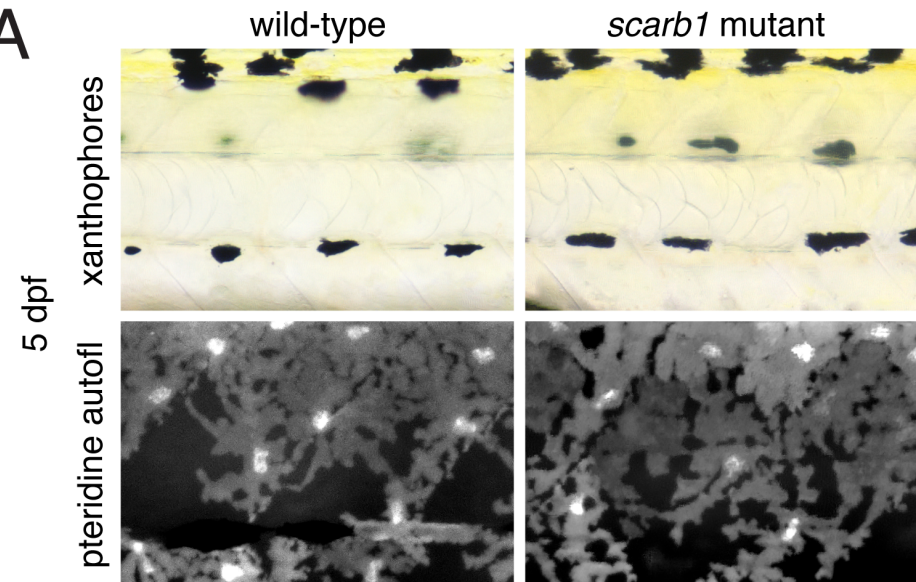
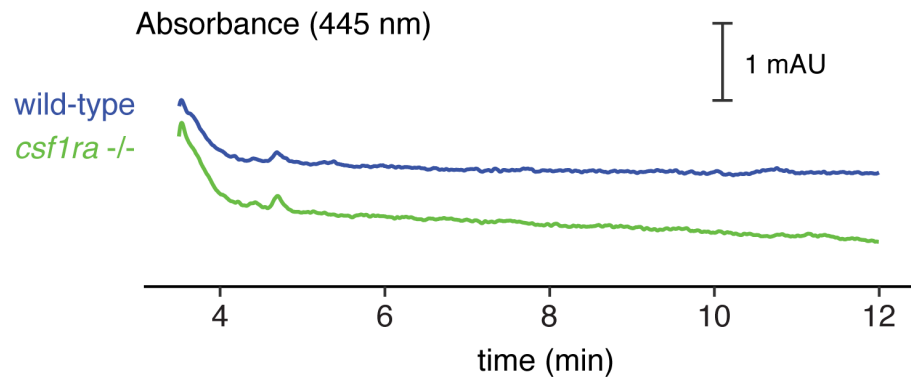
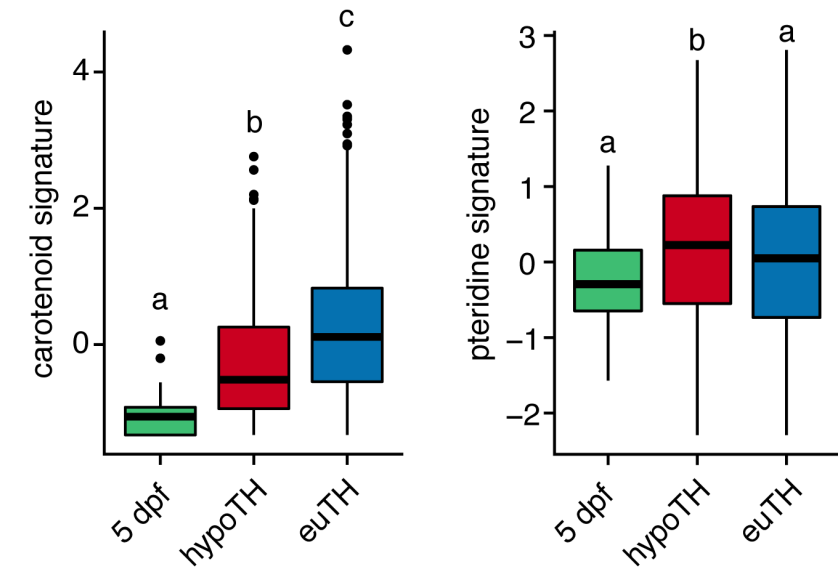
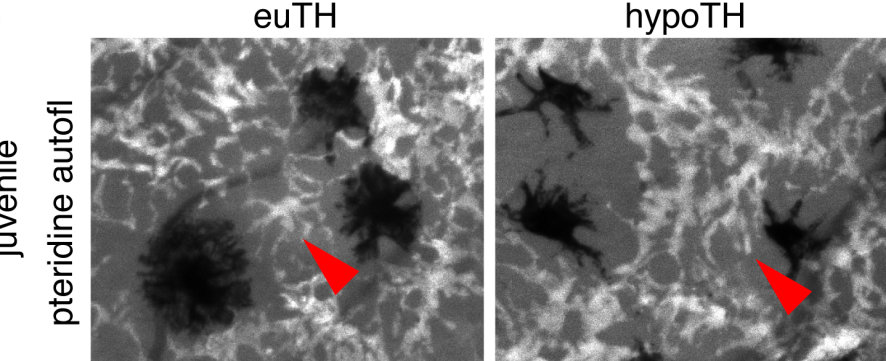
105 bp deletion

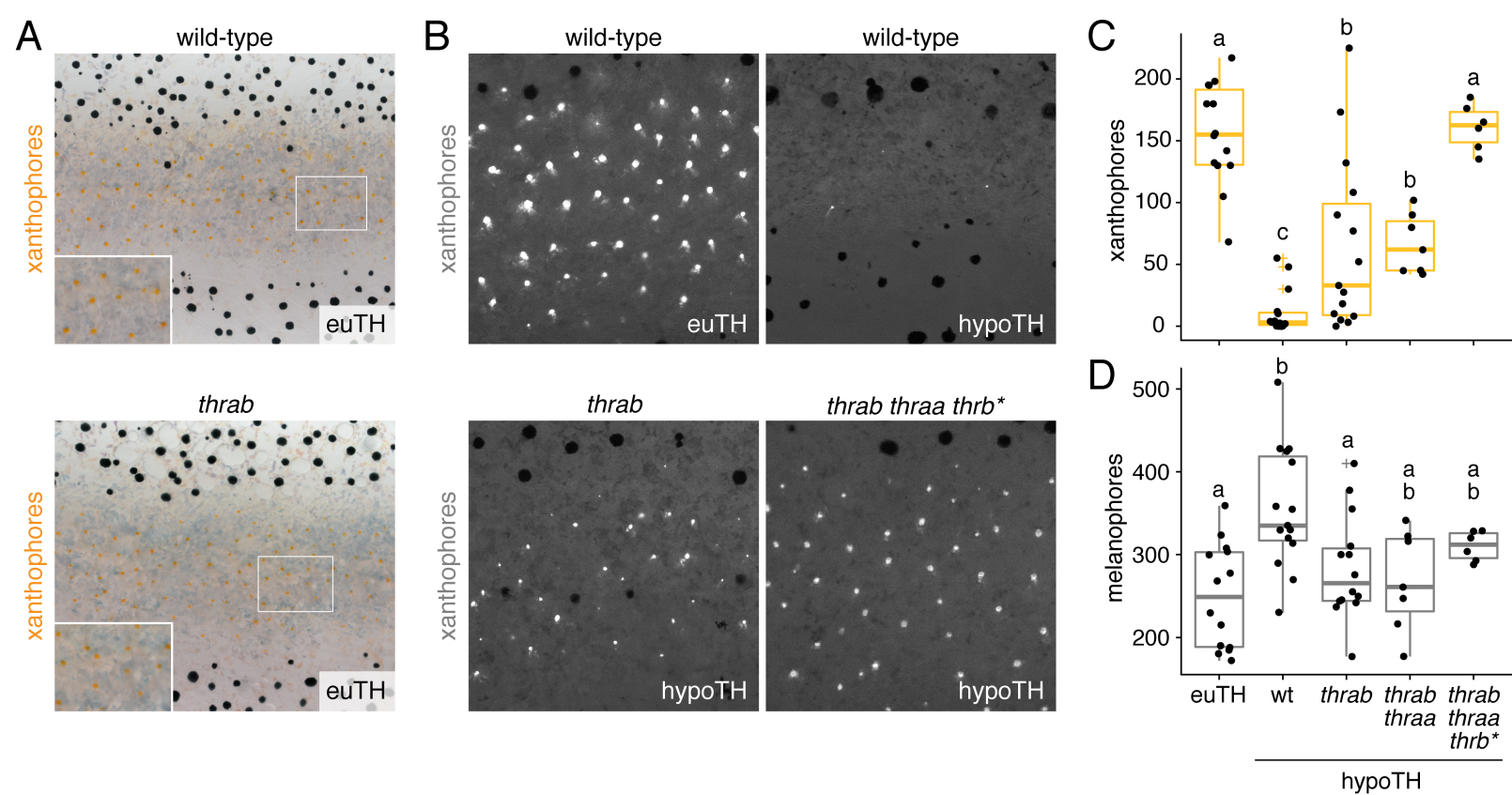
```

zebrafish ---MVSQTTVSIVFLVLGGMALLFGTVLVFVGPIIIDQIVKNVEINPKNDLSYTMWKDIPVPFFMSVYFFHIVNPDEILKGERPMVIQRGPYVYRENRWKDNI...
canary --MAVAQRRLSVGILGLAGLACALLGGCMLLLGPLIVKQQVIKNVRIDPS-SISFQMWKDIPVPFYMTVHFFEVLPKQVLRGEKPVLRQRGPYVYREYRVKTNI...
human MGGSSRARWVALGLGALGLLFAALGVVMILMVPSLIKQQVLKNVRIDPS-SLSFGMWKEIPVPFYLSVYFFEVVNPNEVLNGQKPVVRERGPYVYREFRQKVNI...
mouse MGCSAKARWAAGALGVAGLLCAVLGAVMIVMVPSLIKQQVLKNVRIDPS-SLSFNMWKEIPVFYLSVYFFDVMNPSEILKGEKPQVRERGPYVYREFRHKSNI...

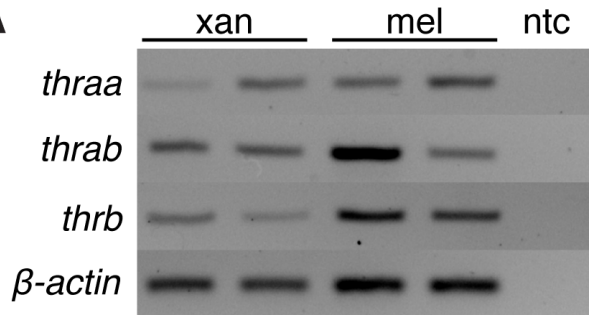
```



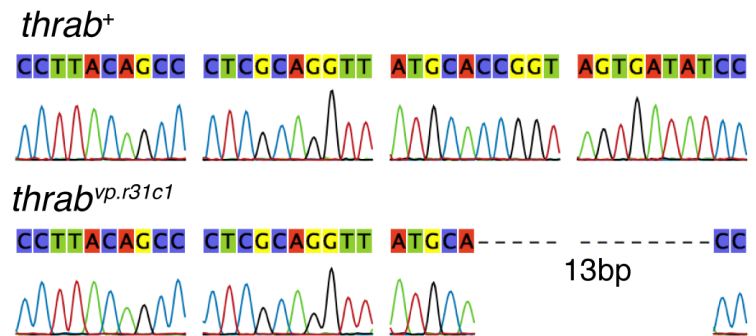
A**B****C****D**



A



B



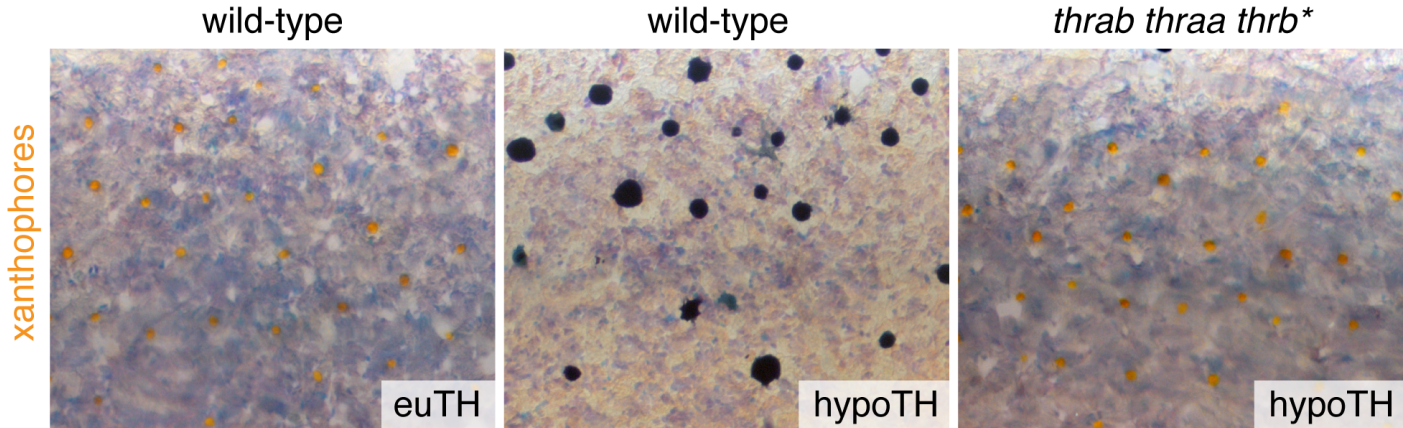
C



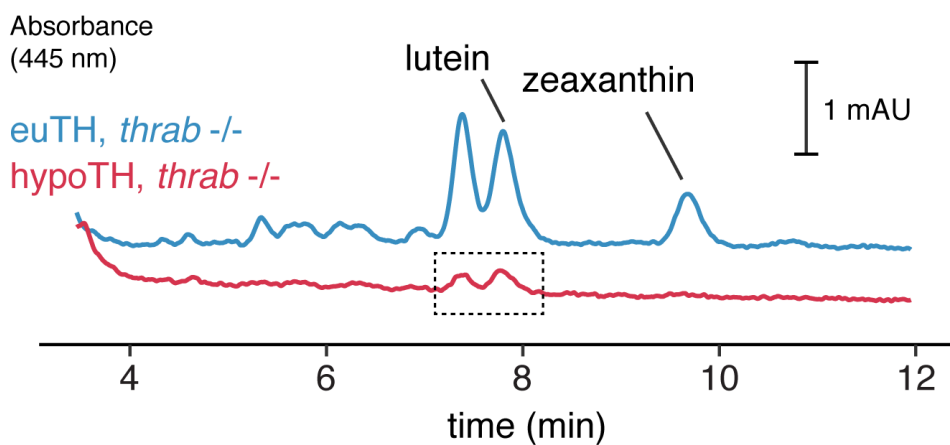
D



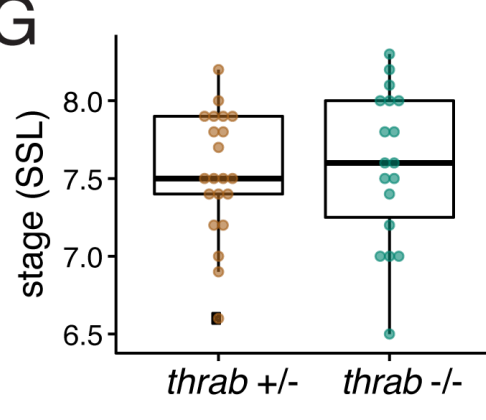
E



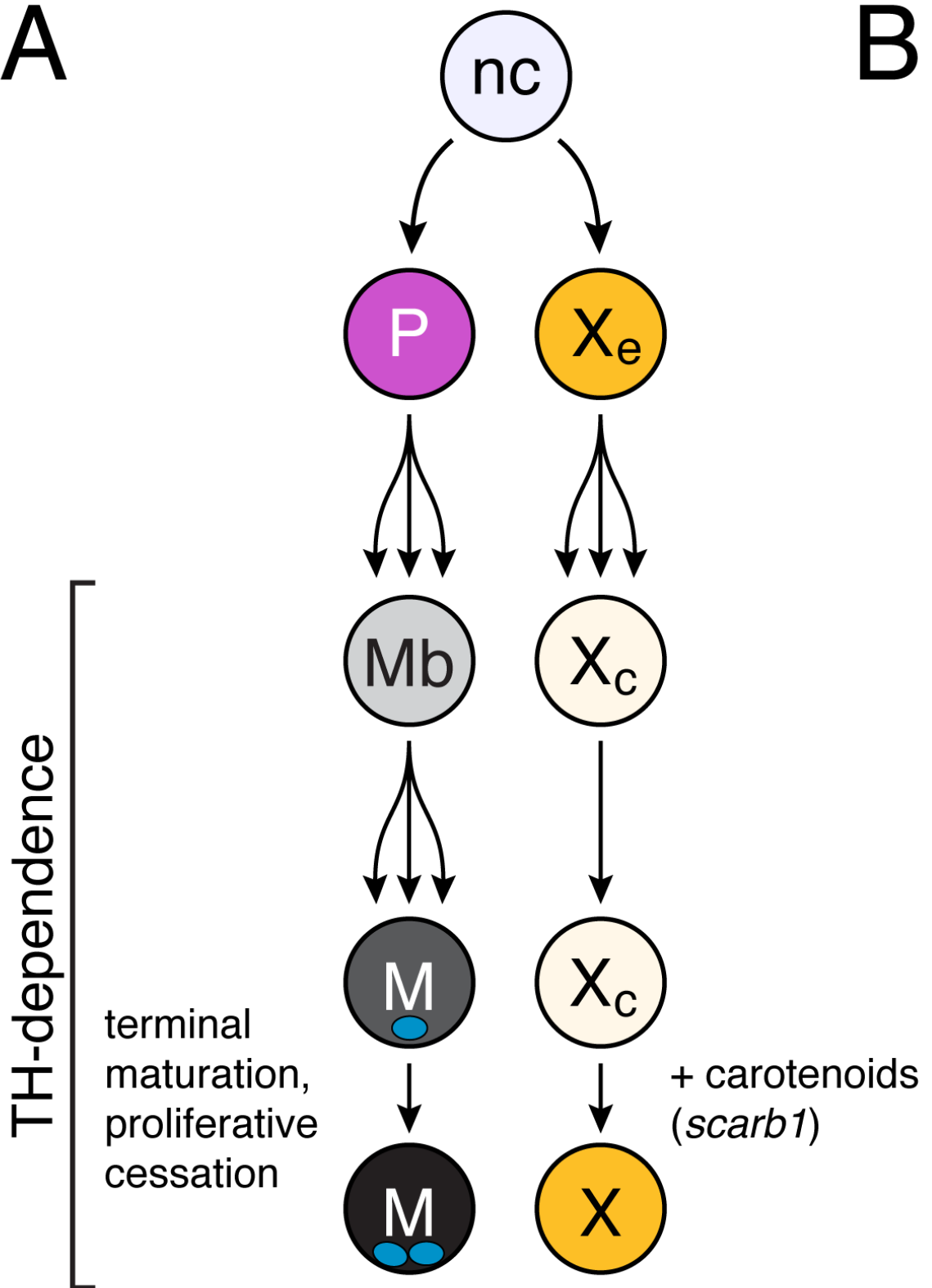
F



G



A



B

